POLITECNICO DI MILANO

School of Engineering

Department of Chemistry, Materials and Chemical Engineering

“G. Natta”

Master of Science in Materials Engineering and Nanotechnology

Graphene Deposition for MEMS Technology

Supervisor: **Prof. Luca MAGAGNIN**
Assistant Supervisor: **Ing. Roberto BERNASCONI**

Pedrazzetti Lorenzo
Student no. 805530

Academic year 2014/ 2015

List of Figures

ABSTRACT

This thesis work aims to develop an optimized process for graphene deposition onto silicon substrates for microelectronics.

Due to the low to absent solubility of carbon into silicon we had to modify the wafer surface in order to let the graphene layer deposit on it; the choice was made considering the most important metals used for microelectronics applications and the effective solubility of carbon in those materials. We ended up using copper and Nickel, which were deposited by galvanic displacement processes, in order to achieve a homogeneous metal layer.

For graphene deposition we did use atmospheric CVD process involving methane as gaseous precursor together with hydrogen as reducing agent; carbon solubility is bradly different for the chosen metals so we had to design two different processes in order to obtain wide graphene layers (or sub-layers).

In order to gather data from the samples we had to make use of different techniques; Raman shift is a well established way of detecting graphene domains while optical microscopy is very useful to explore samples surface morphology.
A wider characterization of the samples required Scanning Electrons Microscopy (SEM) and Atomic Force Microscopy (AFM); to investigate possible technological issues we performed hardness tests.
Last but not the least X-rays diffraction (XRD) has been use to make a strict control of composition and thickness of metallic displacement layers.

INTRODUCTION

Semiconductor technology is, nowadays, the cornerstone of the entire electronics industry and, in particular, of MEMS development. These devices have already proven their utility in everyday life and are growing in popularity, thanks to their reduced dimension but extremely wide plethora of applications.
In order to improve MEMS (and all systems in which are embedded) reliability, many efforts have to be made towards a deeper understanding of surfaces interactions and characteristics. Recent advances in the growth of graphene by chemical vapour deposition have enabled preparation of graphene films of high quality on transition metals surfaces, despite their polycrystalline structure and orientation. To realize many of the potential applications of graphene, there remains a need for scalable methods of transferring graphene from the metal film or foil growth substrate, which is often Copper or Nickel, to application specific substrates. Moreover, graphene transfer methods typically require multiple steps, and can damage the graphene. A more attractive opportunity would be to fabricate directly onto dielectric substrates, thereby avoiding wet chemical processing and the use of a support layer for transfer. It has been shown [57] that graphene grows at the interface of dielectrics and Copper of Nickel films, under the same conditions that, simultaneously, result in growth on top of the metal film. By the way, the costs for depositing metal films on Silicon substrates by physical vapour deposition techniques are burdening for large scale industry applications.

Our goal is to develop a cheaper route to plate Silicon with Copper or Nickel films and to prove their compatibility with the already existing CVD methods for graphene growth.

In order to do so, galvanic displacement was pointed out as a valid alternative to PVD methods of plating semiconductors surfaces with homogeneous and coherent transition metal films.

Galvanic displacement is an electrochemical process that allow obtaining polycrystalline metals with good adherence on dielectric, or semiconducting, surfaces without the need of external applied current. This technology is already exploited in solar cells industry and it have to be customized for the intended technology.

Prior the plating process characterization and optimization, both Copper and Nickel had to be tested, in order to understand which of the two metals better suited the available CVD technique. In CVD process, the methane was used as precursor. The hydrocarbon is decomposed on the metal surface, enabling graphene growth either by a combination of surface nucleation and two dimensional growth, as in the case of Copper, or by a surface segregation process of Carbon from the metal, as in the case of Nickel.

After a qualitative Raman analysis of both the substrates, Nickel resulted in a better quality of the graphene deposit, actually presenting a heterogeneous, but highly ordered, graphene/FLG thickness.

In order to achieve a well rounded Nickel film on the Silicon surface 5 different plating times was inspected: 10 minutes, 15 minutes, 25 minutes, 30 minutes and 40 minutes. Plating characterization featured XRD analysis for grasping crystallographic structure of the plating, SEM analysis to obtain informations about metal film growth rate and AFM analysis for mean roughness and profile data collecting.

Graphene deposition was then performed on the better quality yielding plating time, for the sake of having the most compact and adherent metal film possible. Again, the reported CVD process was employed and a complete characterization followed.

Alongside with the already cited Raman spectroscopy, SEM and AFM analysis, the FLG/Ni/Si samples were subjected to XPS analysis for a better understanding of the deposit chemistry and GDOES analysis for catching composition profile. A Raman peak deconvolution was carried out in order to have another evaluation of the deposit thickness.

Finally, the presented graphene deposition route was applied to existing MEMS, in order to prove the feasibility of the whole process. SEM analysis was performed to glimpse MEMS integrity status and the Raman peak deconvolution was performed for these samples too.

CHAPTER 1:

State of The Art

1.1 Graphene

Carbon is one of the most important elements in the universe for what is concerned the human life; it literally the backbone of our entire biologic system, it is the basis of a wide industrial chemistry branch and during the XX century, thanks to the advent of the quantum mechanics model, it has been found being the constituent of some of the more useful materials.

Carbon has mainly 3 allotropic forms, which are graphite, diamond and amorphous carbon [1].

Until 1947 these were believe to be the only aspect of large carbon systems; however P.R. Wallace theorized the graphene as the basic to understand the structure of graphite, which had been solved thanks to powders diffraction in 1916.

As it was, graphene was supposed to be a two dimensional, atomic-scale, hexagonal lattice in which one atom forms the vertex [2].

Interestingly graphene has been only and mainly a pure theoretical entity, until 2003, when the physics Nobel prizes Andre Geim and Kostantin Novoselov managed to isolate a free standing, two-dimensional, hexagonal carbon cells layer simply by cleavaging a graphite block with the aid of the simplest Scotch ® tape [3].

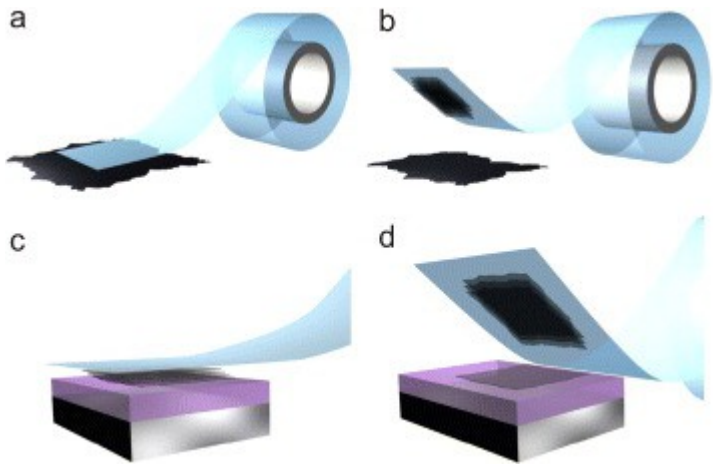

Fig. 1.1: graphene mechanical exfoliation with tape

1.1.1 Graphene Characteristics

The importance of graphene lays of course in its characteristics and the scale at which they can be exploited. The term graphene was coined as a combination of graphite and the suffix “ene” by Hanns-Peter Boehm [4], who described single-layer carbon foils in 1962 [5].

Graphene is a crystalline allotrope of carbon, in which the carbon atoms are densely packed in a regular hexagonal pattern.

Each atom has 4 bonds: one σ bond with each of its three neighbours and one π-bond that is oriented out of plane; the bond length is roughly 1,42 Å.

Graphene hexagonal lattice can be regarded as two interleaving triangular lattices. This perspective was successfully used to calculate the band structure of graphite using the tigh-binding approximation[6].

Graphene's stability is a very important feature in order to obtain self-standing sheets; it is due to the tight packed carbon atoms and to the sp^2 orbital hybridization that constitute the σ bond. These bonds are responsible for the structural properties of graphene, such as a specific strength 100 time that of the steel.

The remaining p_z orbitals for a π-bond which in turns give birth to the half-filled π “band”.

In this work we focused on the electronic properties of graphene, all belonging to the conjugation of those p, out-of-plan, orbitals.

This peculiar structure makes graphene a zero-gap semiconductor: its valence and conductions bands meet each others at the so-called “Dirac point” or k-points [7].

Dirac points are six locations in the reciprocal lattice space, on the edge of the Brillouin zone; they are divided into two different sets, K and K' made up of three points. The two sets give graphene band structure a degeneracy of $g_v = 2$.

so electrons which travel through the graphene's honeycomb lattice effectively lose their mass at the Dirac points and so being described by a Dirac equation for relativistic particles instead of by the purely quantum mechanical Schrödinger equation.

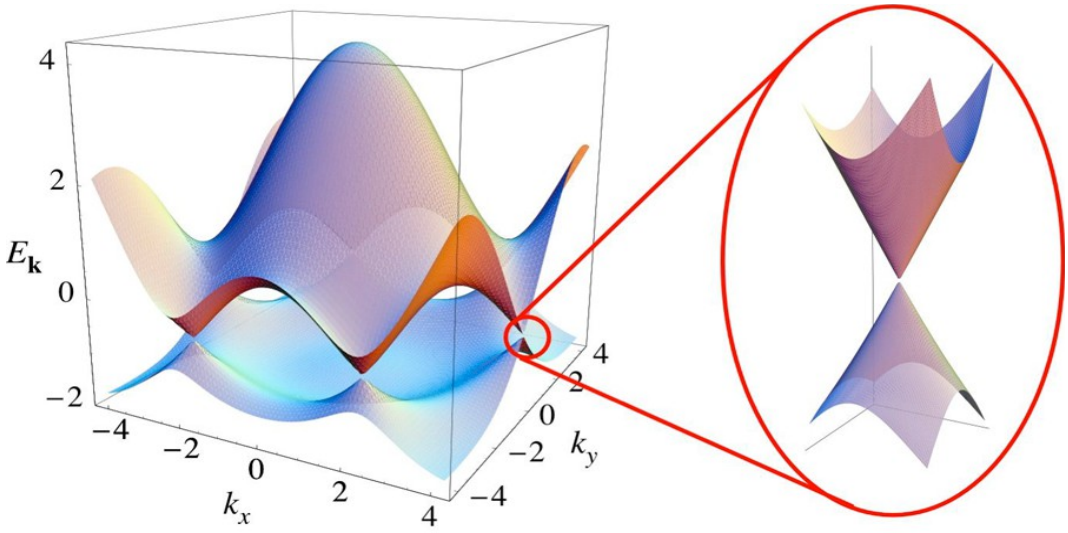

Fig. 1.2: graphene's band structure particular: K points

In the low-energy limit, the energy-momentum dispersion relation in linear (relativistic Diriac's equation) and carriers are seen as zero-rest mass relativistic particles with an effective “speed of light”, c*~106 m/s. The peculiar local electronic structure, thus allows the observations of several phenomena which are typical of a two-dimensional Dirac fermions gas [8]. In the high-energy limit, the linear energy-momentum relation is no longer valid and the bands are subjected to a distortion leading anisotropy, also known as trigonal warping [9]. Upon stacking layers on top of each others, one first obtain bilayered graphene, which exhibits its own set of very specific properties. The centre of aromatic rings of the upper graphene sheet sits on the top of an atom of the lower sheet, so that the symmetry is trigonal rather than hexagonal. With the inter-plane interaction, the charge carriers acquire a mass and the dispersion recovers a parabolic dispersion described by the Schröedinger formalism. Nevertheless, bilayer graphene remains gap less if one ignores trigonal warping. The interaction of the π and π* bands of each graphene sheets produces two other bands. In the presence of an external potential, a gap can be opened close to the K point [10,11]. Further generalization of the perfect stacking results in graphite with alternating (ABAB, Bernal type) or staggered (ABCABC, rhombohedral type) arrangement depending on whatever the lateral carbon atom shift changes direction from one layer to the next or not. The interplanar distance of ideal graphite is 3.45 Å but if successive planes are rotated with respect to each other, this spacing can increase.

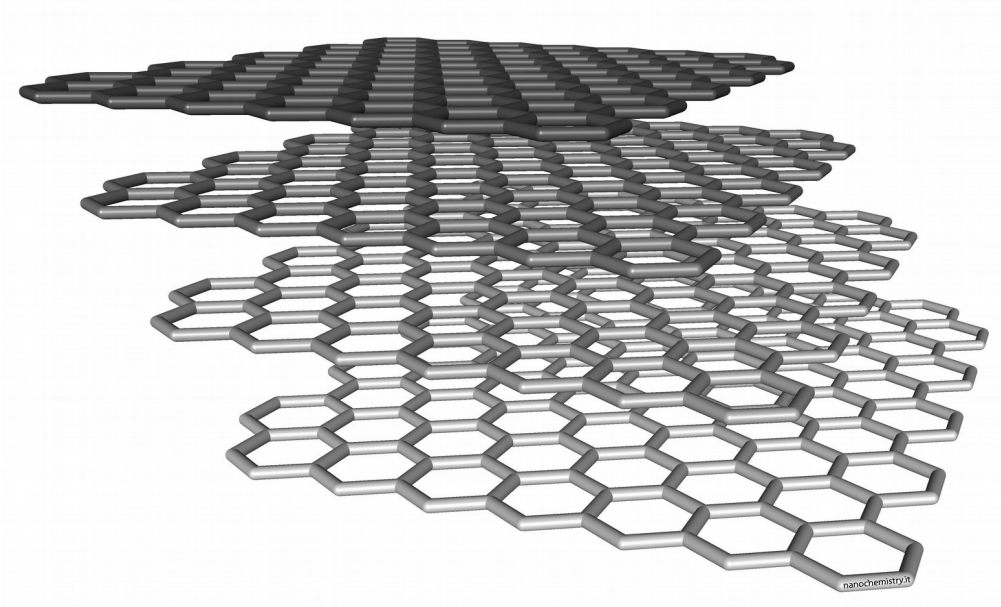

Fig. 1.3: graphene stacking to form graphitic system

1.1.2 Graphene properties

Graphene mechanical properties are the best among materials tested until now : its tensile strength reaches 130 GPa and has a 1 TPa Young modulus, its spring constant has been measured by AFM techniques and it has been found that ranges from 1 to 5 N/m with a 0.5 TPa stiffness (different from graphene bulk one).

These properties are just very good for MEMS industry applications and the only real limit is to obtain a coherent, self-standing, graphene layer.

From the chemical point of view graphene is the only carbon-based system in which every single atom of carbon is available for chemical reaction from two sides (thanks to the 2D); atoms at the edge of a graphene layer have particular chemical reactivity and graphene has the highest edge-to-bulk carbon atoms ratio of all the allotropes.

Graphene burns at relatively low temperature, 620°K, and is generally modified with oxygen- or nitrogen-containing functional groups. Graphene is impermeable to everything but protons.

One of the main properties, which also is important for micro electronics applications and for organic semiconductor technology, is the high electron mobility of graphene structure.

Reported values for room temperature are about 15.000 $cm^2/(Vs)$ and the symmetry of

experimentally measured conductance that holes and electrons mobility should be roughly the same.
Experiments under light that graphene charges mobility is pretty the same ranging from 10 to 100 K, which implies the main scattering mechanism is defect scattering. Nevertheless phonon scattering limits graphene charges mobility when temperature grows, up to 200.000 $cm^2/(Vs)$ with a charge density of 10^{12} $1/cm^2$, which is approximately ten time copper electrons mobility. It goes along with what stated above that graphene resistivity is lower than silver one, which is the lowest resistivity we experimented at room temperature.
Transport in graphene is dominated by two modes : we have ballistic transport, which is temperature independent, which consist in electrons moving without having collisions, the other is temperature activated and of course implies phonons-electrons interactions. Graphene electrons can move for a whole micrometer without having a single scattering event, even at room temperature.
Graphene can be doped with several gaseous species and it can be turned into its pristine form by a gentle heating in vacuum, to avoid the easy oxidation of the carbon layer.

Graphene's unique optical properties produce an unexpectedly high opacity for an atomic monolayer in vacuum, absorbing $\pi\alpha \approx 2.3\%$of red light, where α is the fine-structure constant. This is a consequence of the "unusual low-energy electronic structure of monolayer graphene that features electron and hole conical bands meeting each other at the Dirac point, which is qualitatively different from more common quadratic massive bands [12].

Graphene thermal conductivity has been demonstrated being strictly phonon-dominated; it is also found that different conductivity values, which are very high, can be associated with different graphene qualities and to the isotopes ration of the layer. Nowadays thermal transport in graphene is an active area of research, which has attracted attention because of the potential of thermal management applications; some early measurements of suspended graphene thermal conductivity give about 5.300 W/(mK), which is more than double that of the graphite.

In the 2014 magnetic properties of graphene has been tested by magnetizing a graphene layer using a yttrium-iron garnet, but its electronic properties seemed to be unaffected.

1.1.3 Methods for Graphene Production

Unfortunately it is, in principle, impossible to produce a 2D crystal by chemical synthesis because the rapid growth of phonon density along with increasing lateral size forces the 2D crystallites to bend into the more stable 3D structure.
However there exist a route to produce 2D layers and it is by exploiting the property of 2D systems to grow onto 3D structures, just as naturally happens in graphite, in which we effectively have stacked graphene sheets.

- Mechanical Exfoliation

It is also know as mechanical cleavage of a graphite block and as it can be understande it consists in impressing to a graphite sample the energy required to break the cohesion forces between the planes and exfoliate down to single graphene sheet in matrices.
Once the layer is attached to the tape we must pay attention to not let the domains interact via Van der Waals forces, or it will form irreversible amorphous agglomerates. The force acting between sheets is around 2 eV/nm² and the force required for exfoliation is around 300 nN/μm² [13].
By using High Oriented Pyrolytic Graphite the adhesion forces can be easily achieved using commercial Schotch ® tape, AFM or STM tips and Si/SiO moulds. This process

was first realized by the Noble prizes Novoselov and Geim [14], managing to repeat the stick and peel process until they reached the monolayer; after checking the layer quality by the aid of optical microscopy, the tape is gently pressed on a clean Si substrate. The main drawback of this process is the remnants of glue which can remain on the substrate and lead to an electrons mobility reduction; a post-deposition treatment is generally performed on the samples, better if the atmosphere is made reducent. In order to partially prevent glue to leave behind its remains it is possible to enhance graphene adhesion to the substrate, for example using high voltages: 1-10 to 20 KV can

leave up to a few layer of graphene on the substrate while 3-5 KV can be applied directly to the Silicon wafer to obtain up to three graphene layers. Generally exfoliation-made samples are of very high quality, with optimal charge carriers mobilities, even if it's impossible to strictly control film dimensions; for all those reasons mechanical exfoliation is considered a purely academic process of producing graphene layers.

-Chemical Exfoliation

Unfortunately the poor reproducibility of the mechanical exfoliation methods is a problem for industrial processing, so it was necessary to develop a procedure based on the same approach but using different tools.
The idea behind chemical exfoliation is that we can use surfactants to weaken graphite inter planar bonds and thus obtaining a solution containing graphene monolayer, which have to be sterically stabilized to not cause carbon hybridization, which will lead to the loss of graphene electronics and transport properties.
The process can be carried out both in organic solvents (N-methyl pyrrolidone of phenols) [15,16] or in water [17], with the aid of several hours of sonication and a 1000°C annealing; the main difference is water can produce lower graphene concentration with respect to to organic solvent, but it is clearly a non-toxic solvent.
Several works reported data which suggest we have to reach the CMC solvent concentration (that at which the solvent self-assembly into micelles) to have density-dispersed graphene monolayers, which can be then separated by means of Dendity Gradient Ultracentrifugation (DGU) methods.

Graphite can also be split by intercaling a monomer solvent in between inter planar spacings [18], which are 0,34 to 1 nm wide. For example sodium Dodecyl Sulphate (SDS) is one of the suitable solvents for this purpose. As mentioned above, using a 1000°c thermal treatment it is possible to make the solvent turn to gas and so separate graphene layers while sonicating the solution.

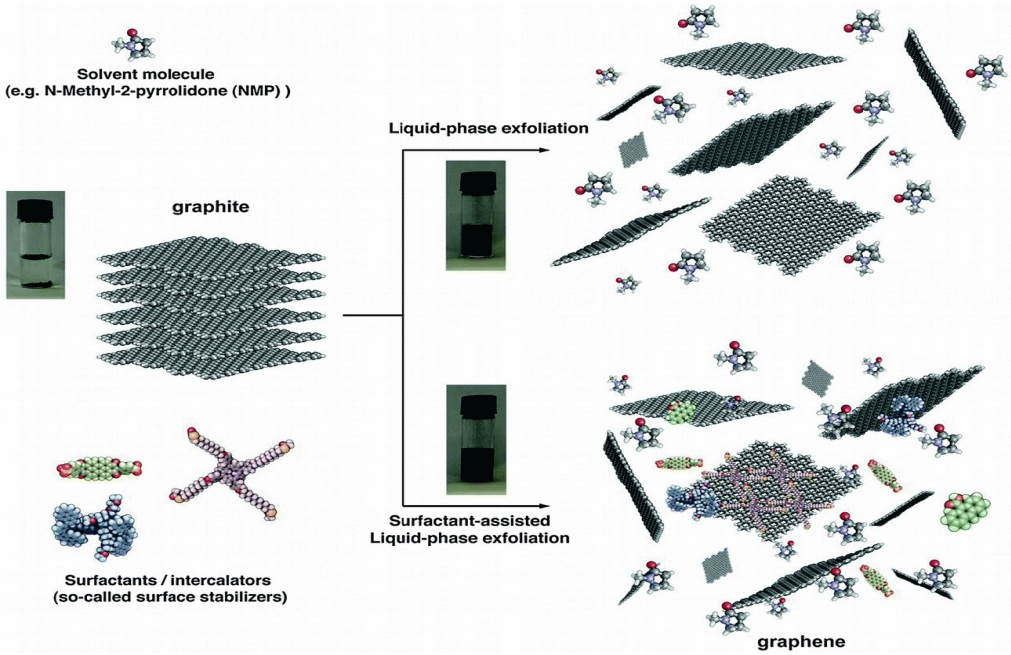

Fig. 1.4: chemical exfoliation method to fabricate graphene sheets

Chemical exfoliation methods can so give sheets maximum 400 nm wide and generally they present irreversible defects and so they cannot be used for the sensors production.

- Chemical Synthesis

A solid alternative to exfoliation has been found among the graphite intercalation compounds, the graphite oxide (GO) or, more precisely, graphite hydroxide [19].
This compound can be obtained in aqueous solution using strong oxidisers onto a crystalline graphite substrate and is a valid alternative to exfoliation processes for graphene production. In fact the theoretical maximum degree of oxidation of the graphite crystallite corresponds to an array of uncoupled graphene sheets, with oxygen atoms and hydroxyl groups grafted on both sides.
Graphene then can easily be obtained reducing the graphite oxide, which means removing all oxygen and all hydroxyl groups grafted onto it.

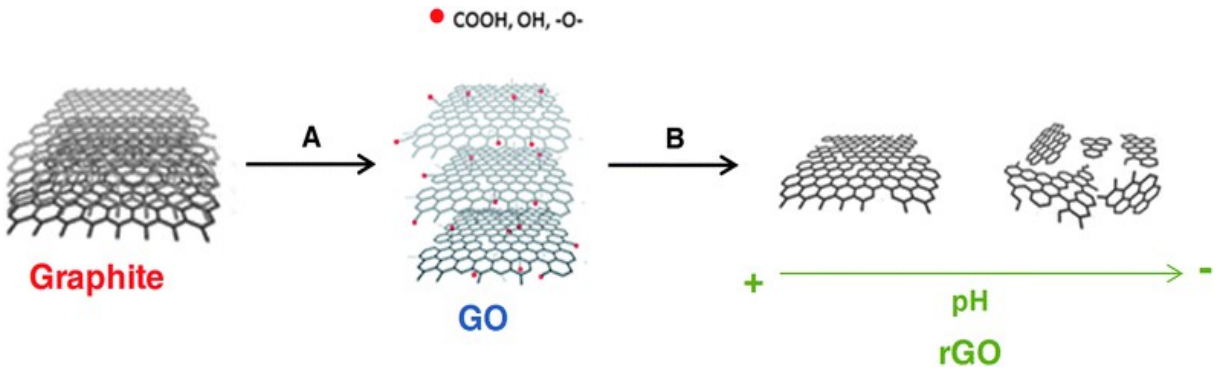

Fig. 1.5: graphene chemical synthesis

Graphite reduction is a simple process and it can be carried out in a very wide range of different conditions, just because graphite oxide is not that chemically stable and so making it a safe process for graphene characteristics.
We are then left with a stable water solution made of graphene monolayers and multilayers, which can be deposited onto several different substrates for a wide range of applications [20,21].

- Substrates Supported Graphene Growth

These techniques can be further divided into 3 categories:

1. Thermal Chemical Vapour Deposition
2. Plasma Enhanced Chemical Vapour Deposition
3. Thermal Decomposition of Substrates.

The thermal CVD is the process we have chosen to deposit graphene monoloayers and we it will be discussed in a proper section more in detail.

Plasma enhanced CVD was first used to produce graphene with a radio frequency system in order to let graphene deposit onto different substrates from a gaseous stream of 5-100% CH_4 in H_2 (total pressure 12 Pa), at 900 W and 680 substrate temperature [22,23].
Afterwards many efforts have been made to improve this technique, in particular to optimize operating conditions to reach graphene monolayers instead of graphitic

structures, which inherently could be present using this process.

Among the substrates used for thermal decomposition in order to obtain graphene we can account for silicon carbide.

Silicon carbide is generally used for large-scale FLG (few layer graphene) production, exploiting the epitaxial growth of the carbon nanostructure which takes place along with substrate thermal decomposition.

The process is made viable by silicon atoms selectively desorbing from the surface as the substrates gets annealed at high temperatures (1300°C), leaving behind carbon atom which self-assemble into FLG.

Silicon carbide is a wide band-gap semiconductor and so the FLG grown on it could serve as a graphene substrate for specific micro electronic applications.

Further on, silicon carbide wafer technology is growing rapidly in terms of production costs and scale and many works shows that thermal decomposition is a suitable process for FLG industrial scale production.

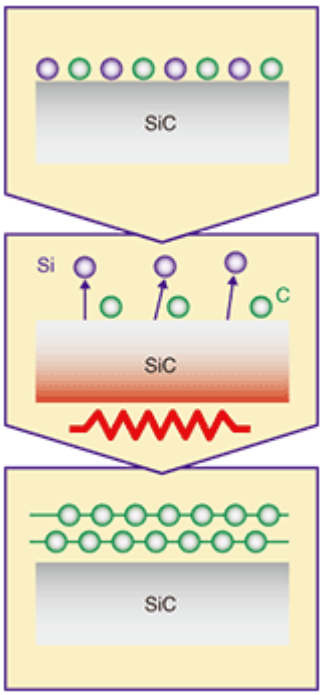

Fig. 1.6: graphene production from Silicon Carbide

There are several other substrates on which graphene can be epitaxially grown by their decompositions: Titanium, Tantalium and Titanium Carbide are very good contenders.
Generally the FLG thickness heavily depends on heating time and process cap temperature; unfortunately thermal decomposition graphene layers presents some defects, along with some thickness inhomogeneities.
The worst drawback this technique presents is a 100 times lower value of charge carries mobility with respect to exfolieted sheets, which could be very detrimental for electronic applications. By the way, two fundamental issues have to be fixed before substrates thermal decomposition achieves an industry-wide viable application. First of all, as already said, there is such a thickness distribution along the graphene layer which makes it very unreliable for electronics, due to the fact that graphene appeal properties are thickness dependant. Second, is it not yet fully understood how silicon carbide quality affects FLG's physical properties and without a well established relation between substrate characteristics and graphene quality it is difficult to choose the optimal FLG appilcation [24,25].

- Graphene Nanoribbons

They are generally produced using several types of carbon nanotubes (CNTs) unzipping [26,27], which could be chemical or even mechanical.

Jiao et al. [28] use a polymeric layer to set a multiwall CNTs forest, which has been then deposited onto a silicon substrate. Afterwards the polymer layer is removed with KOH solution and CNTs forest is subjected to Ar - plasma decomposition to obtain the nanoribbons.
Then polymer residues are removed with acetone and 300°C heating for 10 minutes, obtaining graphene ribbons mono or multilayer 10-20 nanometers wide for electronics applications.

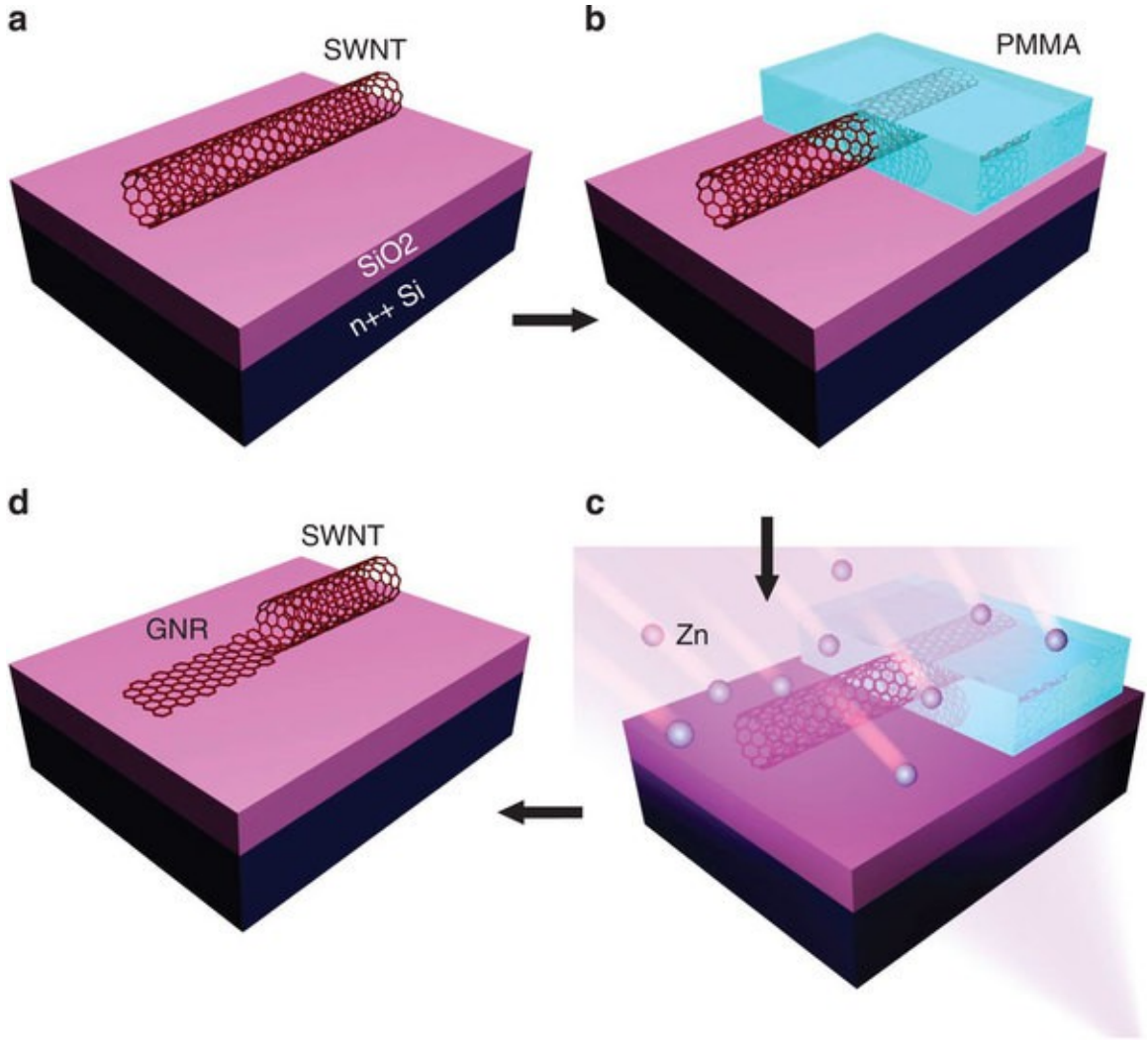

Fig. 1.7: graphene nanoribbons production

Tiwary et al. [29] very recently proposed an alternative to chemical nanotubes unzipping, due to many issues involving toxicity of those compounds.

They use a micro cryo-milling self-designed system.

Mechanical carbon nanotubes unzipping is somewhat deceptive due to the intrinsic anisotropicity of the CNTs system : it is need a very high amount of energy to directionally break those C – C bonds.

The energy requirement is generally fulfilled using very high strain rates (10^8/s) and the machinery is made up of a vibrating ball which can impose a 3 mm displacement amplitude and weights roughly 500 milligrams.

The system has to be kept at 150°K to avoid local melting, cold welding and bridging of the CNTs throughtout a liquid nitrogen flow.

Walled CNTs obtained by water assisted CVD were used; they were grown onto a 10 nm Aluminium / 1,5 nm iron catalyst deposited onto silicon via electron beam deposition.

The whole system was then put into a quartz tube and heated at 775°C in a buffer Ar/H_2 (15% H_2) mix.

After milling CNTs were transformed into a nanoribbons poweder, which can then be water of ethanol dispersed to be further deposited.

Electronic characterization along with Raman spectroscopy revealed a 500 nm wide ribbons suspension, with average number of layers equal to 2.

By the way graphene nanoribbons can also be produced by chemical methods.

For example Mullen et al. [30] proposed a bottom-up route of producing graphene nanoribbons (GNR) on gold surfaces from 10,10'-dobromo-9,9'-bianthryl precursor monomers. In the fabrication process the thermal deposition of the monomers onto a gold surface removes the halogen substituens from the precursors, and provides the molecolar building blocks for the targeted graphene ribbons in the form of surface-stabilazed biradical species. During a first thermal activations step, the biradical species diffuse across the surface and undergo radical addictions reactions to form linear polymer chains (formation of C-C bonds at 200°C) as imprinted by specific chemical functionality patterns of monomers. In a second thermal activations step a surface-assisted cyclodehydrogenation establish an extended fully aromatic system (formation of C hexagons).

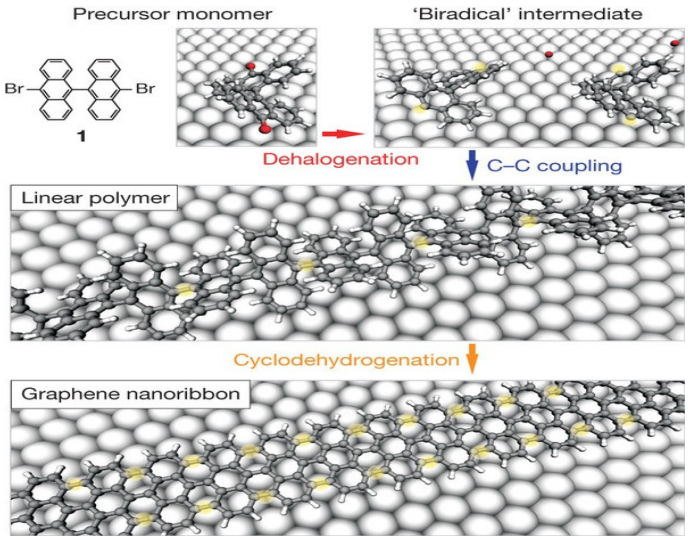

Fig. 1.8: chemical route to fabricate graphene nanoribbons

Unzipping nanotubes and chemical nanoribbons production give the possibility to produce mono-, bi- or even multi-layered graphene nanoribbons which have very good uniformity; generally it is obtained a very good graphene, with all the qualities kept safe.

1.2 CHEMICAL VAPOUR DEPOSITION

Chemical vapour deposition (CVD) is a widely use materials-processing technology vastly applied in the semiconductor industry. The majority of its applications involves applying solid thin-films coating to surfaces, but it is also use to produce high-purity bulk materials and powders, as well as fabricating composite materials via infiltration techniques.
It has been used to deposit a very wide range of materials. The majority of the elements in the periodic table have been deposited by CVD techniques, some used in the form of pure element, but more often combined to form compounds.

CVD involves flowing a precursor gas or gases into a chamber containing one or more heated objects to be coated. Chemical reactions occur on and near the hot surfaces, resulting in the deposition of a thin film on the surface. This is accompanied by the production of chemical by-products that are exhausted out of the chamber along with unreacted precursor gases.

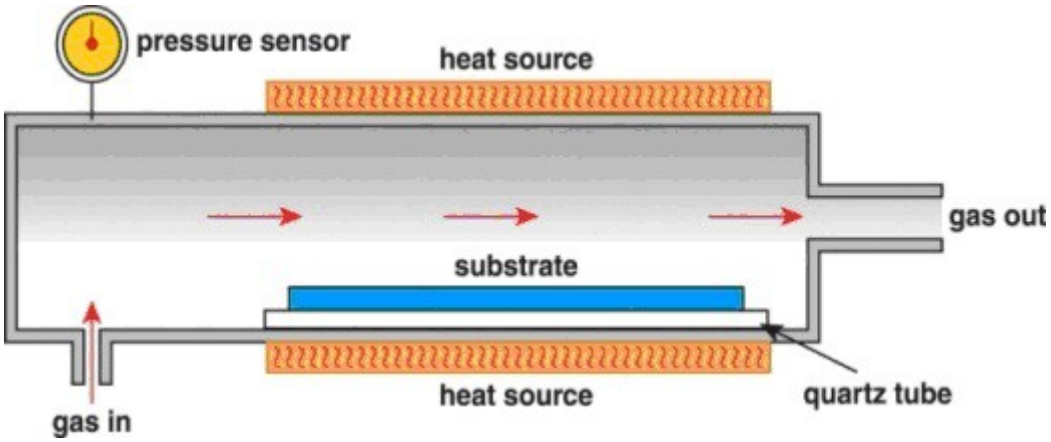

Fig. 1.9: CVD schematics

As it would be expected with the large variety of materials deposited and the wide range of applications, CVD is practised in a variety of formats. These processes generally differ in means by which chemical reactions are initiated.

First of all, CVD processes can be classified by the operating pressure:

- atmospheric pressure CVD (APCVD);
- low pressure CVD (LPCVD), generally carried out at sub-atmospheric pressure. Reduced pressure tends to reduce unwanted gas-phase reactions and improve film uniformity across the substrate;
- ultra-high vacuum CVD (UHVCVD), which is carried out at nearly zero pressure (10^{-8} torr).

The physical characteristics of the vapour used are also worth to make some distinctions:

- areosol-assisted CVD (AACVD), which is CVD with a liquid/gaseous, ultrasonically generated, areosol transporting the precursor; this is a very useful for non volatile precursors;
- direct liquid injection CVD (DLICVD), clearly a CVD process in which precursors are in liquid phase or even solid conveniently dissolved into a liquid solution. Liquid solutions are injected into a vaporization chamber towards injectors (typically car injectors). The precursor vapours are then transported to the substrate as in classical CVD and fairly high growth rates can be reached using this technique.

Among all CVD processes, those who involve the use of a plasma are given very importance:

- microwaves plasma-assisted CVD (MPCVD);
- plasma-enhanced CVD (PECVD), here plasma is used to enhance chemical reaction rates of the precursors. PECVD processing allows deposition at lower temperatures, which is often critical in the manufacture of semiconductor. The lower temperatures also allow for the deposition of organic coatings, such as plasma polymers, that have been used for nanopartile surface functionalization.
- Remote plasma-enhanced CVD (RPECVD), is similar to PECVD except that the wafer substrate is not directly in the plasma discharge region. Removing the

wafer from the plasma region allows processing temperatures down to room temperature.

There is also a variety of enhanced CVD processes, which involve the use of ions, photons, LASERS, hot filaments or combustion reactions to increase deposition rates and/or lower deposition temperatures. There are also a lot of many derivatives of the CVD terminology, such as *metal-organic chemical vapour deposition* (MOCVD) or, less commonly, *organo-metallic chemical vapour deposition* (OMCVD), which are sometimes used to note the class of molecules used in deposition process. Some practitioners chose to differentiate epitaxial film deposition from polycrystalline or amorphous film deposition, so they introduced a variety of terms that include *epitaxy* in the acronym. Two of the more common variants are *organometallic vapour phase epitaxy (OMVPE)* and *metal-organic vapour phase epitaxy* (MOVPE) which are often used in the semiconductor compound epitaxy literature.

1.2.1 Main CVD process characteristics

CVD has a number of advantages as a method for depositing thin films. One of the primary advantages is that CVD films are generally quite conformal, i.e., the film thickness on the sidewalls of the features is compatible to the thickness on the top. This means that films can be applied to elaborately shape pieces, including the insides and undersides of the features, and that high aspect ratio holes and other features can be completely filled.

Another advantage of CVD is that, in addition to the wide variety of materials that can be deposited, the purity of the deposit itself is very high. This results from the relative ease with which impurities are removed from gaseous precursors using distillation techniques. Other advantages include relatively high deposition rates, and the fact that CVD often doesn't requires as a high vacuum as PVD processes.

On the other hand CVD process have some disadvantages. First of all the properties of the precursor: ideally it should be volatile at a near-room temperatures. This is a non-trivial problem for many elements of the periodic table, although the use of metal-organic precursors has eased this situation. CVD precursors can also be highly toxic

($Ni(CO_4)$),explosive (B_2H_6) or corrosive ($SiCl_4$). The byproducts of CVD reactions can also be hazardous (CO, H_2, HF). Some of the precursors, especially the organo-metallic ones, can be quite costly .

Another CVD issue is the high temperatures needed to deposit such high quality films because it clearly limits the number of substrates that could be coated. Further more, and more problematic, the high temperatures induce thermal stresses in the films if they have different thermal expansion coefficient with respect to their substrates. So a gross mechanical instability of the film may results from this process.

1.2.2 Thermal CVD

The CVD growth appears to be the most promising technique for large-scale production of mono- or few-layered graphene films. Although the formation of a “monolayer graphite” was mentioned in the early CVD studies on metal single crystals, the first successful synthesis of few-layered graphene films using CVD was reported in 2006 by Somani and co-workers using camphor as the precursor and Ni foils as the substrate [31]. This study opened up a new graphene synthesis route with several unsolved issues, like controlling the number of layers and minimizing monolayers folding. Since then many progresses have been made to obtain graphene layers on several types of metal substrates with controlled thickness. After a chemical etching of the metal substrate, the graphene layers detach and can be transferred to another substrate, providing high quality graphene layers without difficult mechanical or chemical treatments. The growth mechanism of graphene on substrates with high to mean carbon solubility (>0.1 atomic %), such as Co and Ni, proceed with the diffusion of the carbon into the metal thin film at the growth temperature and the subsequent precipitation of carbon out of the bulk metal straight to the surface upon cooling.

On the other hand, graphene growth on low Carbon solubility (<0.001 atomic %) substrates like Cu mainly happens on the surface through the four-steps process described by Li and co-workers [32]:

1. catalytic decomposition of hydrocarbon precursor on Cu to form C_xH_y;
2. formation of nuclei as a result of supersaturation of C_xH_y;

3. nuclei grow to form graphene islands on Cu surface saturated, or supersaturated with C_xH_y species;

4. full Cu surface coverage by graphene under certain temperature, hydrocarbon flow rate and partial pressure.

If the amount of available C_xH_y on the exposed Cu surface is insufficient to expand the C to the island edges, the Cu surface is only partially covered with graphene islands.

With the understanding of the graphene growth mechanism, various approaches were applied to control the graphene growth rate to obtain monolayered graphene.

The thermal CVD process is characterized by:

- the use of multiple polycrystalline substrates (Ni, Cu, Ir, Pt, Ru, Co) play the role of catalyst for growth
- the growth mechanism varies from metal to metal and depends on the structure and growth conditions
- the wet etching allows the transfer of graphene on other substrates
- the CVD seems to be one of the most promising growth mechanisms for the production of graphene on industrial scale

The sample that can be produced by CVD usually have very good electrical properties; often monolayers or at least bilayers are found by using thermal CVD; the time the process takes is small and it can be applied on a large (industrial) scale of production.

1.2.3 Industrial Applications of the CVD Process

CVD has applications across a wide range of industries such as:

- **coatings**: coatings for a variety of applications such as wear resistance, corrosion resistance, high temperature protection, erosion protection and combinations thereof;
- **semiconductors and related devices**: integrated circuits, sensors and optoelectronic devices;
- **dense structural parts**: CVD can be used to produce components that are

difficult or uneconomical to produce using conventional fabrication techniques. Dense parts produced via CVD are generally thin walled and maybe deposited onto a mandrel or former;

- **optical fibres**: for telecommunications;
- **composites**: performs can be infiltrated using CVD techniques to produce ceramic matrix composites such as carbon-carbon, carbon-silicon carbide and silicon carbide-silicon carbide composites. This process is sometimes called chemical vapour infiltration or CVI;
- **powder production**: production of novel powders and fibres;
- **catalyst;**
- **nanomachines.**

1.3 Electrodeposition

Electrodeposition is the application of metallic coatings to metallic or other conductive surfaces by electrochemical processes.

The workpiece to be plated is the cathode (negative terminal). The anode (positive terminal), can be one of the two types: sacrificial anode (dissolvable anode) and permanent anode (inert anode) [33]. The sacrificial anodes are made of the metal that is to be deposited. The permanent anodes can only complete the electrical circuit, but cannot provide a source of fresh metal to replace what has been removed from the solution by deposition at the cathode. Platinum and carbon are usually used as inert anodes.

The electrolyte is the electrical conductor in which current is carried by ions rather than by free electrons (as in a metal). Electrolyte completes an electric circuit between two electrodes. Upon application of electric current, the positive ions in the electrolyte will move toward the cathode and the negatively charged ions toward the anode. This migration of ions through the electrolyte constitute the electric current in that part of the circuit, while the migration of electrons into the anode through the wiring and an electric generator and then back to the cathode constitutes the current in the external circuit. The metallic ions of the salt in the electrolyte carry a positive charge and are thus attracted to the cathode. Since the cathode is attached to the negative pole of the

electric source, it supplies electrons to the electrolyte, and when ions reach the negatively charged work piece, it provides electrons to reduce those positively charged ions to metallic form. The metal atoms will thus be deposited onto the surface of the negatively charged work piece. On the contrary, the anode is connected to the positive pole of the electric source and therefore it accepts electrons from the electrolyte.

The rate at which the anode is dissolved is equal to the rate at which the cathode is plated, unless parasitic reactions take place at the electrodes. These mainly include hydrogen reduction from water, a reaction that is in competition with the metal deposition. In this manner, the ions in the electrolyte bath are continuously replenished by the anode.

Electroplating changes the chemical, physical, and mechanical properties of the workpiece. An example of a chemical change is when nickel plating improves corrosion resistance. An example of a physical change is a change in the outward appearance. An example of a mechanical change is a change in tensile strength or surface hardness which is a required attribute in tooling industry [34].

1.3.1 Electrodeposition Applications

Electrodeposition is used industrially for producing a dense, uniform, and adherent coating of pure metal or alloy upon a surface by the passage of an electric current. The coating produced is usually for decorative or protective purposes, or enhancing specific properties of the surface.
Electroplating products are widely used for many industries, such as auto-mobile, ship, airspace, machinery, electronics, jewellery, defence and toy industries.

Electroplating finds numerous applications as thin films and as three-dimensional, thick structures in microdevices. The properties of interest for both thick and thin films cover a broad range, including corrosion resistance, wear resistance, thermal, magnetic and optical characteristics. Applications include materials for printed-wiring boards, contacts, connectors, and magnetic recording.

High-resolution lithographic techniques has enabled electronic device integration, with electrodeposits several hundred microns thick. The importance of electrodeposition as a fabrication technology in the microelectronics industry is growing. For some of the fabrication processes involved, electrodeposition offers advantages over competing technologies such as physical and chemical vapour deposition, in that it requires simpler instrumentation and operating conditions.

With the trend toward miniaturization, electrodeposition has established itself as the manufacturing technology of choice. Electrodeposition also holds great promise to conformal deposit metals and alloys for microelectronic fabrication and HARMs (High Aspect Ratio Microdevices). Fabrication of high aspect ratio microstructures by electrodeposition is of increasing interest for a multitude of applications in microelectromechanical systems (MEMS).

Lithography comprises one step of the LIGA process. LIGA is the German abbreviation of the three major process steps, lithography (Lithographies), electroplating (*G*alvanoformung) and moulding (*A*bformung) [35]. The use of the LIGA process overcomes many drawbacks of other traditional fabrication methods and pattern transfer techniques such as chemical etching, sputter etching, reactive ion etching. Electrodeposition is an integral part of the LIGA process. It is employed after exposure and development of the resist and is used to build up a complementary pattern onto a metal substrate by filling the empty spaces of the electrically non-conductive resist starting from the electrically conducting base. The metal pattern produced in such a way can then be used as the microdevice itself or can serve as a mould for plastic replication.

Electrodeposited alloys and composites are of particular interest because of their unique and often superior properties compared with their metal counterparts. Often in alloy electrodeposition the deposition rate of the more noble metal is diffusion controlled. Therefore, the control of the deposit composition in the recess becomes a transient problem and complicates the electrodeposition behaviour.
Properties of electroplated composites such as wear resistance and hardness were found to be better. Particles in the nanometric range can extend the use of composites

for microdevice fabrication. Since microdevices are inherently on the order of micrometers then the composite material that these devices are created from must contain particles that are at least an order of magnitude smaller, nanometric. Even on unrecessed electrodes, few studies have confronted an alloy-composite system and the effect of particles on the metal deposition rate. None have been concerned with this issue in deep recess plating [36].

1.3.2 Electrical Relationships

Electrical Relations

In 1833, the English scientist Michael Faraday, developed Faraday's laws of electrolysis. Faraday's first law of electrolysis and Faraday's second law of electrolysis state that the amount of a material deposited on an electrode is proportional to the amount of electricity used.

- *Faraday's First Law of Electrolysis:* the mass of a substance altered at an electrode during electrolysis is directly proportional to the quantity of electricity transferred at that electrode. Quantity of electricity refers to the quantity of electrical charge, typically measured in coulomb.
- *Faraday's Second Law of Electrolysis:* for a given quantity of D.C. electricity (electric charge), the mass of an elemental material altered at an electrode is directly proportional to the element's equivalent weight.

Faraday's laws can be summarized by:

$$m=(\frac{Q}{F})\circ(\frac{M}{z})$$

where: m is the mass of the substance liberated at an electrode in grams

Q is the total electric charge passed through the substance

F = 96485 C mol^{-1} is the Faraday constant

M is the molar mass of the substance

z is the valency number of ions of the substance (electrons transferred per ion).

Note that M/z is the same as the equivalent weight of the substance altered.

For Faraday's first law, M, F, and z are constants, so that the larger the value of Q the larger m will be. For Faraday's second law, Q, F, and z are constants, so that the larger the value of M/z (equivalent weight), the larger m will be.

Current Efficiency

It is stated in Faraday's laws that the amount of chemical charge at an electrode is exactly proportional to the total quantity of electricity passing. However, if several reactions take place simultaneously at the electrode, side reactions may consume the product. Therefore, inefficiencies may arise from the side reactions other than the intended reaction taking place at the electrodes. Current efficiency is a fraction, usually expressed as a percentage, it indicates the ratio of the desired chemical change to the total chemical change multiplied by 100:

$$CE = 100 \circ \frac{Act}{Theo}$$

where: CE is current efficiency in percent

Act is the weight of metal deposited or dissolved

Theo is the corresponding weight expected from Faraday's laws

Cathode efficiency is current efficiency as applied to the cathode reaction, and anode efficiency is current efficiency as applied to the anode reaction.

Current Distribution

Except for the simplest geometries of a cell, such as when the anode and cathode are concentric, the current is not uniform over the surface of an electrode. In fact, the manner in which the current distributes itself over an electrode surface in any practical case is quite complicated, usually far too much so to be simply calculated from geometry. Current will tend to concentrate at edges and points, and unless the resistance of the solution is extremely low (lower than in any practical case), it will flow more readily to parts near the opposite electrode than to more distant parts. Thus, except for the simplest parts subject to electroplating, the thickness of deposit, which depends on the current density, will not be uniform over the surface.

1.3.3 Copper and Nickel Electroforming

Copper and Nickel are relatively easy metals to electroform via amperostatic deposition. Deposition baths electrochemistry is well know and the processes are well established in the surface engineering industry for both the chosen metals: no kind of solutions electrochemical characterization was needed in order to obtain 99.99% purity metal layers.
Electrolytic baths conditions data were gathered by Manuale di Trattamenti e Finiture hand book and were fixed as follows:

- Copper
    - current density 15 mA/cm^2;
    - PH 5;
    - room temperature;

- Nickel
    - current density 15 mA/cm^2;
    - PH 4,5;
    - temperature 65°C;

Experimental set – up was exactly that of a standard electrolytic cell; a EA – PSI 8065 – 05 T LCD current generator was employed, making it work in amperostatic conditions

and leaving at 60V the cells tensions in order to dampen the possible tension drops caused by the increase in electrical resistivity of the substrates while the metal layers were growing.
In order to obtain metals layers thick enough to be self-standing, the plating baths were left in the above mentioned conditions for 30 minutes.
It is possible to foresee the final metal substrate thickness by means of the analytic form of the Faraday laws:

$$m=(\frac{Q}{F})\circ(\frac{M}{z})$$

where:

- m is the mass of a substance liberated at an electrode in grams;
- Q is the total electric charge passed through the substance;
- F is the Faraday constant which is 96485 C/mol;
- M is the molar mass of the substance;
- z is the valency of ions of the substance

Alternatively the cited handbook can procure the value of millimetres, at a given current density, of the chosen metal that will be deposed in a given time [34,38.

1.3.4 Galvanic Displacement

Among electrochemical processes used to enable the plating of many different surfaces, there is a very important and widely used class of electrochemical phenomena which do not involve the use of an active circuit to feed the electrochemical cell with electrons.
They are known as electroless deposition techniques and are defined as the deposition of a metallic coating on a substrate without the use of an external voltage or current.
They are commonly referred to as chemical rather than electrochemical methods in order to emphasize the absence of an external power supply, even if their mechanisms can be explained by taking account of their electrochemical red – ox potential.

Among the electroless plating processes, a distinction can be made between autocatalytic method and *galvanic displacement* methods. The autocatalytic method is an electroless process in which the reduction of the metallic ions in solution and film deposition can be carried out through the oxidation of a chemical compound present in the solution itself, namely, of a reducing agent. This reducing compound, under a defined temperature which depends on the reducing agent itself and on the bath's composition, spontaneously oxidises, freeing electrons for the reduction of the metallic ions. It is properly named autocatalytic, because the oxidation of the reducing agent can start or become self-sustained only at the depositing metal surface. This is the reason why for some non-catalytic base materials, the activation of the deposition with catalytic metals such as palladium is required. In this work the main processes implemented in the preparation route of the samples are the Nickel deposition from Hypophosphite based solution (used in microelectronics) and the elctroless copper process for the deposition of the first thick conductive layer for copper interconnects in integrated circuits (IC).
In comparison to electrodeposition, autocatalytic deposition avoids current distribution, improves thickness uniformity and allows film deposition with a thickness that mainly depends on the deposition time. Complexing agents and stabilizers can be added to the solution in order to avoid the reduction and precipitation of metallic powders in the bulk solution.

Galvanic displacement or immersion plating (sometimes also called cementation) on a substrate takes palace when the base material is displaced by a metallic ion solution that has a lower oxidation potential than the displaced metal ion. The base material is dissolved into the solution; meanwhile the metallic ions in the solution are reduced on the surface of the base material. Such a mechanism differs completely from autocatalytic deposition because, in immersion plating, reducing agents are not required to reduce the metal ions to metal, as the base material behaves as the reducing agent.

Galvanic displacement deposition processes are widely used, since they yield high value finishes on a variety of metals. The following characteristics of the galvanic displacement process can be pointed out:

- the thickness of the deposited film obtained by immersion plating is limited (typically, in the range of hundreds of nanometers), because the deposition stops when the entire surface of the metal is coated. As a consequence of such complete coverage and dense morphology of the film, the source of reducing agent is hindered;
- reaction rate increases with the increased temperature;
- stirring is sometimes beneficial to the characteristics of the coating, by improving uniformity and reducing surface roughness;
- immersion reaction rates are not easily controllable, due to the fast exchange of charges between oxidizing and reducing species. Due to the nature of the displacement process, the deposition occurs by downward growth. The surface of the coating reproduces almost exactly that of the base material, both in contour and in a location, avoiding current distributions issues and the absence of electrical connections among areas of the substrate.

Immersion plating allows deposition on difficult surfaces, such as the inside vias, and on surfaces that are not in the line of sight, or in cases where it is difficult to make electrical connections to isolated areas of the base materials.
Clearly it is possible to extend this process to non conductive surfaces, thanks to the intrinsic chemical-only nature of the displacement phenomenon.
A natural consequence of this possibility, galvanic displacement has been widely used in the semiconductor industry, in order to produce compact and homogeneous metallic layers on top of semiconductor material, one above all, Silicon.
Galvanic displacement on Silicon from solutions containing HF is a red – ox reaction in which both anodic and cathodic processes occur simultaneously at the Si surface while the charge may be exchanged through the substrate. Fluoride ions in solution help sustain the reaction by dissolving the silicon substrate as silicon hexafluoride, avoiding the formation of silicon oxide, thus exposing new silicon surface.

As commonly reported the global chemical reaction of the red – ox couple is:

$$M^{n+}(aq) + Si^{0}(s) + 6F^{-}(aq) = M^{0}(s) + SiF_{6}^{2-}(aq)$$

where “aq” and “s” indicate the aqueous and solid phases, respectively. The above

reaction can be divided in two half-cell processes:

$$M^{n}+(aq)+n\,e^{meno}=M^{0}(s)$$

$$SiF_{6}^{2minus}(aq)+4\,e^{minus}=Si^{0}(s)+6\,F^{minus}(aq)$$

$$E^{0}(Si^{4\,plus}/Si^{0})=-1.20\,V_{SHE}$$

Silicon is dissolved in solution as silicon hexafluoride, while the metal is deposited from solution with a deposition rate related to the concentration of HF in the solution.
Usually, the silicon surface shows an increase in surface roughness, particularly at the region close to the metal deposit, and sometime pitting is observed. The oxidation of silicon followed by the galvanic displacement of the metal ions in solution is believed to initiate defects on the surface such as kinks, steps, contaminated sites, or areas chemically more reactive than H-terminated regions. As such, the deposition rates can be enhanced by increasing the density of surface defects (for example by Ar ions bombardment). Doping of the silicon substrate can affect the deposition mechanism, due to the transfer of the charged carriers through the substrate during displacement.
Galvanic displacement is thermodynamically more favourable for metals with higher red – ox potential values, for example is better for gold or palladium than for copper or nickel. The efficiency of the metal deposition on the silicon surface is expected to vary according to the composition and the pH of the solution. In addition, the presence of the first metallic nuclei on top of the silicon surface can modify the dissolution mechanism and catalytically enhance the evolution of hydrogen [].

1.4 MEMS

Micro-Electro-mechanical systems are typically defined as microscopic devices designed, processed, and used to interact or produce changes within a local environment. A mechanical, electrical or chemical stimulus can be used to create a mechanical, electrical or chemical response in a local environment. These smaller, more sophisticated devices that act, sense, and communicate are replacing their bulk counterparts in many traditional applications.

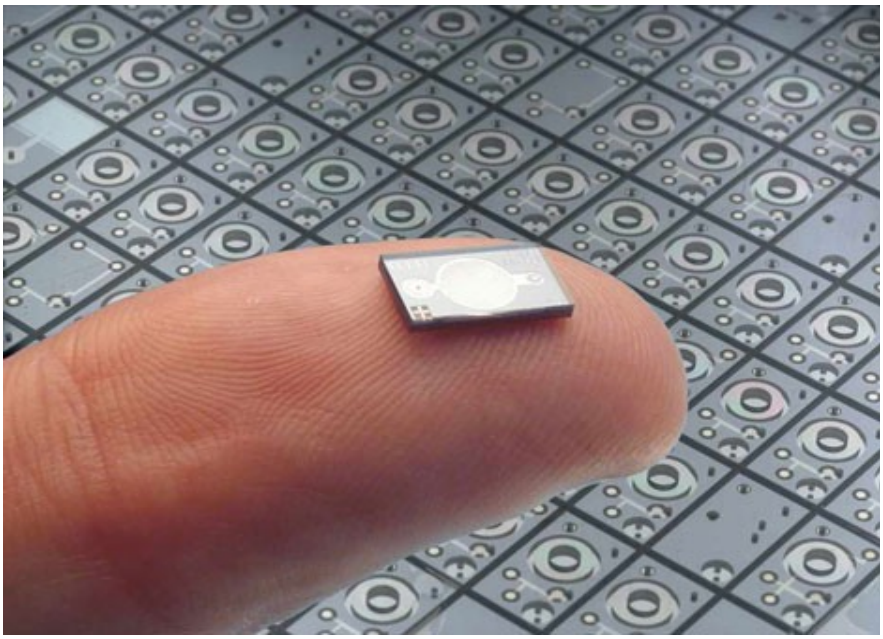

Fig. 1.10: MEMS dimensions

Micro-Electro-Mechanical systems (MEMS) technology is the integration of mechanical elcentimetressors, actuators, and electronics on a common silicon substrate through microfabrication technology. These devices replace bulky actuators and sensors with micron scale equivalent that can be produced in large quantities by fabrication process used in integrated circuits in photolitography. They reduce cost, bulk, weight and power consumption while increasing performances, production volume and functionality by orders of magnitude [38].

As a general rule of thumb, MEMS typically have dimensions ranging from nanometers to centimetres; however, very little has been done with MEMS below one micrometer. On the contrary, recent developments in IC technologies can now mass produce chips with features as small as 0.13 microns.
They usually consist of a central unit that processes data (the microprocessor) and several components that interact with the surroundings such as microsensors. At these size scales, the standard construct of classical physics are not always useful. Because of the large surface area-to-volume ratio of MEMS surface effects such as electrostatic sand wetting dominate over volume effects such as inertia and thermal mass.

1.4.1 Components of MEMS

MEMS components are categorized in one of the six distinct applications. These include:

- **sensors** are a class of MEMS that are designed to sense changes and interact with their environment. These classes of MEMS include chemical, motion, inertia, thermal and optical sensors;
- **actuators** are a group of devices designed to provide power or stimulus to other components or MEMS devices. In MEMS, actuators are either electrostatically or thermally driven;
- **RF MEMS** are a class of devices used to switch or transmit high frequency, RF signals. Typical devices include metal contact switches, shunt switches, tunable capacitors, antennas, etc.;
- **optical MEMS** are devices designed to direct, deflect, filter, and/or amplify light. These components include optical switches and reflectors;
- **microfluidic MEMS** are devices designed to interact with fluid-based environments. Devices such as pumps and valves have been designed to move, eject, and mix small volumes of fluid;
- **bio MEMS** are devices that, much like microfluidic MEMS are designed to interact specifically with biological samples. Devices such as these are designed to interact with proteins, biological cells, medical reagents, etc. and can be used for drug delivery or other in-situ medical analysis [39].

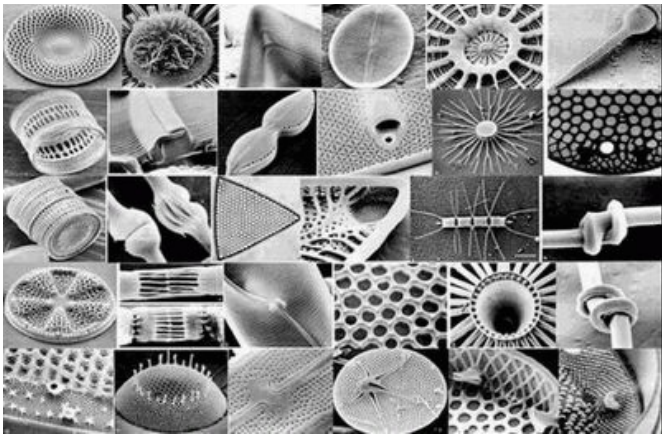

Fig. 1.11: MEMS plethora

1.4.2 MEMS Applications

Sensors

Sensors based on MEMS technology have a wide range of applications. Applications range from motion and inertial sensors to chemical and biological sensors. MEMS technology is particularly well suited to this arena where traditional technology may fail. This may be due to surrounding environments, system level limitations, or design/size constrains. One commercial success using MEMS technology involves the application of MEMS as a sensor for automobile airbag deployment systems. In this application, an accelerometer was designed and fabricated to sense rapid changes in acceleration to deploy an airbag. The MEMS device is surrounded by CMOS technology to process the output signals sensed from the accelerometer. Other devices have been fabricated to sense motion along both the x and the y axis. Over 100 million airbag sensors have been sold over the past ten years, putting MEMS-based sensors solidly in the commercial marketplace.

Efforts are currently under wary to design and fabricate high sensitivity 3-axis (x, y, z) gyroscopes. The use of MEMS technology enable gyros to be smaller, more accurate, more reliable and more economical than their bulk counterparts, while exhibiting excellent resistance to both shock and vibrations. Potential application of these devices include automotive safety, commercial avionics and industrial equipment [40].

Other sensors applications include air quality and trace chemical analysis. One example is the combustible gas sensor developed at Sandia Laboratories; it consists of a conductive filament, coated with a catalytic layer, that is heated by electrical current. Micromachining technology allows the filament to be made very small and suspended above the substrate for thermal isolation, resulting in low-power operation. Combustible gas react on the catalytic surface, releasing heat that changes filament resistance. This device is proposed for use in exhaust gas analysis to indicate combustible gas hazards.

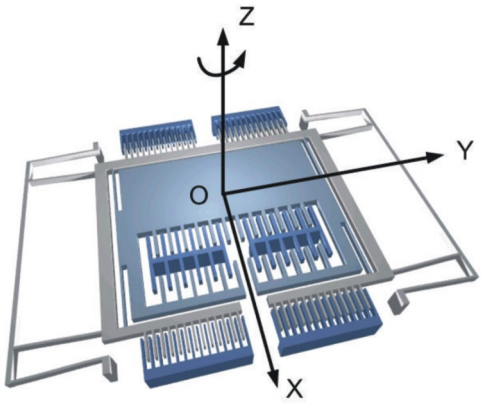

Fig. 1.12: MEMS gyroscope schematics

Actuators

Actuators are a family of MEMS components designed to produce motion or provide driving force for moving other MEMS fabricated components. Actuators are powered using an electronic-based signal. The drive signal can be in any waveform (square, sine, sawtooth, etc.) to produce motion. Two types of actuators, electrostatic and thermal, have been used to enable motion in various MEMS components.

Electrostatic actuators operate using an applied electric field between fixed and movable structures. One structure is fixed to the substrate and biased producing electric fields along the edges of the structure itself. The fixed components are typically the only biased structures in the device. This structure is typically a multi-fingered component where electric fields are present along the comb fingers.

The movable components of an electrostatic actuator is typically a multi-fingered component to create an inter-digitated comb-like structure. The movable comb fingers are attracted to the powered ones via the electric field fringes, pulling them towards the biased components. Restoring springs are fabricated with the comb fingers to provide the required restoring force to bring the movable comb fingers back to their original position. Linear motion can be translated into rotational or out-of-plane motion by coupling linear actuators [41].
Most MEMS devices operate by using some form of electrostatic actuation.

Thermal actuators operate using current in elongated structure fabricated slightly off-axis [42]. The off-axis fabrication creates the direction for thermal actuators to move. When current passes through the horizontal arms of the thermal actuator, the arms heat and expand causing displacement, (or throw) in its designed direction. This result in a linear output. One potential application for actuators may be in the hard drive/memory market.

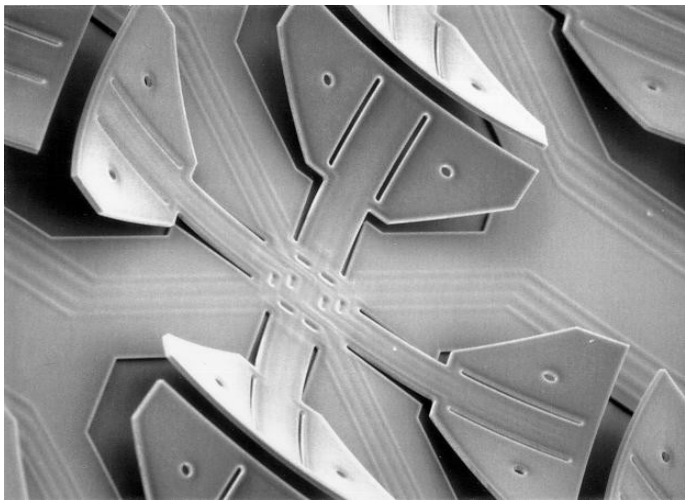

Fig. 1.13: MEMS thermal actuator

RF MEMS

RF MEMS are becoming recognized as an excellent alternative to existing solid-state RF technologies. Although the field of RF MEMS is relatively new, results have shown that performance enhancements and manufacturing costs reduction make this technology a viable competitor with large-scale and solid-state counterparts [43].
In many cases, RF MEMS components can function as well as an equivalent solid-state circuit (depend upon its application). Research is currently under wary to develop and commercialize RF products such as switches, tunable capacitors, high-Q inductors, high-Q mechanical resonators and filters, as well as microwave and millimeter-wave components. Industries may apply this technology to satellite and military communications, navigation, sensors, and avionics.

Current state-of-the-art RF circuits use a combination of gallium arsenide FETs, PIN diodes and/or varactor diodes to achieve required tuning, filtering and/or switching

functions. These devices typically require high power consumption, are expensive to fabricate and have limited reliability. In some instances, poor RF performance (such as high insertion loss per switching cycle) serves as the impetus driving RF MEMS production.

As has been discussed, several commercial and government applications exist for RF MEMS capabilities. Very few RF MEMS components are commercially available due to the relative infancy of the field, technological hurdles and reliability issues that must be overcome for successful implementation. One area of research is the RF signal switching arena. Two types of switches have been developed for this application. These include the metal-contact series switch and a shunt switch. Metal-contact series switches offer the ability to switch both AC and DC signals through metal-to-metal contact. Shunt switches allows AC switching through a thin dielectric and eliminate metallurgical contact issues caused by hot and cold switching, but have limited bandwidth.

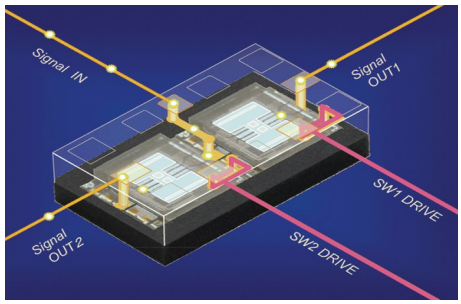

Fig. 1.14: RF MEMS schematics

Optical MEMS

Optical MEMS is a unique application where MEMS are used to direct, guide, filter, and in some stances, amplify light. Well known application of optical MEMS include optical switching and digital protection.

In optical switching application, micromirrors are used to steer light from an incoming fibre optic input to a fibre optic output. Many different types of MEMS micromirrors have been designed and fabricated. The function of the mirrors are divided into 3 categories: 1-d, 2-d and 3-d configurations. These configuration correspond to the degrees of motion of micromirror operation. The 1-d configuration allows the micromirror to control reflected light by tilting about a single axis, typically parallel to the plane of the micromirror array. The 2-d configuration allows tilting of the micromirror along the orthogonal positions parallel to the plane of the micromirror array. The 3-d architectures steer light along orthogonal positions parallel to and perpendicular to the plane of the micromirror array. By rerouting optical signal directly, MEMS technology enables maintaining signal fidelity and continuity by creating an all-optical switching network. This technology may potentially replace existing electronics used for re-routing optical signals though an opto-electronic-opto conversion [44,45]. arrays of micromirrors have been fabricated and tested at 3x3, and 256x256 array sizes. Note that the size of each micromirror is smaller than the eye of a pin.

Other applications of optical MEMS include digital light projection systems for displays. Commercially available MEMS components such as the Digital Mirror Device (DMD™) fabricated by Texas Instruments improve image quality and resolution. Televisions, home theatre systems, and business projectors using DLP™ (Digital Light Projection) technology rely on a single DMD™ chip configuration for light projection. DLP™ technology enabled projectors for very high image quality or high.
brightness applications such as cinema and large venue displays rely on a 3-DMD-chip configuration to produce static and dynamic images [46].

Fig 1.15: MEMS micromirror

Microfluidic MEMS

Microfluidic MEMS are devices that transport, dispense, combine and/or separate fluids at the microscopic level. Industries are now beginning to realize the potential of MEMS-based microfluidic ejection, transport, delivery and detection system. Applying MEMS in fluidic-based applications reduces the amount of fluid used, reduces waste and can be processed in serial or parallel (multiple devices).

Typical application for microfluidic MEMS include valves, pumps and ink jet delivery systems[47,48], MEMS are used to increase printing resolution (increased DPI) and reduce ink consumption, resulting in longer lifetimes of the ink cartridge. By increasing the density of ejection devices (using MEMS), and reducing droplet size, more ink drops can fit into a given area, this must increase DPI.

Other potential applications for microfluidic MEMS include water sampling detection, in situ/non-invasive fluidic testing, etc. Multiple devices can be placed in strategic regions of water supplies of other fluidic systems to monitor toxicity and contaminant levels.

Bio MEMS

Like microfluidic MEMS, bio MEMS are designed to transport, combine and/or separate fluids at the microscopic level. One pertinent difference between these two devices is the ability to manipulate biological material contained within the fluid or manipulate biological fluid itself. Applications of biomedical MEMS such as microdialysis [49],

biosensors [50] and laboratory analysis on chip [51] are areas currently under research and development. Companies such as Molecular Devices [51] and i-Stat [51] have produced microphysiometers [52] and chemical laboratory analysis methods at the microscopic scale.

Some benefits of microscale fluidic technology for medical applications include reduced fluid consumption, reduced waste products, decreased reaction times and improved parallel chemical processing capability. The promise of packaging a variety of diagnostically relevant, otherwise expensive tests into a tiny amount of microfabricated real estate would represent a major advancement for many clinical situations [51].

Employing MEMS components for biological fluid analysis not only enables the benefits of a microfluidic component, but other mechanical can be used to manipulate biological material, such as blood cells contained within the biological fluid.

Fig. 1.16: MEMS lab - on - chip

1.4.3 Silicon as Mechanical Material

Any consideration of mechanical material devices made from silicon must certainly take into account the mechanical behaviour and properties of single-crystal silicon (SCS). Although SCS is a brittle material, yielding catastrophically rather than deforming

plastically, it certainly is not fragile as is often believed. The Young's modulus of silicon (27E6 psi), for example, has a value approaching that of stainless steel, nickel, as well above that of quartz and most other borosilicate, soda-lime, and lead-alkalisilicate glasses. The knoop hardness of silicon (850) is close to quartz, just below chromium (935), and almost twice as high as nickel (557), iron and most common glasses (530).
Silicon single crystals have a tensile yield strength (10E6 psi) which is 3 times higher than stainless-steel wire. In practice, tensile stresses *routinely encountered* in seed crystal during the growth of large SCS boules, for example, can be over 18000 psi.
The primary difference is that silicone will yield by fracturing (at room temperature) while metals usually yield by deforming inelastically.
Despite this quantitative evidence, we might have trouble intuitively justifying the conclusion that silicon is a strong mechanical material when compared with everyday laboratory and manufacturing experience.
Wafers do break sometimes without apparent provocation; silicon wafers and parts of wafers may also easily chip. These occurrences are due to several factors which have contributed to the misconception that silicon is mechanically fragile. First, single-crystal silicon is normally obtained in large (5-13 cm diameter) wafers, typically only 10-20 mils (250-500 μm) thick. Even stainless steel of these dimensions is very easy to deform inelastically. Silicon chips with dimensions of the order of 6.0 cm x 0.6 cm, on the other hand, are relatively rugged under normal handling conditions unless scribed. Second, as a single-crystal material, silicon has a tendency to cleave along crystallographic planes, especially if edge, surface, or bulk imperfections cause stresses to concentrate and orient along cleavage planes. Slip lines and other flaws at the edge of the wafer, in fact, are usually responsible for wafer breakage. In recent years, however, the semiconductor industry has attacked this yield problem by contouring the edges of waters and by regularly using water edge inspection instruments, specifically designed to detect mechanical damage of wafer edges and also to assure that edges are properly contoured to avoid the effects of stress concentration. As a result of these quality control improvements, wafer breakage has been greatly reduced and the intrinsic strength of silicon is closer to being realized in practice during wafers handling. Third, chipping is also a potential problem with brittle materials such as SCS. On whole wafers, chipping occurs for the same qualitative reasons as breaking and the solution is identical. Individual die, however, are subject to chipping as a result of saw- or scribe-induced edge damage and defects. In extreme cases, or during rough handling, such damage

can also cause breakage of or cracks in individual die. Finally, the high-temperature processing and multiple thin-film depositions commonly encountered in the fabrication of IC devices unavoidably result in internal stresses which, when coupled edge, surface, or bulk imperfections, can cause concentrated stresses and eventual fracture along cleavage planes.

These factors make it clear that although high-quality SCS is intrinsically strong, the apparent strength of a particular mechanical component or device will depend on its crystallographic orientation and geometry, the number and size of surface, edge, and bulk imperfections, and the stresses induced and accumulated during growth, polishing, and subsequent processing. When these considerations have been properly accounted for, we can hope to obtain mechanical components with strengths exceeding that of the highest strength alloy steels.

One excellent example of the unique qualities of silicon in the realization of high reliability mechanical components can be found in the analysis of mechanical fatigue in SCS structures. Since the initiation of fatigue cracks occurs almost exclusively at the surface of stressed members, the rate of fatigue depends strongly on surface preparation, morphology and defect density. In particular, structural components with highly polished surface have higher fatigue strengths than those with rough surfaces. Passivated surfaces of polycrystalline metal alloys (to prevent intergrain diffusion of H_2O) exhibit higher fatigue strengths than unpassivated surfaces, and, for the same reasons, high water vapour content in the atmosphere during fatigue testing will significantly decrease fatigue strength. The mechanism of fatigue, as these effects illustrate, are ultimately dependent on a surface-defect-initiation process. In polycrystalline materials, these surface defects can be inclusions, grain boundaries, or surface irregularities which concentrate local stresses.

It is clear that the high crystalline perfection of SCS together with the extreme smoothness and surface perfection attainable by chemical etching of silicon yields mechanical structures with intrinsically high strength [52].

Fig. 1.17: Silicon monocrystals

1.4.4 Microfabrication

Microfabrication is the process of fabrication of miniature structures of micrometre scales and smaller. Historically, the earliest microfabrication processes were used for integrated circuits fabrication, also known as "semiconductor manufacturing" or "semiconductor device fabrication".

Miniaturization of various devices presents challenges in many areas of science and engineering: physics, chemistry, material science, computer science, ultra-precision engineering, fabrication processes, and equipment design. It is also giving rise to various kinds of interdisciplinary research [53]. The major concepts and principles of microfabrication are microlithography, doping, thin films, etching, bonding, and polishing.

Traditional machining techniques such as *electro-discharge machining*, *spark erosion machining*, and *laser drilling* have been scaled from the millimetre size range to micrometer range, but they do not share the main idea of microelectronics-originated microfabrication: replication and parallel fabrication of hundreds or millions of identical structures. This parallelism is present in various imprint, casting and moulding techniques which have successfully been applied in the micro regime. For example, injection moulding of DVDs involves fabrication of submicrometer-sized spots on the disc.

To fabricate a microdevice, many processes must be performed, one after the other, many times repeatedly. These processes typically include depositing a film, patterning the film with the desired micro features, and removing (or etching) portions of the film. Thin film metrology is used typically during each of these individual process steps, to ensure the film structure has the desired characteristics in terms of thickness (t),refractive index (n) and extinction coefficient (k), for suitable device behaviour.

Here's an overview about the basics of lithography technique and, in particular, the photolithography; this is not the only way to manufacture MEMS components but is surely the most common process implemented in a *top-down* fabrication approach.

In this process, a pattern is transferred to a photosensitive polymer (a photoresist) by exposure to a light source through an optical mask. An optical mask usually consists of opaque patterns (usually chrome or iron oxide) on a transparent support (usually quartz) used to define features on a wafer.
The pattern in the photoresist is then further transferred to the underlying substrate by subtractive (etching) or additive (deposition) techniques. The combination of accurate alignment of a successive set of photomasks and exposure of these successive patterns leads to complex multilayered structures. Photolithography has matured rapidly by continuous improvements in the ability to resolve ever-smaller features. Research in high-aspect-ratio resist features, driven by the field of Micro-Electro-Mechanical systems, is also being actively pursued, as opposed to the essentially two-dimensional processes used traditionally. This is especially important in the fabrication of microfluidic moulds.
Photolithography and pattern transfer involve a set of process steps, as is described below.

As an example, we use an oxidized silicon (Si) wafer and a negative photoresist to transfer a pattern from a mask to a layer of silicon dioxide. An oxidized wafer is coated with a 1-μm-thick negative photoresist layer. After exposure, the wafer is rinsed in a developing solution or sprayed with a spray developer, which removes the unexposed areas of photoresist and leaves a pattern of bare and photoresist coated oxide on the wafer surface. The resulting photoresist pattern is the negative image of the pattern on the photomask.

In a typical next step after development, the wafer is placed in a solution of HF or a mixture of HF and NH4F that attacks the oxide at a much faster rate than the photoresist or the underlying Si. The photoresist prevents the oxide underneath from being attacked. Once the exposed oxide has been etched away, the remaining photoresist can be stripped off with a solution that only attacks the photoresist, such as a strong acid (e.g., H2SO4) or an acid-oxidant combination (e.g., piranha, H2SO4:H2O2). Other liquid strippers include organic solvent strippers and alkaline strippers (with or without oxidants). The oxidized Si wafer with etched windows in the oxide now awaits further processing. Recently, photoresists are increasingly being used in applications in which the resist is a permanent part of the final device rather than just a sacrificial layer for patterning the substrate.

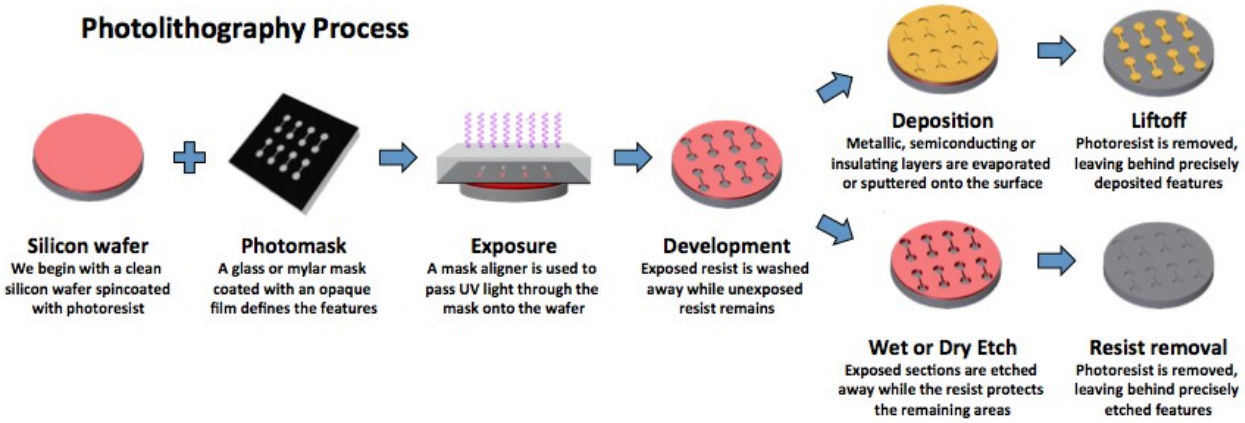

Fig. 1.18: photolithography process flow

Preparation of Wafer

Cleaning of Wafer. Physical contaminants such as dust particles can hinder the lithography process by preventing light from exposing the photoresist or by disturbing the surface uniformity of a coated photoresist. Chemical contaminants may also react with various materials used in the lithography process, creating unwanted effects. A silicon wafer is the most commonly used platform for microfabrication, but there is a trend toward different substrate materials, especially in the field of BioMEMS. A variety of cleaning methods can be used to prepare a wafer for the lithography process.

Usually, new wafers do not need further cleaning, because they are cleaned before shipping and are kept in a contamination-free container. If cleaning of the wafer is necessary, a variety of methods (HF dip, RCA1, RCA2, use of piranha, and so on) can be used to remove different types of contaminants. The presence of water or water vapour compromises the adhesion between the photoresist and the wafer. Before the photoresist is applied, a dehydration bake is performed to remove water from the surface of the wafer. Adhesion can be further promoted by applying an adhesion promoter (hexamethyldisilizane) or by roughening the surface of the wafer by plasma etching. This is referred to as wafer priming.

Oxide growth. In many cases, an oxide layer is desired as a mask for subsequent processes (e.g., an etch or an implant process) or as an insulating layer. This is usually achieved by heating a silicon wafer to between 900 and 1150°C in a dry or humidified oxygen stream in a tube furnace.

Resist Spinning and Soft Bake

As the first step in the lithography process itself, a thin layer of an organic polymer, a photoresist sensitive to ultraviolet (UV) radiation, is deposited on the oxide surface. The liquid photoresist is dispensed onto a wafer that is held by a vacuum chuck in a resist spinner. The wafer is then spun in one or more steps at precisely controlled speeds. The spin speed (between 1500 and 8000 rpm) allows the formation of a uniform film. At these speeds, the centrifugal force causes the liquid to flow to the edges, where it builds up until expelled when the surface tension is exceeded. The resulting polymer thickness, *t*, is a function of spin speed, solution concentration, and molecular weight (measured by intrinsic viscosity). The spin curves for various photoresists can be obtained from the manufacturer.

The spinning process is of primary importance to the effectiveness of pattern transfer. The quality of the resist coating determines the density of defects transferred to the device under construction. After spin coating, the resist still contains up to 15% solvent and may contain built-in stresses. The wafers are therefore soft baked (prebaked) at 75–100°C to remove solvents and stress, and to promote adhesion of the resist layer to the wafer.

Exposure and Postexposure Treatment

Pattern transfer onto a photoresist is done by shining light through the mask. One typically uses the g-line (435 nm) or i-line (365 nm) of a mercury lamp. In general, the smallest feature that can be printed using projection lithography is roughly equal to the wavelength of the exposure source. The action of light on a photoresist either increases or decreases the resist solubility depending on whether it is a positive or negative photoresist, respectively. Thus, for a positive-tone photoresist, the opaque pattern on the mask will determine the features remaining in the resist layer after development. Conversely, after development of a negative photoresist, the clear pattern of the mask determines the remaining photoresist features. The profile of the photoresist side walls is critical to many applications such as patterning of hard-to-etch metals (lift-off) and mould fabrication. The resist wall profile can be controlled by adjusting resist tone, exposure dose, developer strength, and development time, as well as by other means.

Post-exposure treatment is often desired because the reactions initiated during exposure might not have run to completion. To halt the reactions or to induce new ones, several post-exposure treatments can be used: postexposure baking, flood exposure with other types of radiation, treatment with reactive gas, and vacuum treatment.

Development, Descumming, and Postbaking

During the development process, selective dissolving of resist takes place. Development can be done using a liquid (wet development), a gas, or plasma (dry development). Positive resists are typically developed in aqueous alkaline solutions (e.g., tetramethyl ammonium hydroxide), and negative resists in organic solvents.
Unwanted residual photoresist sometimes remains after development. Descumming is a procedure for removing this unwanted photoresist with a mild plasma treatment. In this process, highly energetic oxygen ions react and essentially burn away the unwanted photoresist. Postbaking or hard baking removes residual solvents and anneals the film to promote interfacial adhesion of the resist that has been weakened either by developer penetration along the resist/substrate interface or by swelling of the resist (mainly for negative resists). Hard baking also improves the hardness of the film. Improved hardness increases the resistance of the resist to subsequent etching and

deposition steps. Postbaking is usually done at higher temperatures (120°C) and for longer times (e.g., 20 min) than soft baking or prebaking.

Pattern Transfer

In cases in which the photoresist is a permanent part of the final device (e.g., microfluidics, carbon MEMS [C-MEMS]), further processing may not be necessary. In most other cases, the sacrificial photoresist pattern is used as a mask for etching (subtractive) or deposition (additive) on the underlying substrate (a subtractive process). In a subtractive process, the resist acts as a protective barrier to the etching agent, which can be a liquid solution, a gas, or plasma. After pattern transfer, the resist can be removed for further process steps. Similarly, pattern transfer can involve a deposition technique: chemical vapour deposition or e-beam evaporation.

CHAPTER 2:

Experimental Methods

Here the experimental set – up used during practical work is presented and examined.

In the fist part of the project amperostatic equipment has been employed, in order to electroform Nickel and Copper substrate; in the second section standard laboratory equipment has been used to set up a galvanic displacement process onto flat and microstructured silicon wafers.
In the final part chemical vapour deposition was needed to obtain graphene sheets on top of the substrates, by means of a tubular furnace.

In order to investigate samples features during all the steps, several characterization techniques was performed:

- X-rays fluorescence;
- X-rays diffraction;
- optical microscope;
- glow discharge optical emission spectroscopy;
- scanning electrons microscopy;
- atomic force microscope;
- Raman spectroscopy.

2.1 Chemicals and Deposition Processes

2.1.1 Electroforming

Both Nickel and Copper electroforming solutions were made available by TECNOCHIMICA and used as received. Solutions volume was kept at 150 ml; silica beakers were used and no magnetic stirring was necessary.

The processes were carried out using a 15 mA/cm^2 current density for both metals. The forming areas were 2 by 1 cm rectangles, marked by means of Capton ®.

Electroforming mandrel was a stainless steel AISI 316 plate, cleaned in 65% nitric acid aqueous solution.

Counter electrodes were, respectively, Nickel rack and 99% pure Copper plate. Amperostatic deposition was carried out by using a EA – PSI 8065 – 05 T LCD, with 0 to 60V tension scale and 0 to 5 A current scale; the maximum instrument output power was 325W.

2.1.2 Galvanic Displacement

The Nickel displacement solution was prepared by dissolving Nickel(II) Sulphate Hexahydrate and ammonium fluoride into a high density polyethylene beaker. Solution volume was generally kept at 100 ml by adding deionized water and no magnetic stirring was necessary.

The Copper displacement solution was prepared by dissolving Copper(II) Sulpahte pentahydrate, ammonium fluoride, methanol, Sodium – Magnesium Tartate and Ascorbic Acid in the end. As for Nickel, high density polyethylene beakers were employed but magnetic stirring was necessary here. Solution volume was kept at 100 ml by adding small amounts of deionized water.

The substrates to cover were 2 by 1 cm^2 pieces of a monocrystalline silicon wafer, supplied by ST Microelectronics; the silicon shards were cleaned using acetone and etched using hydrofluoric acid.

All the chemical were made available by CARLO ERBA and used as received.

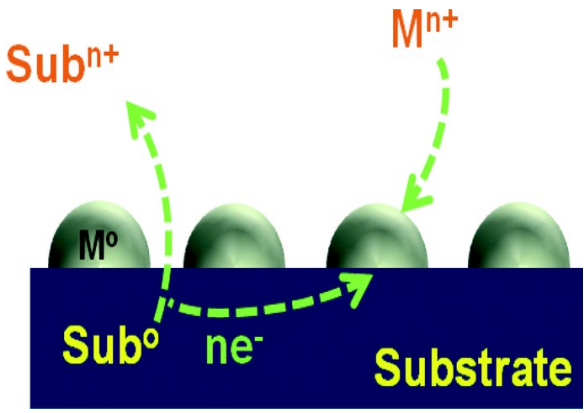

Fig. 2.1: Galvanic displacement process schematics

2.2 Analysis and Characterization

2.2.1 Optical Microscope

The optical microscope, often referred to as the "light microscope", is a type of microscope which uses visible light and a system of lenses to magnify images of small samples. Optical microscopes are the oldest design of microscope and were possibly invented in their present compound form in the 17th century. Basic optical microscopes can be very simple, although there are many complex designs which aim to improve resolution and sample contrast. The image from an optical microscope can be captured by normal light-sensitive cameras to generate a micrograph. Originally images were captured by photographic film but modern developments in CMOS and charge-coupled device (CCD) cameras allow the capture of digital images. Purely digital microscopes are now available which use a CCD camera to examine a sample, showing the resulting image directly on a computer screen without the need for eyepieces.

There are two basic configurations of the conventional optical microscope: the simple microscope and the compound microscope. The vast majority of modern research microscopes are compound microscopes while some cheaper commercial digital microscopes are simple single lens microscopes. A magnifying glass is, in essence, a single lens simple microscope. In general, microscope optics are static; to focus at different focal depths the lens to sample distance is adjusted, and to get a wider or narrower field of view a different magnification objective lens must be used. Most modern research microscopes also have a separate set of optics for illuminating the sample.

All modern optical microscopes designed for viewing samples by transmitted light share the same basic components of the light path. In addition, the vast majority of microscopes have the same structural components. For this project a LEICA DMLM was available.

Fig. 2.2: LEICA DMLM optical microscope

2.2.2 X-rays Fluorescence

X-ray fluorescence (XRF) is the emission of characteristic "secondary" (or fluorescent) X-rays from a material that has been excited by bombarding with high-energy X-rays. The phenomenon is widely used for elemental analysis and chemical analysis. When materials are exposed to short-wavelength X-ray, ionization of their component atoms may take place. Ionization consists of the ejection of one or more electrons from the atom, and may occur if the atom is exposed to radiation with an energy greater than its ionization potential. X-rays can be energetic enough to expel tightly held electrons from the inner orbitals of the atom. The removal of an electron in this way makes the electronic structure of the atom unstable, and electrons in higher orbitals "fall" into the

lower orbital to fill the hole left behind. In falling, energy is released in the form of a photon, the energy of which is equal to the energy difference of the two orbitals involved. Thus, the material emits radiation, which has energy characteristic of the atoms present. The term fluorescence is applied to phenomena in which the absorption of radiation of a specific energy results in the re-emission of radiation of a different energy (generally lower). The radiation emitted from the deposit is proportional to the deposit thickness. The system maybe calibrated with a known thickness and composition standard for additional accuracy. XRF is a nondestructive method and can be adapted to work for many different plating applications. The instrument used for the analysis of the elemental composition and thickness of the alloy electroplated was a FISCHERSCOPE X-RAY XAN.

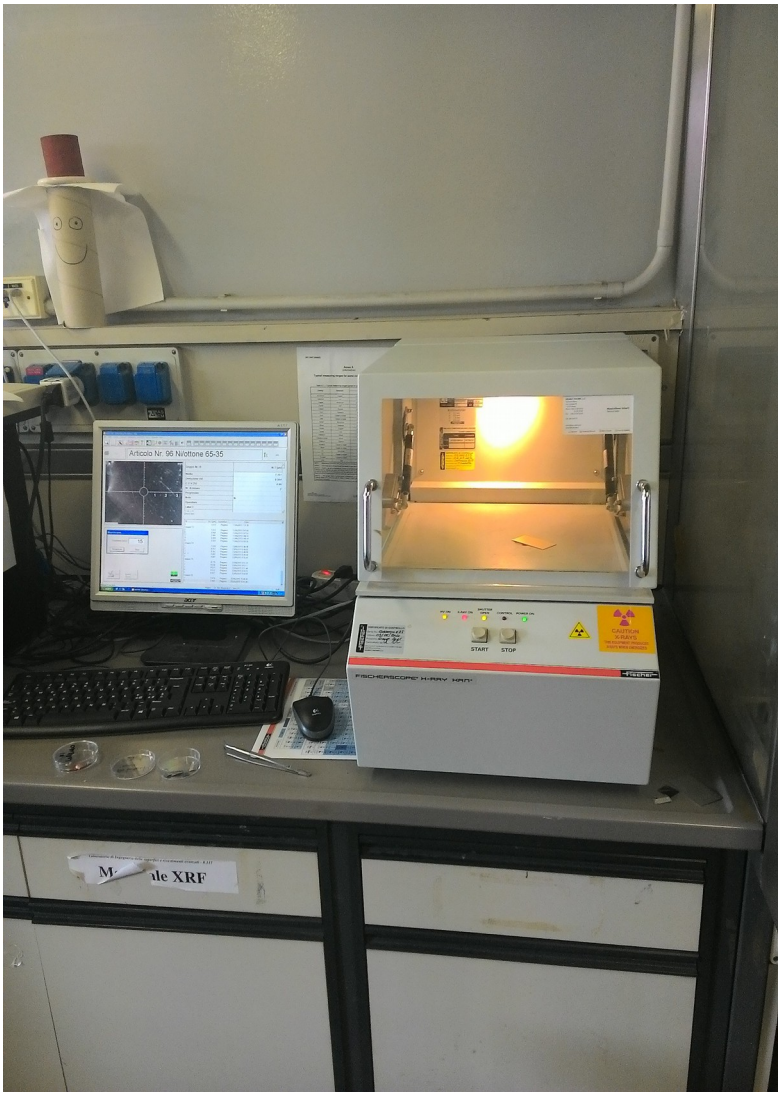

Fig. 2.3: XRF machinery

2.2.3 X-rays Diffraction

X-ray crystallography is a tool used for determining the atomic and molecular structure of a crystal, in which the crystalline atoms cause a beam of X-rays to diffract into many specific directions. By measuring the angles and intensities of these diffracted beams, crystallographer can produce a three-dimensional picture of the density of electrons within the crystal. From this electron density, the mean positions of the atoms in the crystal can be determined, as well as their chemical bonds, their disorder and various other information. X-ray crystal structures can also account for unusual electronic or elastic properties of a material, shed light on chemical interactions and processes.

In an X-ray diffraction measurement, a crystal is mounted on a goniometer and gradually rotated while being bombarded with X-rays, producing a diffraction pattern of regularly spaced spots known as reflections. The two-dimensional images taken at different rotations are converted into a three-dimensional model of the density of electrons within the crystal using the mathematical method of Fourier transforms, combined with chemical data known for the sample. Poor resolution (fuzziness) or even errors may result if the crystals are too small, or not uniform enough in their internal make-up.

For all X-ray diffraction methods, the scattering is elastic; the scattered X-rays have the same wavelength as the incoming X-ray. X-rays range in wavelength from 10 to 0.01 nm; a typical wavelength used for crystallography is 1 Å (0.1 nm), which is on the scale of covalent chemical bonds and the radius of a single atom. This is the reason for using this type of electromagnetic radiation. Waves with longer wavelength would not have sufficient resolution to determine the position of atoms. A monochromatic X-ray beam is sent onto the sample to be analysed, atoms scatter X-ray waves, primarily through electrons. When X-rays are incident on an atom, they make the electronic cloud move deflected away from the direction where they originally travel, as does any electromagnetic wave. If the movement of these scattered waves occurs with the same wavelength of the incident waves, there is the condition elastic scattering (meaning that X-ray photons did not lose any energy).

The intensity of the diffracted radiation is maximum when the condition of constructive interference given by, Bragg's law:

$2d \sin \theta = n\lambda$

where:

- d is the spacing between diffracting planes;
- θ is the incident angle;
- n is any integer;
- λ is the wavelength of the beam.

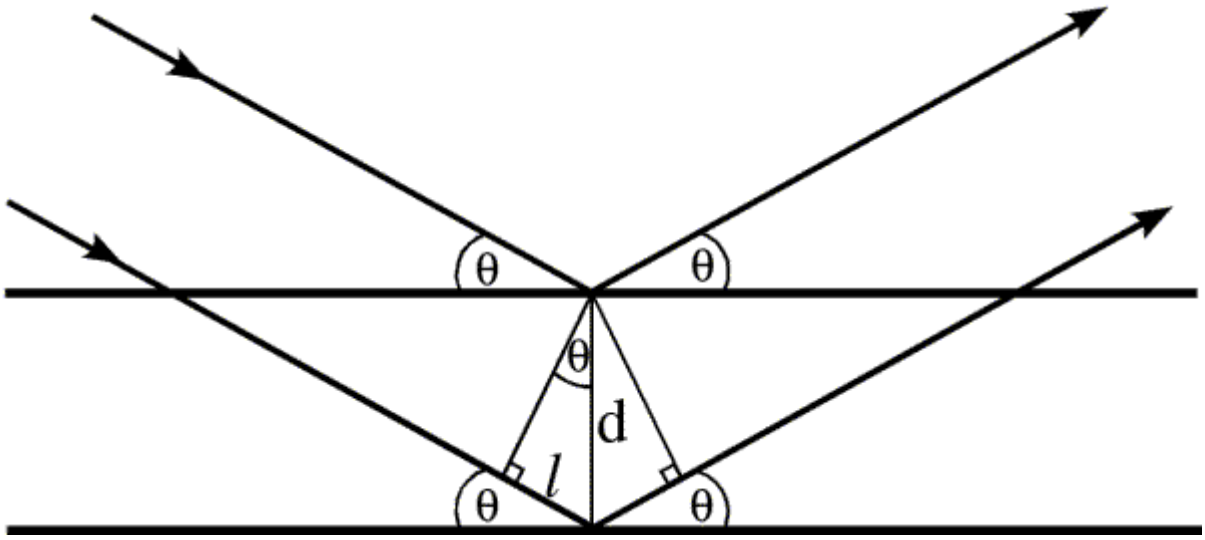

These specific directions appear as spots on the diffraction pattern. The diffraction spectra were obtained with a diffractometer Philips PW 1830, equipped with a vertical goniometer PW 1820. The measures were done in thin film mode, using a Cu target to generate X-rays.

Fig. 2.4: Philips PW 1830 XRD machinery

2.2.4 Glow Discharge Optical Emission Spectroscopy

Glow Discharge Optical Emission Spectrometry (GDOES) is used to perform chemical analysis and surface profiles on solid conductive materials. The glow discharge is basically a plasma, formed by the passage of electric current through a low pressure gas. It is obtained by means of a voltage applied between two metal electrodes in a glass chamber containing the gas. When the applied voltage exceeds the 'striking voltage', which is the voltage critical value, the gas in the tube ionizes and a plasma is

obtained. The simplest type of glow discharge is a direct-current glow discharge. In its simplest form, it consists of two electrodes in a cell held at low pressure (0.1–10 torr; about 1/10000th to 1/100th of atmospheric pressure). The cell is typically filled with neon, but other gases can also be used. An electric potential of several hundred volts is applied between the two electrodes. A small fraction of the population of atoms within the cell is initially ionized through random processes (thermal collisions between atoms or with gamma rays, for example). The ions (which are positively charged) are driven towards the cathode by the electric potential, and the electrons are driven towards the anode by the same potential. The initial population of ions and electrons collides with other atoms, ionizing them. As long as the potential is maintained, a population of ions and electrons remains. Some of the ions' kinetic energy is transferred to the cathode. This happens partially through the ions striking the cathode directly. The primary mechanism, however, is less direct. Ions strike the more numerous neutral gas atoms, transferring a portion of their energy to them. These neutral atoms then strike the cathode. Whichever species (ions or atoms) strike the cathode, collisions within the cathode redistribute this energy until a portion of the cathode is ejected, typically in the form of free atoms. This process is known as sputtering. Once free of the cathode, atoms move into the bulk of the glow discharge through drift and due to the energy they gained from sputtering. The atoms can then be excited by collisions with ions, electrons, or other atoms that have been previously excited by collisions. Once excited, atoms will lose their energy fairly quickly. Of the various ways that this energy can be lost, the most important is radiatively, meaning that a photon is released to carry the energy away. Below the ionization voltage or striking voltage there is no glow, but as the voltage increases to the ionization point the Townsend discharge [?[happens just as glow discharge becomes visible; this is the start of the normal glow range. As the voltage is increased above the normal glow range, abnormal glow begins. If the voltage is increased to the point the cathode glow covers the entire cathode arc-discharge begins. Glow discharge can be used to analyse the elemental, and sometimes molecular, composition of solids, liquids, and gases, but elemental but elemental analysis of solids is the most common. In this arrangements, GDOES is made up of a discharge lamp, an optical spectrometer, and a data acquisition and processing system; the sample to investigate is put on a copper electrode and used as the cathode (the copper is the anode).

The discharge is applied between the cathode and the anode, triggering off a sample surface erosion, sputtering indeed. The sputtered atoms, now in the gas phase, can be detected by atomic absorption, but this is a comparatively rare strategy. Instead, atomic emission of atomic emissions and mass spectroscopy are usually used. Collisions between the gas-phase sample atoms and the argon plasma pass energy to the sample atoms. This energy can excite atoms, after which they can lose their excess energy through an X – photon emission. Emitted photons, whose energy is characteristic of a chemical element's energy level, are then collected by photomultipliers, that allows to quantify elemental composition of a material. By observing the intensity of the emission, the concentration of atoms of that type can be determined.

Both bulk and depth analysis of solids may be performed with glow discharge. Bulk analysis assumes that the sample is fairly homogeneous and averages the emission signal over time. Depth analysis relies on tracking the signal in time, therefore, is the same as tracking the elemental composition in depth. Depth analysis requires greater control over operational parameters. For example, conditions (current, potential, pressure) need to be adjusted so that the crater produced by sputtering is flat bottom. In bulk measurement, a rough or rounded crater bottom would not adversely impact analysis. Under the best conditions, depth resolution in the single nanometre range has been achieved (in fact, within-molecule resolution has been demonstrated).

The surface profile analysis, which is the gathering of signal for each element as a function of time, were made using SPECTRUMA Analyser 750.

Fig 2.5: Spectruma analyser 750

2.2.5 Scanning Electrons Microscope

A scanning electron microscope (SEM) is a type of electron microscope that produces images of a sample by scanning it with a focused beam of electrons. The scanning electron microscope (SEM) uses a focused beam of high-energy electrons to generate a variety of signals at the surface of solid specimens. The signals that derive from electron-sample interactions reveal information about the sample including external morphology (texture), chemical composition, and crystalline structure and orientation of

materials making up the sample. In most applications, data are collected over a selected area of the surface of the sample, and a 2-dimensional image is generated that displays spatial variations in these properties. Areas ranging from approximately 1 cm to 5 microns in width can be imaged in a scanning mode using conventional SEM techniques (magnification ranging from 20X to approximately 30000X, spatial resolution of 50 to 100 nm). The SEM is also capable of performing analyses of selected point locations on the sample.

Accelerated electrons in an SEM carry significant amounts of kinetic energy, and this energy is dissipated as a variety of signals produced by electron-sample interactions when the incident electrons are decelerated in the solid sample. These signals include secondary electrons (that produce SEM images), backscattered electrons (BSE), diffracted backscattered electrons (EBSD that are used to determine crystal structures and orientations of minerals), photons (characteristic X-rays that are used for elemental analysis and continuum X-rays), visible light (cathode luminescence-CL), and heat.

Secondary electrons and backscattered electrons are commonly used for imaging samples: secondary electrons are most valuable for showing morphology and topography on samples and backscattered electrons are most valuable for illustrating contrasts in composition in multiphase samples. X-ray generation is produced by inelastic collisions of the incident electrons with electrons in discrete orbitals (shells) of atoms in the sample. As the excited electrons return to lower energy states, they yield X-rays that are of a particular wavelength (that is related to the difference in energy levels of electrons in different shells for a given element). Thus, characteristic X-rays are produced for each element in a mineral that is "excited" by the electron beam. SEM analysis is considered to be "non-destructive" so it is possible to analyse the same materials repeatedly.

In a typical SEM, an electron beam is thermoionically emitted from an electron gun fitted with a tungsten filament cathode. Tungsten is normally used in thermionic electron guns because it has the highest melting point and lowest vapour pressure of all metals, thereby allowing it to be heated for electron emission, and because of its low cost. Other types of electron emitters include lanthanum hexaboride (LaB6) cathodes.

The instrument used was a ZEISS EVO 50 EP, equipped with an OXFORD INCA ENERGY 200 EDS unit.

Fig. 2.6: ZEISS EVO 50 EP SEM equipment

2.2.6 Raman Spectroscopy

Raman spectroscopy is a spectroscopic technique used to observe vibrational, rotational, and other low-frequency modes in a system. It relies on inelastic scattering, or Raman scattering, of monochromatic light, usually from a laser in the visible, near infra-red, or near ultraviolet range. The laser light interacts with molecular vibrations, phonons or other excitations in the system, resulting in the energy of the laser photons

being shifted up or down. The shift in energy gives information about the vibrational modes in the system. In general, an incident light beam passes through the sample or is absorbed without change (depending on the wavelength of the light and of the nature of the sample). A small part of the incident beam is scattered elastically, i.e. with the same frequency (Rayleigh effect). An even smaller percentage of light undergoes inelastic scattering (Raman effect): it is spread with a frequency higher or lower than the original.
The Raman interaction leads to two possible outcomes:

- the material absorbs energy and the emitted photon has a lower energy than the absorbed photon. This outcome is labelled Stokes Raman scattering;
- the material loses energy and the emitted photon has a higher energy than the absorbed photon. This outcome is labelled anti-Stokes Raman scattering.

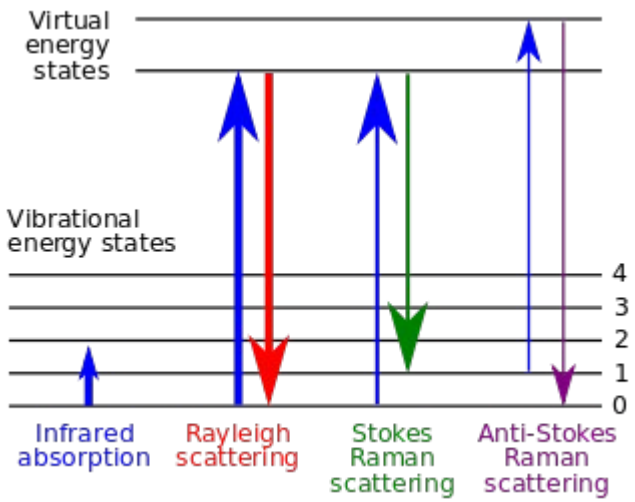

Fig. 2.7: Raman scattering phoenomena

The energy difference between the incident photons and those released inelastically corresponds to the vibrational energy levels of the diffusing molecule: the analysis of the shift of the spectral lines due to Raman effect can therefore provide information on the chemical composition, molecular structure, intermolecular interactions of the sample. Moreover the energy difference between the absorbed and emitted photon corresponds to the energy difference between two resonant states of the material and is independent of the absolute energy of the photon.
The spectrum of the scattered photons is termed the Raman spectrum. It shows the intensity of the scattered light as a function of its frequency difference Δv to the incident photons. The locations of corresponding Stokes and anti-Stokes peaks form a

symmetric pattern around Δv=*0*. The frequency shifts are symmetric because they correspond to the energy difference between the same upper and lower resonant states.

If the final vibrational state of the molecule is more energetic than the initial state, the emitted photon will be shifted to a lower frequency for the total energy of the system to remain balanced. This shift in frequency is designated as a Stokes shift. If the final vibrational state is less energetic than the initial state, then the emitted photon will be shifted to a higher frequency, and this is designated as an anti-Stokes shift. Raman scattering is an example of inelastic scattering because of the energy transfer between the photons and the molecules during their interaction.

The intensities of the pairs of features will typically differ, though. They depend on the populations of the initial states of the material, which in turn depend on the temperature. In thermodynamic equilibrium, the upper state will be less populated than the lower state. Therefore, the rate of transitions from the lower to the upper state (Stokes transitions) will be higher than in the opposite direction (anti-Stokes transitions). Correspondingly, Stokes scattering peaks are stronger than anti- Stokes scattering peaks. Their ratio depends on the temperature (which can practically be exploited for the measurement of temperature).

A change in the molecular polarization potential (or amount of deformation of the electron cloud) with respect to the vibrational coordinate is required for a molecule to exhibit a Raman effect. The amount of the polarizability change will determine the Raman scattering intensity. The pattern of shifted frequencies is determined by the rotational and vibrational states of the sample. This dependence on the polarizability differs from infra-red spectroscopy where the interaction between the molecule and light is determined by the dipole moment.

Raman shifts are typically reported in wavenumbers, which have units of inverse length, s this value is directly related to energy. In order to convert between spectral wavelength and wavenumbers of shift in the Raman spectrum, the following formula can be used:

$$\Delta w = \left(\frac{1}{\lambda_0} - \frac{1}{\lambda_1}\right)$$

where:

- Δ*w* is the Raman shift expressed in wavenumber;
- λ0 is the excitation wavelength;
- λ1 is the Raman spectrum wavelength.

Most commonly, the unit chosen for expressing wavenumber in Raman spectra is inverse centimetres (cm−1). Since wavelength is often expressed in units of nanometers (nm), the formula above can scale for this unit conversion explicitly, giving:

$$\Delta W\left(cm^{-1}\right)=\left(\frac{1}{\lambda_0(nm)}-\frac{1}{\lambda_1(nm)}\right)\circ\frac{\left(10^7\,nm\right)}{cm}$$

The toll for the simplicity of Raman measurements is paid when it comes to spectral interpretation. In laboratory it was used the model LABRAM HR 800 UV HORIBA JOBIN YVON. The analysis was conducted using as light source the Argon ions laser with a wavelength of 514 nm, lens with magnification 50X (spot laser of 1-2 μm). The potential used was D1 and D2: the acronym indicates the reduction of the power intensity of the laser by a factor equal to 10-1 and 20-1 (the sample will hit with a power intensity equal to 10 mV).

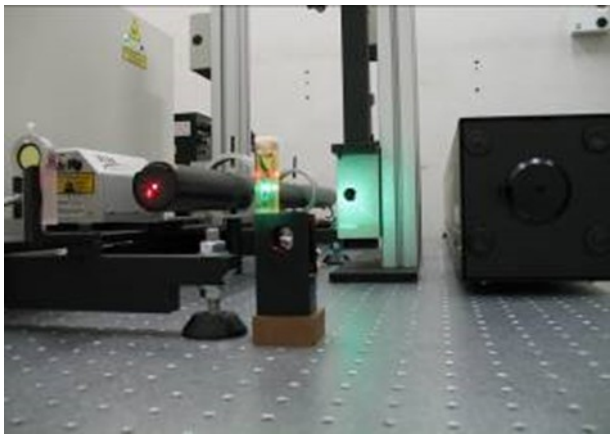

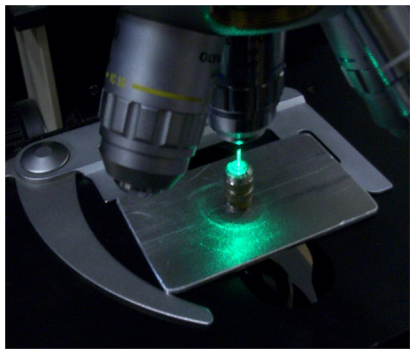

Fig. 2.8: LASER apparatus

2.2.7 Atomic Force Microscope

Atomic force microscopy (AFM) or scanning force microscopy (SFM) is a very high-resolution type of scanning probe microscopy, with demonstrated resolution on the order of fractions of a nanometre, more than 1000 times better than the optical diffraction limit. The AFM is one of the foremost tools for imaging, measuring, and manipulating matter at the nanoscale. The information is gathered by "feeling" the surface with a mechanical probe. Piezoelectric elements that facilitate tiny but accurate and precise movements on (electronic) command enable the very precise scanning. In some variations, electric potentials can also be scanned using conducting cantilevers. The AFM consists of a cantilever with a sharp tip (probe) at its end that is used to scan the specimen surface. The cantilever is typically silicon or silicon nitride with a tip radius of curvature on the order of nanometers. When the tip is brought into proximity of a sample surface, forces between the tip and the sample lead to a deflection of the cantilever according to Hooke's law. Typically, the deflection is measured using a laser spot reflected from the top surface of the cantilever into an array of photo diodes.
If the tip was scanned at a constant height, a risk would exist that the tip collides with the surface, causing damage. Hence, in most cases a feedback mechanism is employed to adjust the tip-to sample distance to maintain a constant force between the tip and the sample. The AFM can be operated in a number of modes, depending on the application. In general, possible imaging modes are divided into static (also called *contact*) modes and a variety of dynamic (non-contact or "tapping") modes where the cantilever is vibrated. The instrument used was a NT-MDT SOLVER PRO.

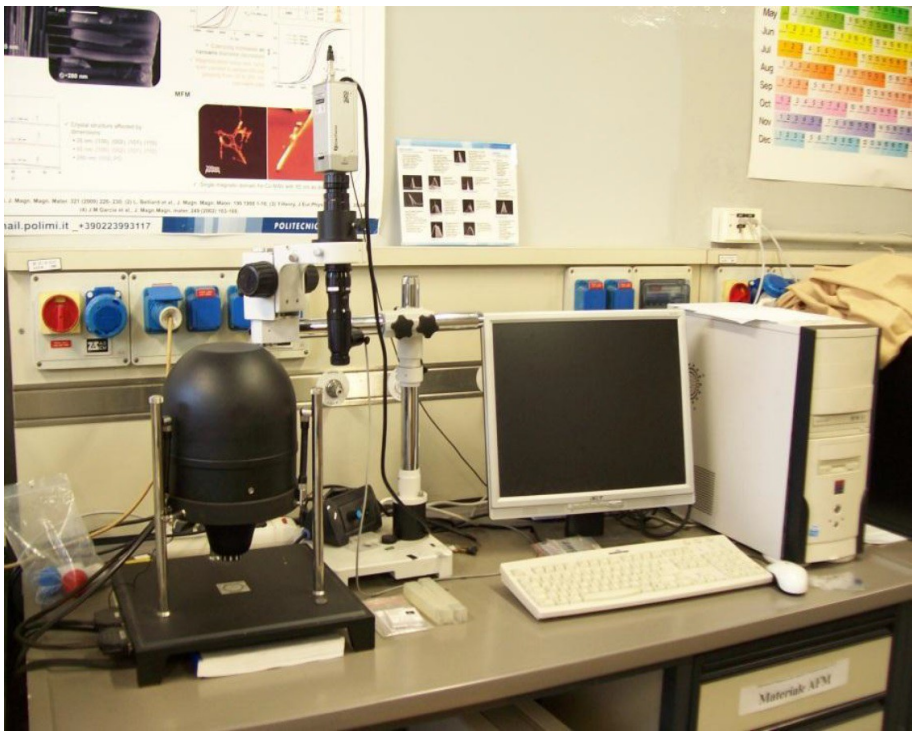

Fig. 2.9: AFM apparatus

2.2.8 X – Rays Photoelectron Spectroscopy

X-Ray Photoelectron Spectroscopy (XPS), also known as Electron Spectroscopy for Chemical Analysis (ESCA), is an analysis technique used to obtain chemical information about the surfaces of solid materials. Both composition and the chemical state of surface constituents can be determined by XPS. Insulators and conductors can easily be analysed in surface areas from a few microns to a few millimetres across.

The sample is placed in an ultrahigh vacuum environment and exposed to a low-energy, monochromatic x-ray source. The incident x-rays cause the ejection of core-level electrons from sample atoms. The energy of a photoemitted core electron is a function of its binding energy and is characteristic of the element from which it was emitted. Energy analysis of the emitted photoelectrons is the primary data used for XPS. When the core electron is ejected by the incident x-ray, an outer electron fills the core hole. The energy of this transition is balanced by the emission of an Auger electron or a characteristic x-ray. Analysis of Auger electrons can be used in XPS, in addition to emitted photoelectrons.

The photoelectrons and Auger electrons emitted from the sample are detected by an electron energy analyser, and their energy is determined as a function of their velocity entering the detector. By counting the number of photoelectrons and Auger electrons as a function of their energy, a spectrum representing the surface composition is obtained. The energy corresponding to each peak is characteristic of an element present in the sampled volume. The area under a peak in the spectrum is a measure of the relative amount of the element represented by that peak. The peak shape and precise position indicates the chemical state for the element.

XPS is a surface sensitive technique because only those electrons generated near the surface escape and are detected. The photoelectrons of interest have relatively low kinetic energy. Due to inelastic collisions within the sample's atomic structure, photoelectrons originating more than 20 to 50 Å below the surface cannot escape with sufficient energy to be detected.

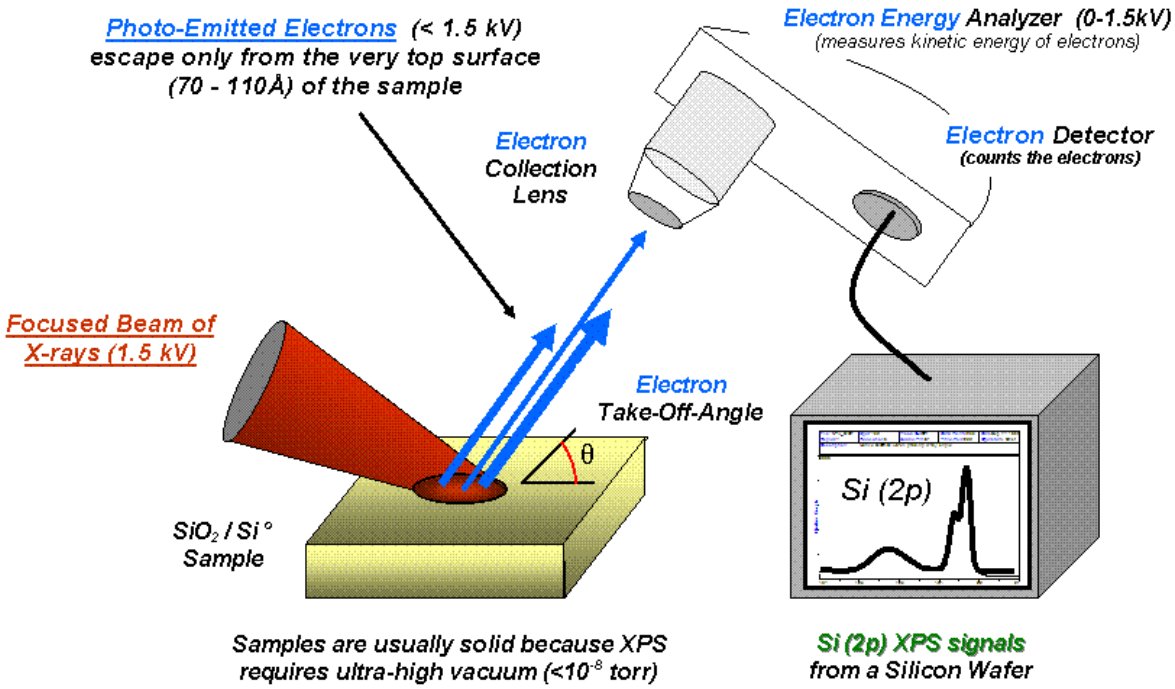

Fig. 2.10: XPS schematics

2.3 Graphene Chemical Vapour Deposition

The reactor consists of a horizontal tube furnace and by a system of pipes, valves and regulators in order to control the flow of gas required for the deposition.
Inside the tubular furnace is inserted a cylindrical tube of quartz, within which are enclosed the samples. Also inside the cylinder is inserted a metallic conduit necessary for bringing the gases within the container; gases flow out through an opening to the aspirator. Everything is sealed by means of a tunable metal clamp.
The deposition of graphene was realized with the CVD technique using hydrocarbons as precursors, in particular it was used CVD at ambient pressure with nitrogen, hydrogen and methane flows.
Once prepared the instrumentation, the a flux of nitrogen was released only in order to eliminate the oxygen inside the cylindrical tube; in fact the presence of oxygen at high temperature can promote oxidation. Then the sample was heated up to a deposition temperature using a specific heating rate, providing a flow of hydrogen. Once this temperature was achieved, growth was started by introducing methane, which acts as the carbon source.
During the holding time, the flux of hydrocarbons and hydrogen was controlled by using two regulators. At the end of this period, every heat source was removed leaving cool the system without imposing any rate of cooling and maintaining the same ratio CH_4/H_2.
Once the tube temperature reached 600°C, flows of methane was stopped because we would expect only a very small precipitation or growth occurring below this temperature.
Once the samples have reached room temperature the flux of hydrogen was removed in favour of nitrogen flux.

Fig. 2.11: CVD tubular furnace

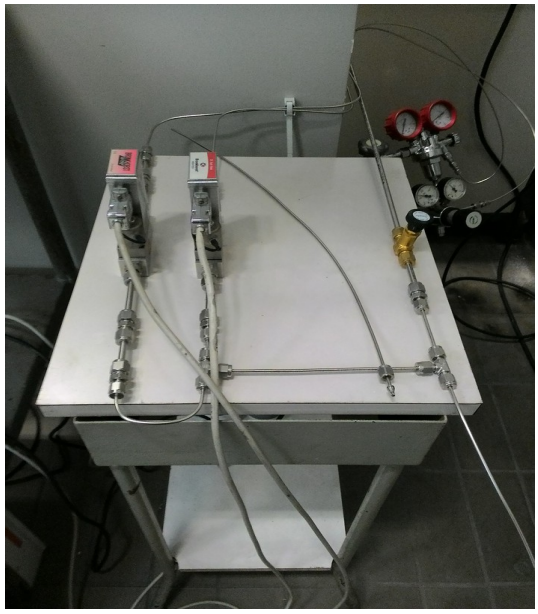

Fig. 2.12: fluxometers

CHAPTER 3:

Experimental work

The first part of the present work was intended to understand how certain substrates do behave when chemical vapour deposition (which will be explained later) is performed onto them.
Simple as they are, metallic Copper and Nickel do not present many issues during the deposition step and therefore a detailed characterization step hasn't been performed, leaving room for the second, and central, part of the project.

3.1 Copper and Nickel Electroforming and Analysis

Electroforming is a metal forming process that forms parts through electrodeposition or electroplating on a model, known in the industry as a mandrel. Conductive (metallic) mandrels are pre-treated chemically to allow subsequent separation of the finished electroform, non-conductive (glass, silicon, plastic) mandrels require the deposition of a conductive layer. Conductive layers can be deposited chemically, or using vacuum deposition techniques. The outer surface of the mandrel forms the inner surface of the form. A thick layer of electroplating is applied until the plate itself is strong enough to be self-supporting. The mandrel is most often separated intact or dissolved away after forming, but occasionally (as in the case in decorative electroforming) left in place. The surface of the finished part that was in intimate contact with the mandrel is rendered in fine detail with respect to the original, and is not subject to the shrinkage that would normally be experienced in a foundry cast metal object, or the tool marks of a milled part. The side of the part that was in contact with the plating solution is less well defined, and that loss of definition increases with thickness of plating. In extreme cases, where a thickness of several millimetres is required, there is preferential build-up of material on sharp outside edges and corners. This tendency can be reduced by a process known as periodic reverse, where the plating current is reversed for short periods during electroforming and the excess is preferentially etched away. The finished plated form can either be the finished part, or can be used in a subsequent process to produce a positive of the original mandrel shape.

3.1.1 Electroforming

Both Copper and Nickel electroforming solutions were provided by TECHNOCHIMICA and were used as received.
The solution volumes was kept around 200 ml, adding water when needed. As already stated in the previous chapter, a Copper and Nickel rack counter electrodes were employed: this is done to avoid solutions salts depletion.
An AISI 316 stainless steel mandrel were employed as electrode; a 2 – by – 4 square centimetres electroforming area was drafted by means of Capton ® tape, which is completely inert and insulating and so avoided the contact between plating solutions and the mandrel itself, keeping up the purity of the solutions.

Forming solutions were hosted in 350 ml silica beakers.
In order to provide solutions stirring a magnetic anchors were put into the beakers.

For the purpose of this work, the substrate thickness doesn't really matter because the graphene growth mechanism for both Copper and Nickel does not depend upon the metal metal thickness or mass present in the furnace, as it will be illustrate later.

For the sake of completeness a characterization step has been done for the examined metal foils.

First of all, optical microscopy have to be performed: as a non destructive inspection technique it can be useful to gather some preliminary informations, such as surface morphology on a macroscopic scale and, eventually, some critical defects in the metal layer.

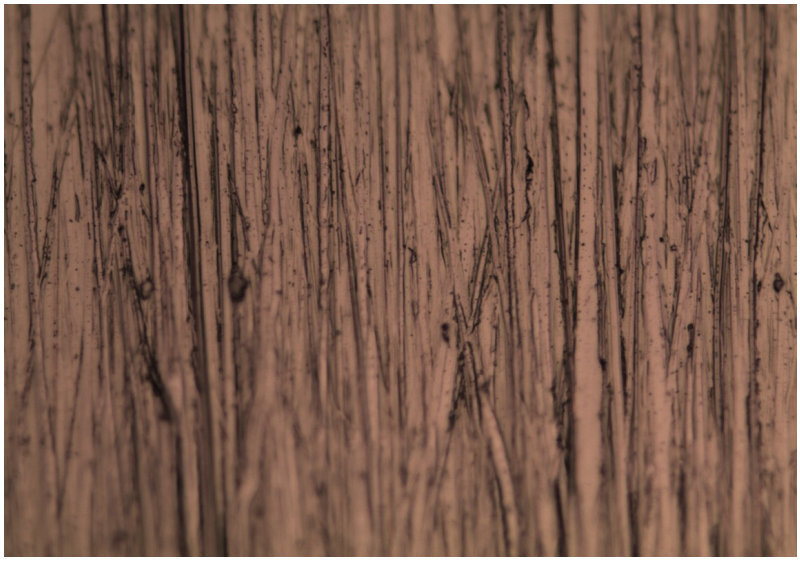

Fig. 3.1: Electroformed Nickel sample (500x)

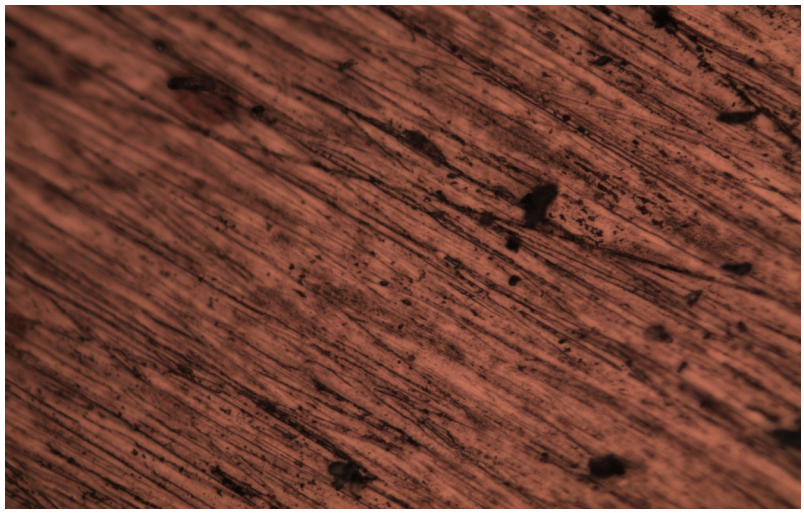

Fig. 3.2: Electroformned Copper sample (500x)

As it can be seen, the grain boundaries are observable and their size should vary after the graphene CVD.

In order to grasp informations about Copper and Nickel depositions, X – rays fluorescence was performed to understand effective metal substrates compositions: before entering the chemical vapour deposition process it must be known which elements do belong to the platings because the graphene deposited quality depends upon substrate composition via specific mechanisms that will be explained later and which are characteristic of each transition metal.

3.1.2 XRF Analysis

To perform an X – rays fluorescence it must be selected a specific support on which the sample is set; in this particular case the 316M AISI steel was pointed out, clearly because it was employed as electroforming mandrel.
The following data were captured:

- Copper thickness

- n= 1 Cu 1 = 9.71 µm;
- n= 2 Cu 1 = 11.2 µm;
- n= 3 Cu 1 = 10.6 µm;
- n= 4 Cu 1 = 9.81 µm;
- n= 5 Cu 1 = 10.2 µm;

Mean **10.29** µm
Standard Deviation **0.595** µm

And for the composition an element analysis was conduced:

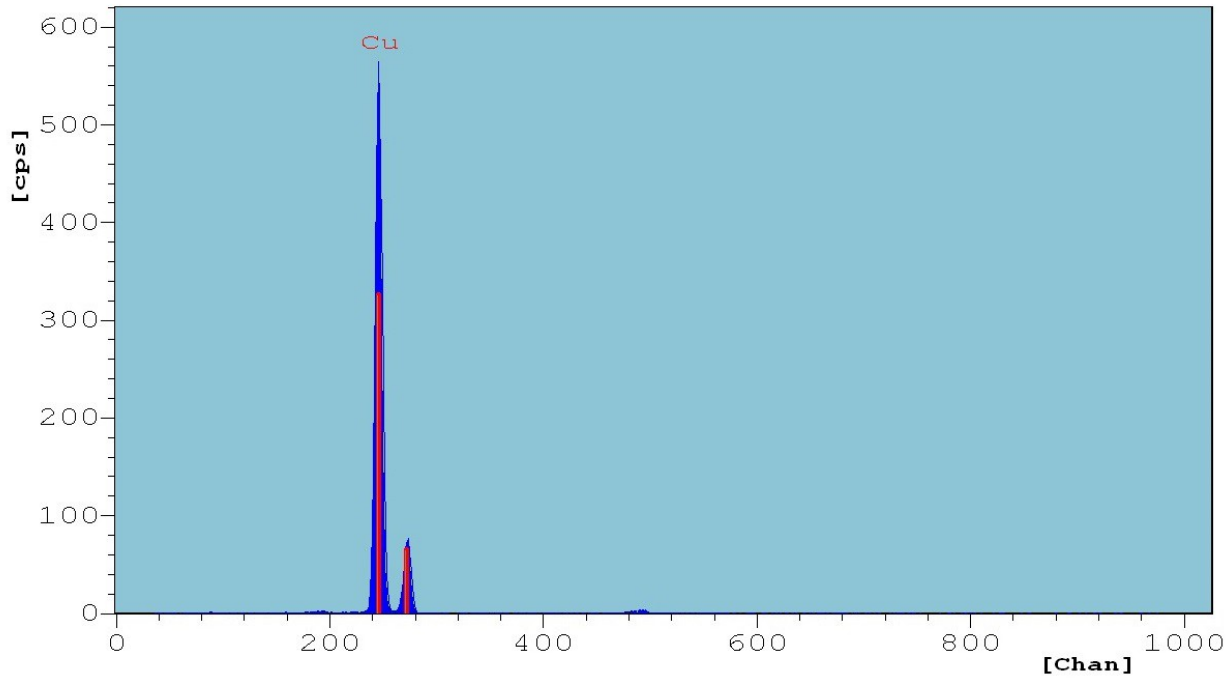

Fig. 3.3: Cu XRF composition analysis

- Nickel thickness:

- n= 1 Ni 1 = 7.979 µm;
- n= 2 Ni 1 = 7.435 µm;
- n= 3 Ni 1 = 7.414 µm;
- n= 4 Ni 1 = 8.437 µm;
- n= 5 Ni 1 = 7.623 µm;

Mean **7.778** µm

Standard Deviation **0.433** µm

And for the composition an element analysis was conduced:

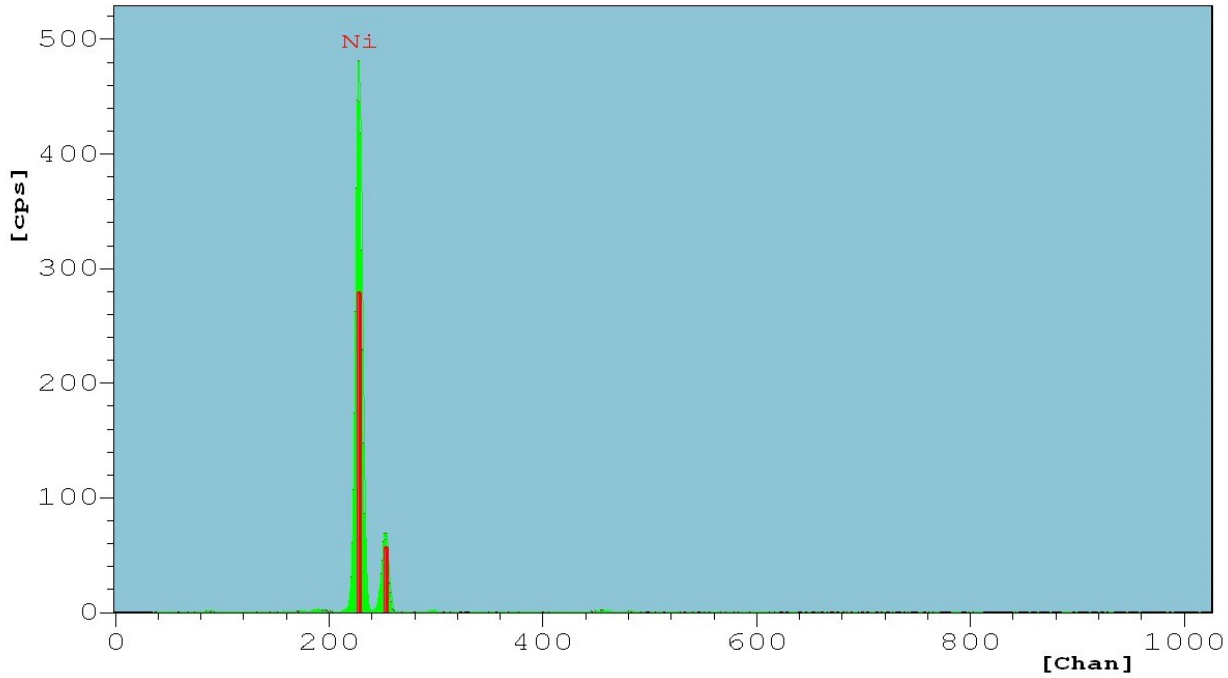

Fig. 3.4: Ni XRD composition analysis

Metal substrate were pure enough to pursue the experimentation without any appreciable influence of substrates composition.

3.1.3 XRD Analysis

Then an X – rays diffraction has been performed for the understanding of metal grains orientation and for another proof of samples composition.

In fact the samples have to be put in the chemical vapour deposition tubular furnace, practically undergoing a thermal treatment know as annealing during the first temperature ramp up of the graphene deposition. This involves the altering of the physical and sometimes chemical properties of a material to increase its ductility and reduce its hardness, making it more workable; more important, annealing, makes atoms migrate in the crystal lattice and decreases the number of dislocations (this is even why a change in ductility and hardness is appreciated).

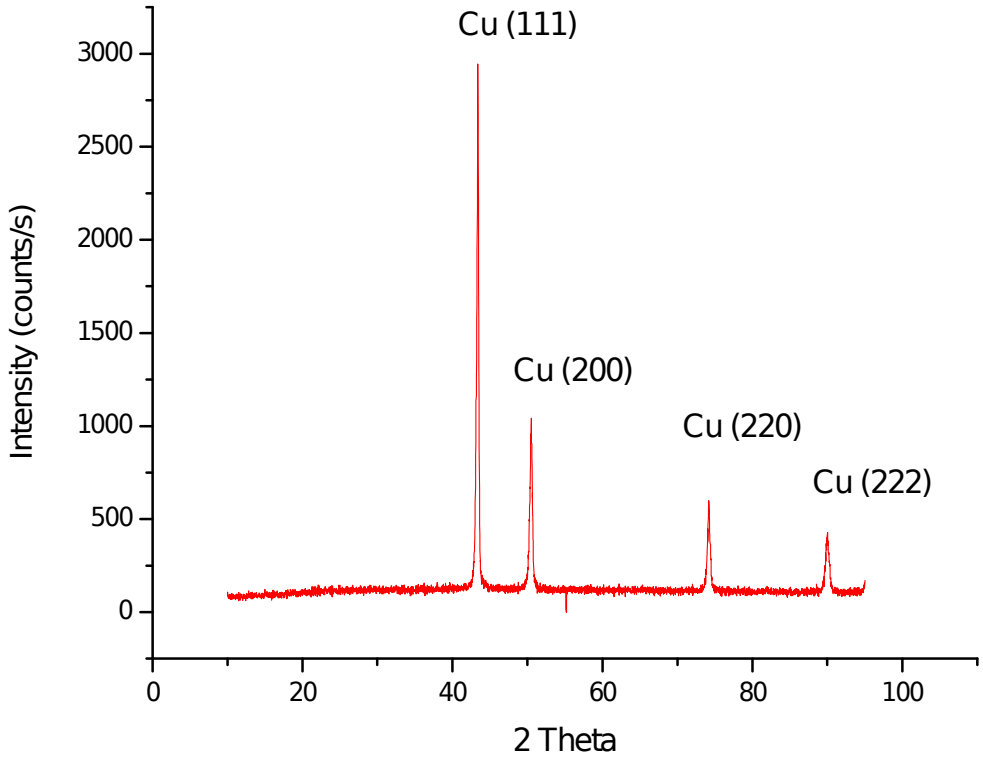

Fig. 3.5: Electroformed Copper XRD spectrum

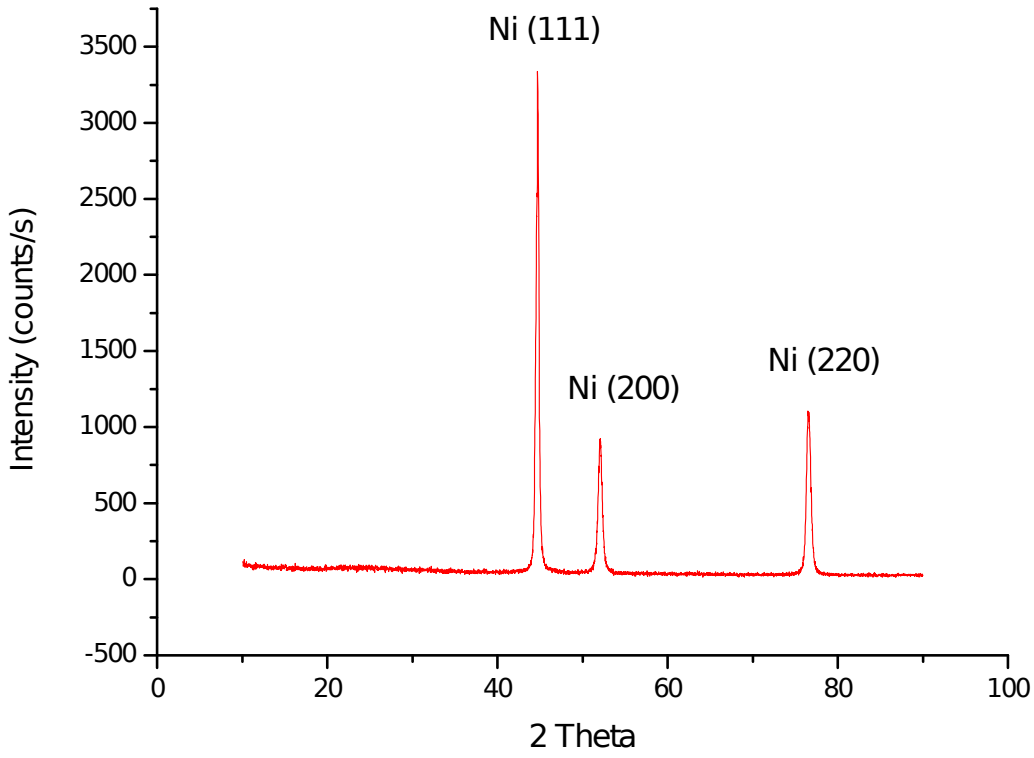

Fig. 3.6: Electroformed Nickel XRD spectrum

Both Copper and Nickel peaks were sharp and intense and no particular features arose. Regular crystallographic structure was present for these electroformed samples. In the case of Copper the (111) orientation is the predominant and the same is true for Nickel A total of 4 samples, 1 by 2 cm^2 wide and presenting the above depicted properties were produced for subsequent graphene deposition.

3.2 Graphene Deposition

In this section two different paths are presented.

On one side it has been necessary to understand the correct dwelling time for the Copper samples to produce a well rounded graphene deposition: in fact copper is a very useful material to cover, because of its wide application in each branch of electronics industry. Unfortunately past literature did not provide enough data to grasp all the parameters, and in particular the dwelling time, to perform the specific chemical vapour deposition process that has been intended in this work.
On the other side, Nickel has proved to be more “docile” when it comes to a deposition process, in particular graphene one. So all the parameters for Nickel substrate to deposit were already clear and fixed.

Furthermore, the two deposition precesses did differ, by a significant amount, in the furnace dwelling time, making not viable a simultaneous deposition for both samples.
The reasons for the different behaviour of the substrates have to be found in the different mechanisms that each metal triggered during graphene chemical vapour deposition.

It has been proposed that CVD growth of graphene on Nickel is due to a Carbon segregation or precipitation process and that a fast cooling rate in conjunction with thin films are needed to suppress the formation of multiple graphene layers. Blakely and co authors have performed extensive studies on the formation of carbon films by cooling Nickel foils saturated with Carbon at high temperatures and found that a monolayer graphite grows first by Carbon segregation, followed by more Carbon precipitation [54].

On the contrary, graphene flakes on Copper seems to grow by surface adsorption, but not by segregation nor precipitation.

The two mechanisms of graphene growth on Nickel and Copper can be understood from the C-metal binary phase diagram. The binary phase diagrams of C-Ni and C-Cu are similar in that Carbon has a limited solubility in the metal without the presence of a metal-carbide line compound. The only significant difference is that the solubility of

Carbon in Copper is much lower than that in Nickel: the former is negligible while the latter is 0.9 at. %. Since only a small amount of carbon can be dissolved in Copper, the source for graphene formation is mainly from the Carbon precursor that is catalytically decomposed on the Copper surface with minimal carbon diffusion into the Copper [1]. Once the surface is fully covered with graphene growth terminates because of the absence of a catalyst to decompose Carbon precursor. In contrast, Nickel can dissolve more carbon atoms and hence it is difficult to get uniform graphene films due to precipitation of extra Carbon during the cool-down.

3.2.1 CVD Process Insight

Both samples underwent the same de-oxidizing process: a 120 s immersion in a 20 g/l Sulfamic Acid solution.
Furthermore, both metal self-standing layers were subjected to the same deposition flow, but, as already said, with different thermal cycles. The chemical vapour was composed by methane and hydrogen flows, which were kept at an 8:1 volume ratio, according to the literature. So inside the chamber were inserted 7.43 sscm of hydrogen and 0.86 sscm of methane, in particular these values were selected considering the load losses that are present moving from the tank to the cylinder.
The generic procedure applied for the CVD onto the metals was kept identical for all the sample presented in this thesis work; it was made of several steps, which are reported below:

- furnace and tubular chamber set up, a very important passage because the effective heated portion of the furnace is a 4 cm spot in the middle, so it was mandatory to fit the sample size to that dimension;
- 5 min of pure gaseous Nitrogen, N_2, wash, in order to replace the air inside the tubular chamber with inert gas (otherwise the high reactive H^2 could react with the Oxygen in the air and crack the tube);
- 5.5 sscm of H_2 unleash and start of the temperature ramp, in this way the heating hydrogen is able to reduce and clean the whole sample surface and avoid further oxidation during the thermal treatment;
- 0.86 sscm of CH_4 unleash and raise of H_2 to 7.43 sscm to set up reaction conditions;

- samples dwelling for a time span depending upon the sample itself;
- CH_4 flow removal, in order to avoid further Carbon deposition and hence graphitic structures formation;
- 5 min of pure gaseous Nitrogen, N_2, wash to remove all Hydrogen residues and avoid reaction with air Oxygen;
- samples removal from the furnace.

3.2.2 Graphene Characterization Approach

Another common feature of graphene layer development onto both Copper and Nickel substrates was the evaluation of the deposit. Optical and Raman spectroscopy methods were applied, in order to glimpse essential characteristics of the carbonaceous thin film.

While informations gathered via optical inspection, even if with high levels of magnifications, could not guarantee the presence nor the quality of graphene layer, Raman spectroscopy has been fundamental throughout all the experimentation.
In particular, a 514 nm wavelength (green light) was employed, due to many literature indications it best suits graphene inspection role; another important parameter to be underlined is the use of a ICS D2 filter, in order to reduce LASER beam power: due to the organic nature of the inspection target, there existed the possibility of modify the film during the Raman shift itself by using a too high energy beam; the mentioned filter decreased by 20 times the beam intensity, removing this issue. Unfortunately it is never mentioned if this correction is made or not. For this reason can be present a shift of the spectrum respect to the spectrum reported in the literature that is evaluated at the same conditions.
It must be said that a 600 lines/mm diffraction grating was used to scatter light on the CCD.

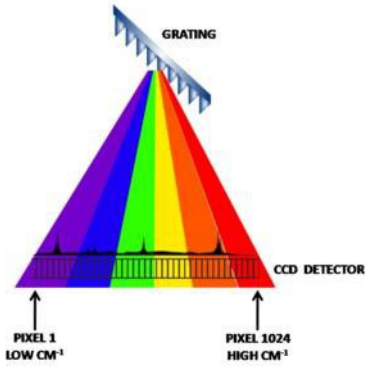

Fig. 3.7: diffraction grating schematics

Using for analysis a magnification of 500X, the laser spot dimension is equal to 1-2 μm. This implies that during the analysis can be detected broader areas between several domains with different number of layers. Therefore the spectrum obtained is a weighted average of the spectra obtained in the various zones at different number of layers present in the volume of analysis. For this reason, it will not be correct to define a specific number of layers but it is better to speak about predominant domains.

The most important parameters to consider in order to characterize a graphene structure are:

- ratio between the intensity of the 2D peak and the intensity of the G peak: in particular if I(2D)/I(G) is higher than 1 it is possible to determine graphene structure, while if this ratio is less than 1 it is possible to determine FLG/graphitic structure;
- shape of 2D peak: graphene has a single, sharp 2D peak, while bi-layer graphene has a much broader band with respect to the graphene and so on with increasing of number of layers;
- Frequencies of the 2D: in particular it is possible to observe a blueshift of the 2D peak frequency increasing the number of graphene layer (see deconvolution section).

To obtain a quantitative evaluation of the number of graphene layers, Malaard et al. [55] work was kept as reference.

3.2.3 Copper Substrate

The first experiment was realized considering the above cited deposition process onto a Copper sample 1 by 2 cm^2 sized, with a furnace dwell time of **2 min**.

The sample surface morphology appears as follows (500x):

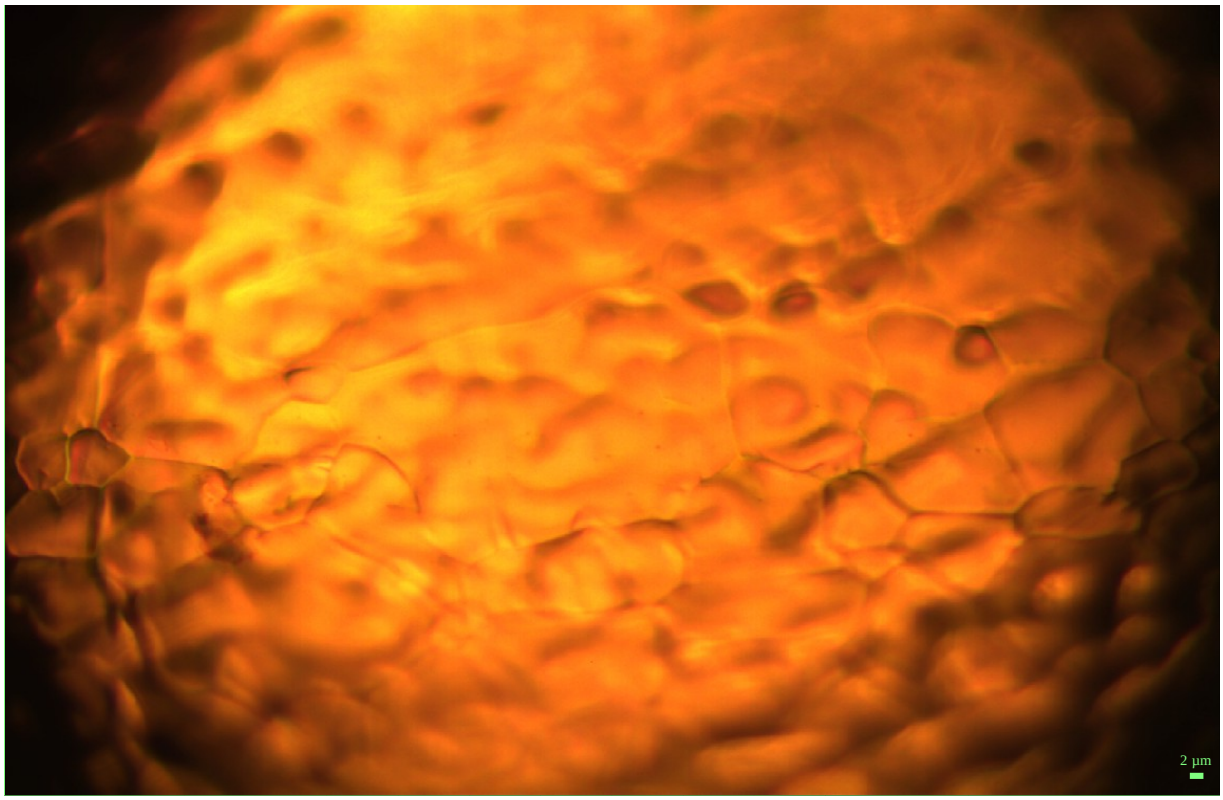

Fig. 3.8: optical image of the first Copper sample

Optical analysis, as anticipated, does not reveal any particular surface feature but Copper grain boundaries: graphene layer (or layers) or graphitic structures/FLG were not seen.
The main difference from the original substrate that could be accounted was the grain size: in fact, the first temperature ramp of the CVD process could be regarded as a 30 minutes thermal treatment, during which the crystal structure had evolved.

At this stage, Raman spectroscopy was employed as a qualitative characterization technique: the aim is to verify the actual presence of graphene; so only spot measure are reported.

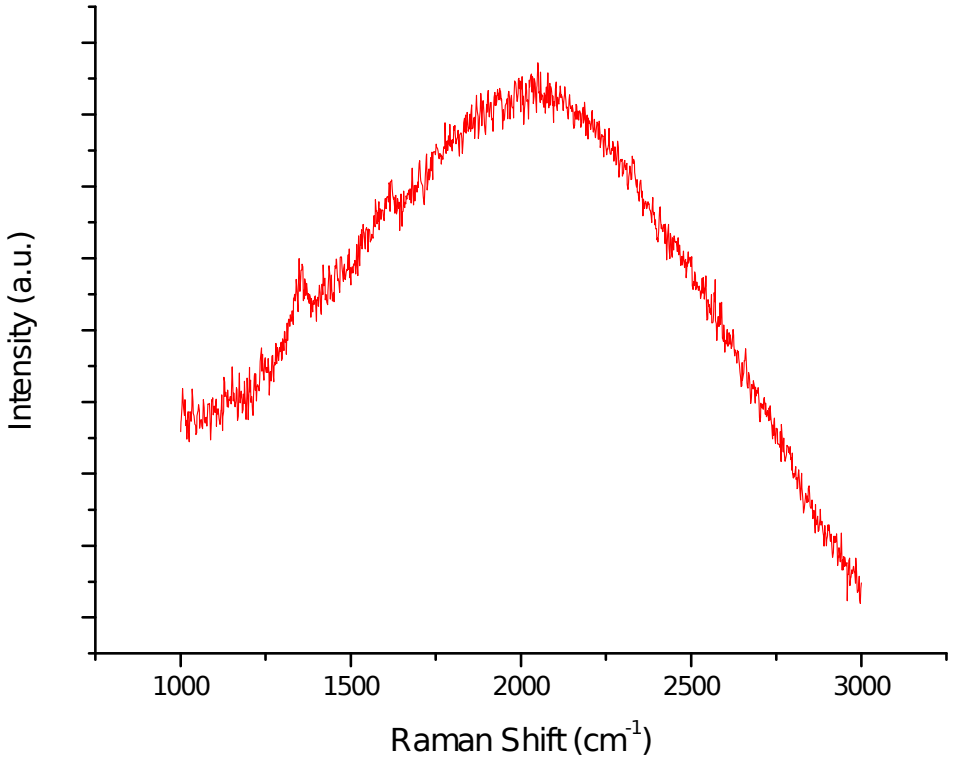

Fig. 3.9: Raman spectrum of 2 min CVD Copper sample

As it can be seen no 2D peak is present, while the G peak and the D peak are at least visible. The broad peak in the middle of the shift was probably due to sample fluorescence, which can be linked to some addictive present in the Copper plating solution.

The shape of the presented spectra clearly shows no presence at all of an ordered Carbon structure: in fact the I(2D)/I(G) ratio clearly suggests a defected, or better amorphous, deposit.

The second experiment has been performed onto a similar sized Copper sample, but raising furnace dwelling time to **4 min**.

The sample surface morphology appears as follows (500x):

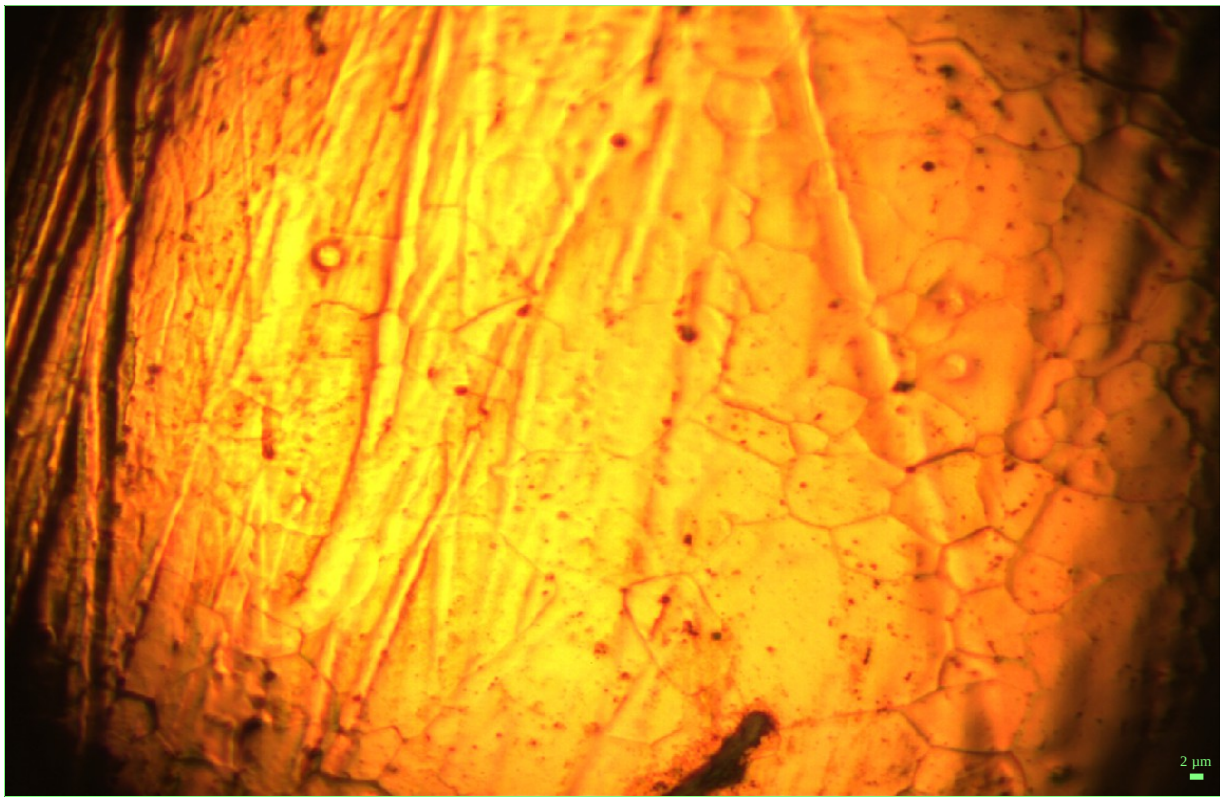

Fig. 3.10: optical image of 4 min CVD Copper sample

The sample appeared slightly different from the previous one; the surface was no more clean and bright but many dark point were visible; this surface texture had been linked to Carbon deposit which turned out to be graphitic one, as can be see by the following Raman spectrum.
Again the influence of the temperature ramp on the grain size could be appreciated.

As before, at this stage just a qualitative spot Raman investigation was carried out:

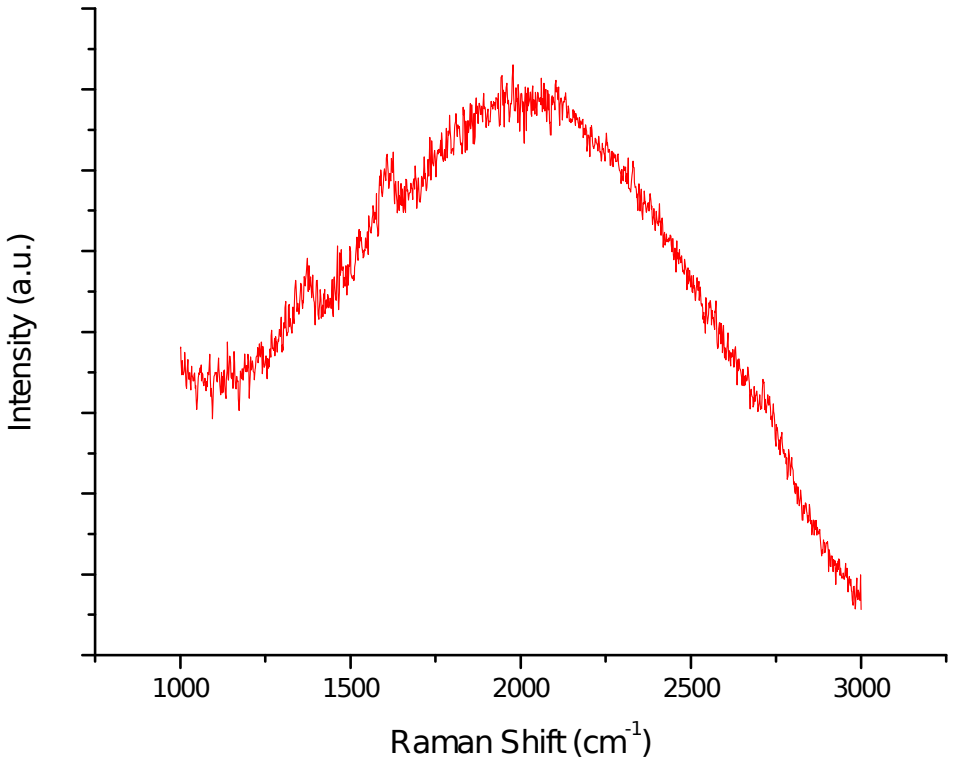

Fig. 3.11: Raman spectrum of 4 min CVD Copper sample

A low intensity 2D peak have appeared in the high frequencies region, remarking that the graphitic layer is progressing towards a more ordered structure; the D peak is clearly less intensive, while the G have risen in intensity. This features were a clear sign of a positive structural evolution of the carbonaceous deposit.

By the way the spectrum was not adequate for our purpose, so a third experiment was carried out.

The third experiment has been performed onto a Copper sample with the above cited features, but raising furnace dwelling time to **6 min**.

Sample surface had the following appearance at optic investigation (500X):

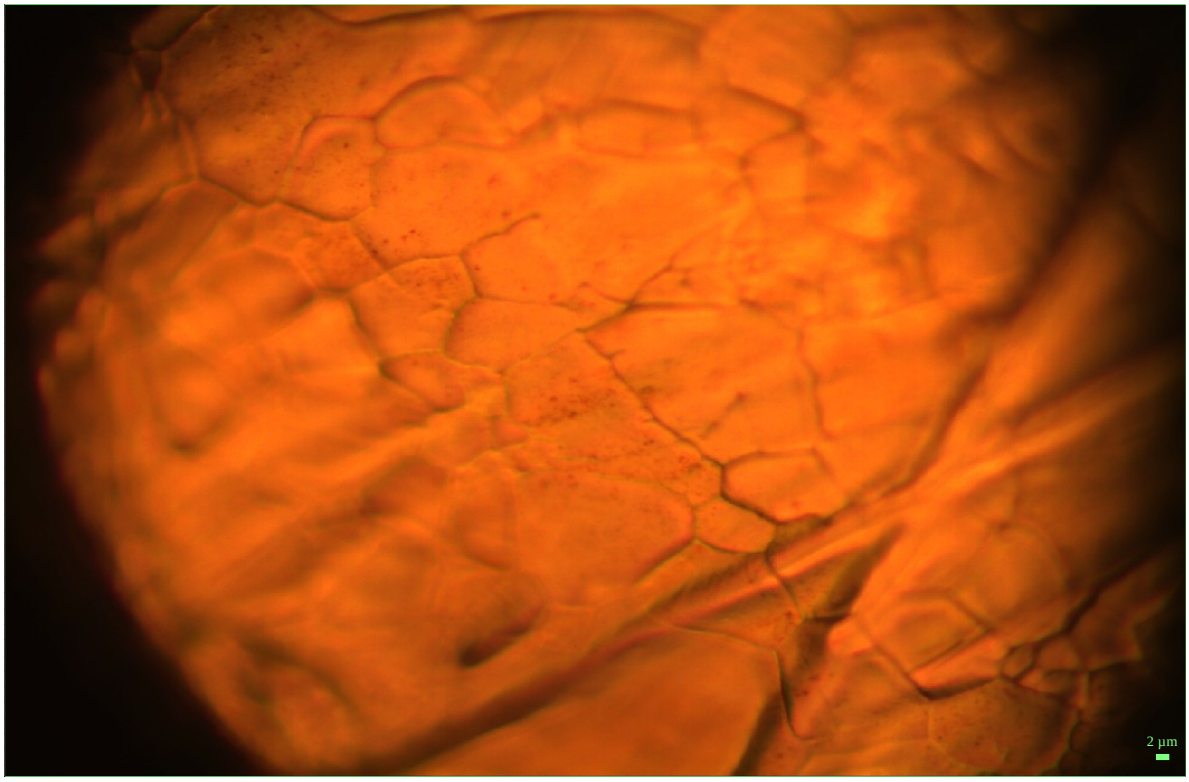

Fig. 3.12: optical image of the 6 min Copper sample

Again the surface did appear different with respect to the 2 minutes sample and the black spots were visible again, as in the 4 minutes sample.

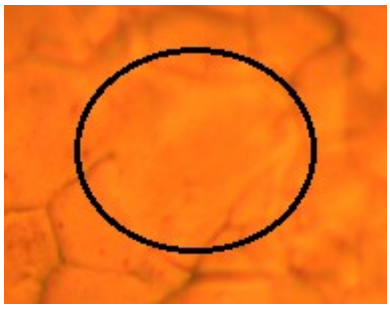

Fig. 3.13: darker areas on the 6 min CVD Copper sample

Furthermore, wide darker areas corresponding to the Copper grains were evident: these were pointed out as FLG domains and the Raman shift confirmed the theory, as can be seen later on.

The spot Raman investigation on the region depicted in fig 3.14 was needed to understand to what could be linked the surface morphology changes:

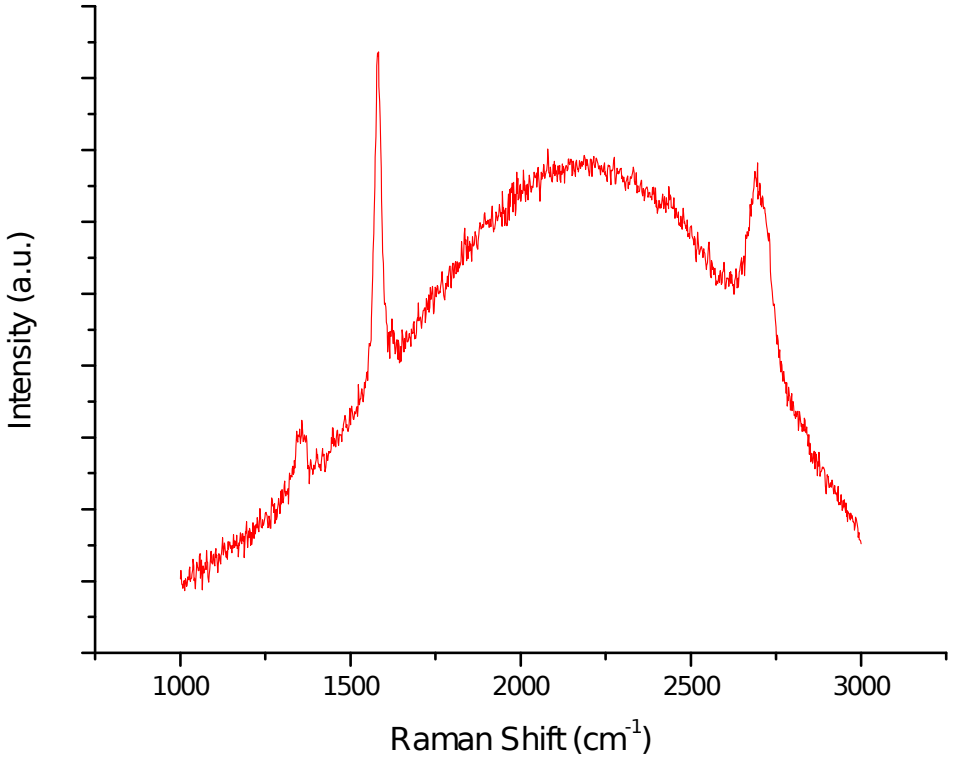

Fig. 3.14: Raman spectrum of the 6 min Copper sample

Here a very intense 2D peak was obvious and a lower – than – one I(2D)/I(G) was present too. Unfortunately the D peak, even if way less intensive, was still present, indicating disorder inside the deposit. This result was probably due, as already has been said, to the large spot size of the instrument: in a single measure amorphous (black spots), graphitic and FLG (or graphene itself) layers were glimpsed together and the presented spectrum was the result. In order to wrap up Copper experimentation

results, a grouped spectrum has been realized. Here was significant the signal evolution with respect to the increasing of the deposition time.

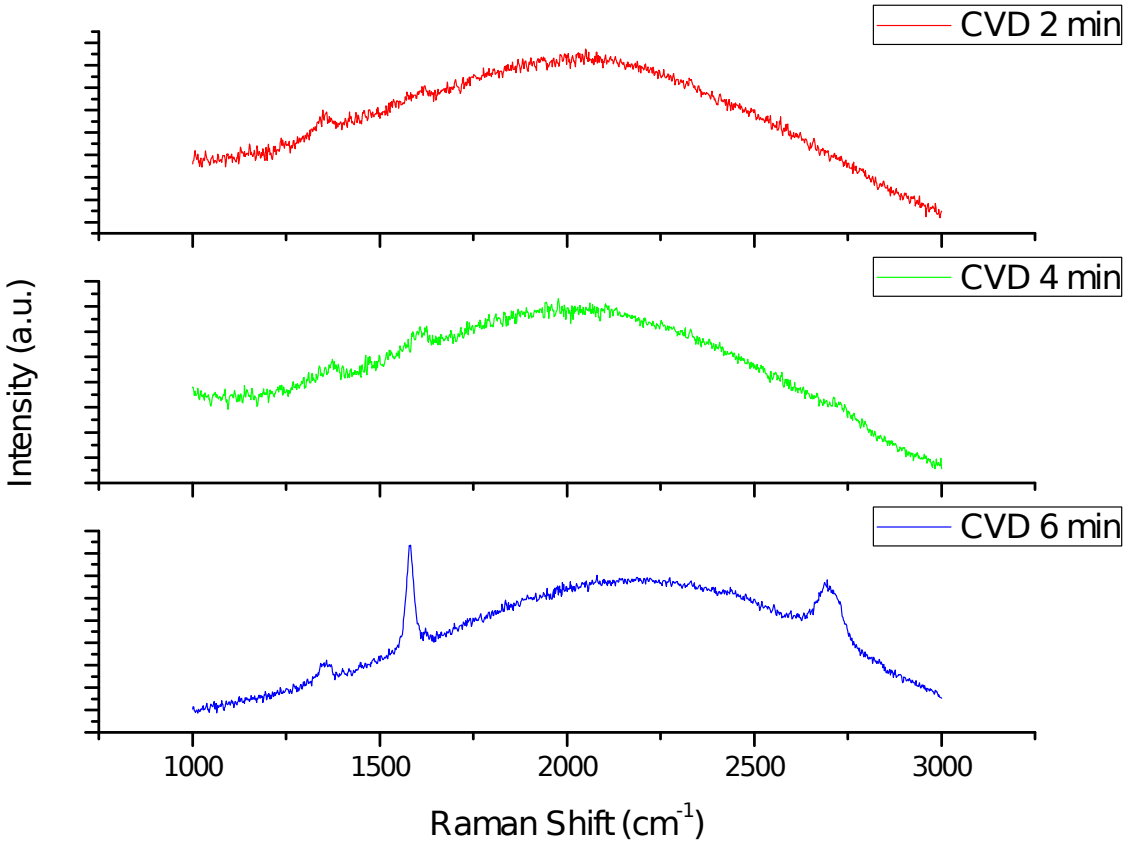

Fig. 3.15: Raman spectra comparison of 2, 4 and 6 min CVD Copper samples

What resulted clear from the previous comparison, was that Carbon deposits in an amorphous way from the very beginning of the CVD process, merging in an ordered fashion as the deposition time goes on. This layer evolution was not fully understood, but the heterogeneous nature of the FLG could be related to the uncontrolled crystallographic structure of the electrodeposited Copper sample: recently Ago et al. [56] showed how the metal grains orientation can influence the quality of the deposited graphene.

Actually they related Copper (111) crystal parameter to the graphene Carbon inter atomic, justifying the quality improvement with a very close match between the two lengths.

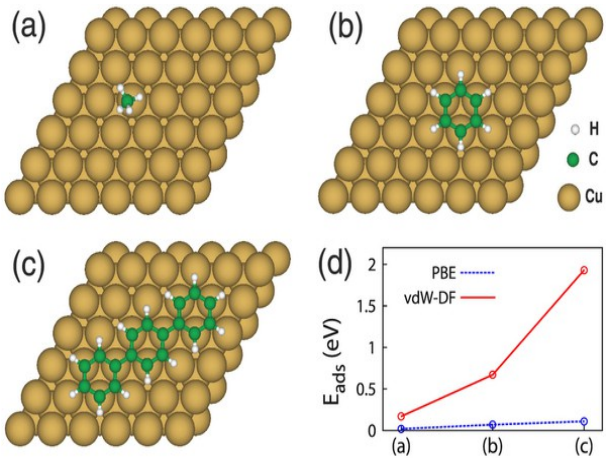

Fig. 3.16: Top views of the optimized structures of (a) methane (CH4), (b) benzene (C6H6), and (c) p-Terphenyl (C18H14) on the Cu(111) surface and an adsorption energy estimation [60].

Therefore, given the dispersive grains orientation of the proposed Copper samples (see Fig. 3.5) the Raman spectrum reported reasonably reflected the different order deposits present on the surface: on the Cu(111) domains the ordered FLG was present, while on the other domains amorphous Carbon was predominant.

3.2.4 Nickel Substrate

The first experiment was realized onto a 1 by 2 cm^2 Nickel sample following all the deposition steps previously reported. The furnace dwelling time was fixed, according to the literature, at **2 min**: indeed, due to the high solubility of Carbon into Nickel and the small amount of metal volume, no long than a couple of minutes were needed to saturate the Nickel film with Carbon.

A preparatory optical surface inspection was performed, using 500x as magnification lens:

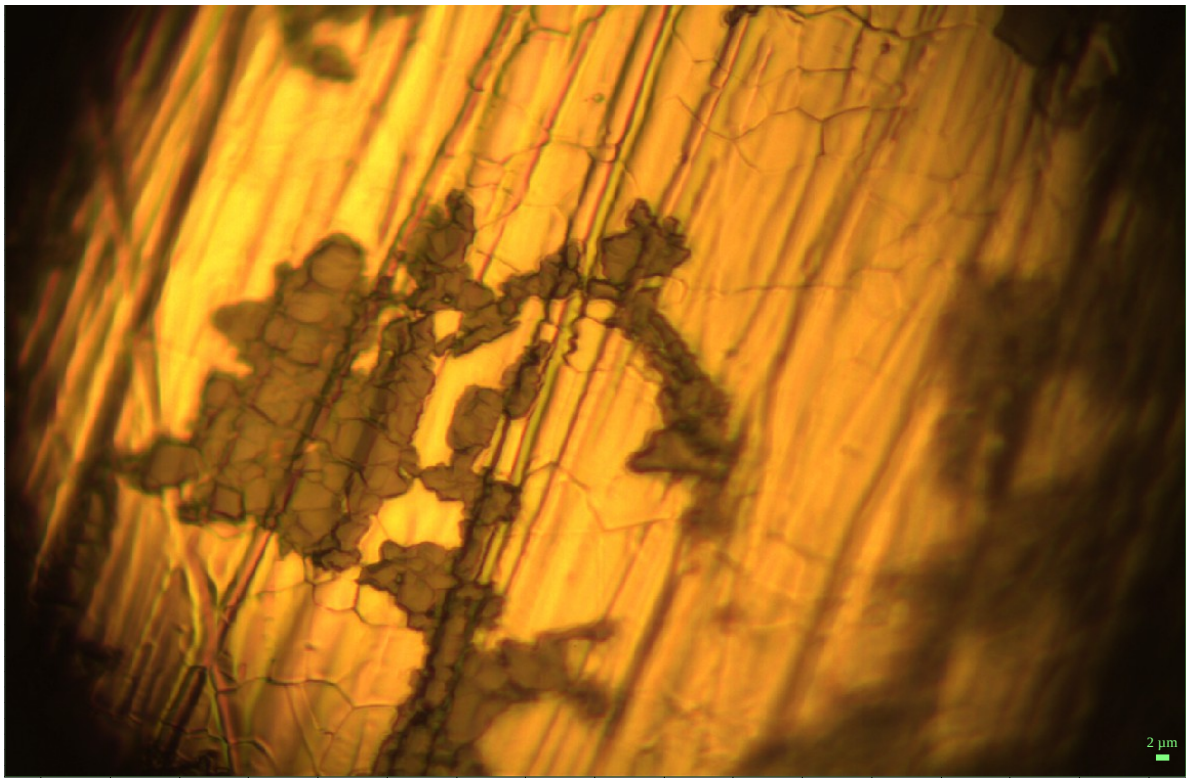

Fig. 3.17: optical image of 2 min CVD Nickel sample

From optical analysis it is possible to distinguish areas with different colours. This happens because the graphene is able to absorb a significant fraction of incident white light; in particular for each graphene layer added there is a reduction of light transmittance. Then it can be concluded that moving from a darker area to a brighter

area of the sample, the number of deposited layers decreases, up to bare Nickel.
This high distribution inhomogeneity was reflected by the Raman spectrum: the darker areas was covered by FLG while the bright one were bare nickel, with no deposit onto them. Here is the spectrum:

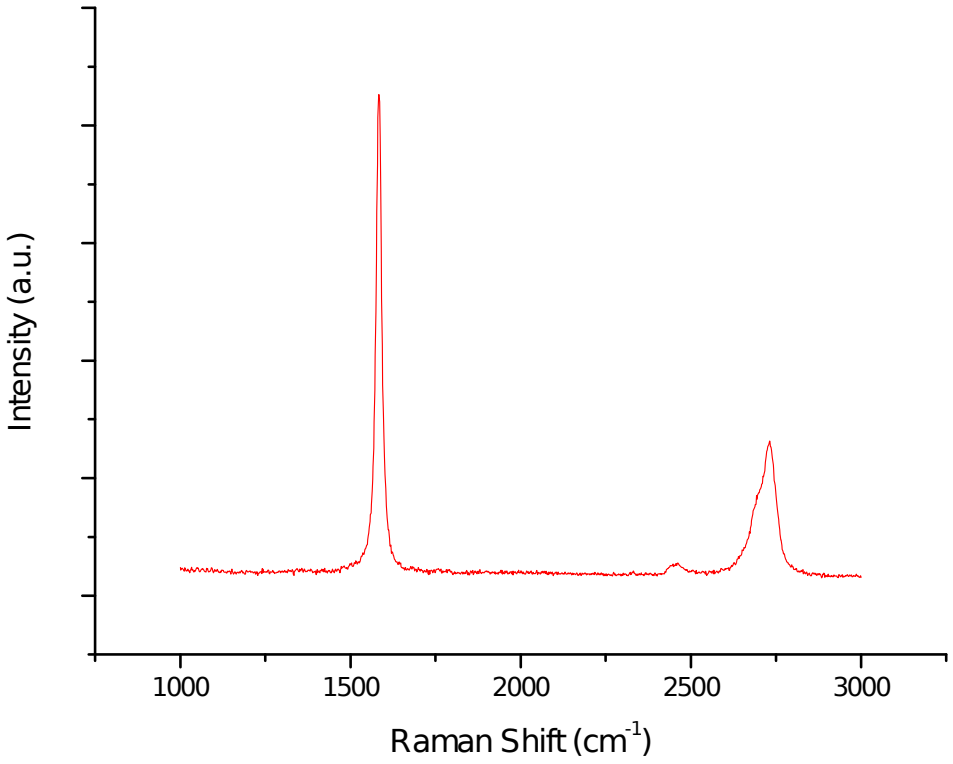

Fig. 3.18: Raman shift of the 2 min CVD Nickel sample

Here can be seen why Nickel best suited the purpose of support layer for graphene deposition. In fact the D pick was completely absent, symptom of a high ordered system; both the G peak and the 2D peak were very sharp, which again was a positive information for what regards graphene/FLG quality: an ordered system would display better transport characteristics and a much better chemical stability. Both these are the qualities why graphene was chosen as active or protective layer for MEMS applications, making Nickel a very good choice for Silicon applications.
On the other side the I(G)/I(2D) was nearly 3.5, which clearly pointed out that more than a single graphene layers were present.

This could be an issue when coming to the transport characteristics of the graphene layer, but, for the purpose of an anti – stiction layer, it is good enough. It must be kept in mind that the CVD process here presented could be embedded in an actual MEMS production process, making it more interesting than a mechanical exfoliation graphene deposition method, which in theory could have given a single graphene layer.
No other experimentations were performed onto Nickel substrate, because the data acquired were, as already said, quite satisfactory.

3.2.5 Summing Up

After a series of 4 total experiments performed onto 2 different substrates, the first part of the iter here reported ended.
The two metals displayed different behaviours when subjected to the graphene chemical vapour deposition process.
This led to a choice in terms of which of the two substrate could be employed for the following experimental session, featuring flat and micro structured Silicon substrates, which have to be covered with a metal layer in order to let graphene deposit on the surface.

3.3 Graphene/Si Substrates Fabrication Enabled by Nickel Galvanic Displacement

Daniel Q. McNerny et al. recently demonstrated how direct production of graphene on SiO_2 could be achieved through CVD growth of graphene onto a metal layer which has been itself grown onto Silicon [57].
They found out that graphene actually was able to grow at the interface between Silicon Oxide and Nickel layer; further on they showed how stress engineering applied to the whole sample (Silicon Oxide with the Nickel layer) could in turn lead to an easy, selective, and clean removal of the metal, leaving Silicon Oxide covered by micro – scale graphene layer (or FLG).
Indeed, when the Nickel film remains adherent after graphene growth, the balance between residual stress and adhesion governs the ability to mechanically remove the Nickel after the CVD process.

In the cited study, Nickel films were deposited by e – beam evaporation on mono crystalline Silicon wafers with 300 nm thermally grown SiO_2.

Electron Beam Physical Vapour Deposition, or EBPVD, is a form of physical vapour deposition in which a target anode is bombarded with an electron beam given off by a charged tungsten filament under high vacuum. The electron beam causes atoms from the target to transform into the gaseous phase. These atoms then precipitate into solid form, coating everything in the vacuum chamber with a thin layer of the anode material.
The PVD process can be carried out at lower deposition temperatures and without corrosive products, but deposition rates are typically lower than a standard chemical vapour deposition process.
Electron beam physical vapour deposition, however, yields a high deposition rate from 0.1 μm/min to 100 μm/min at relatively low substrate temperatures, with very high material utilization efficiency.

Despite all of the reported advantages, EBPVD resulted to be an expensive and technologically burdening (vacuum or ultra – high chambers are needed) deposition process for the purpose of developing a large scale method to obtain graphene onto semiconductor material.

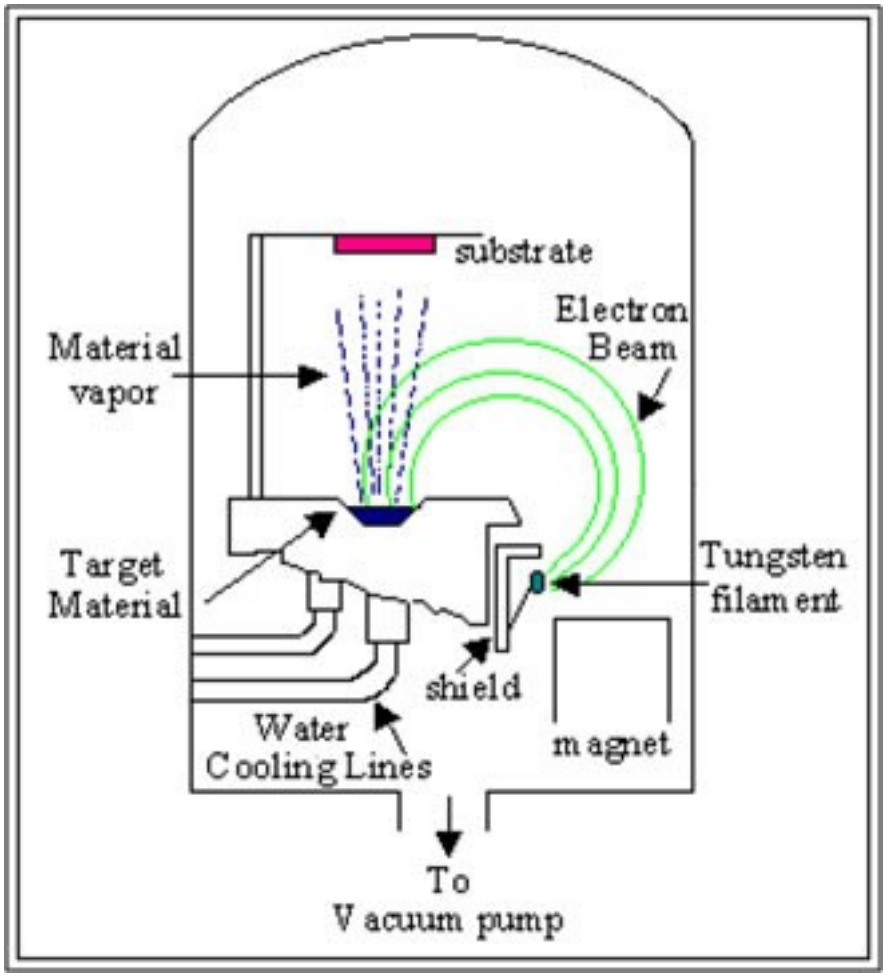

Fig. 3.19: EBPVD process schematics

Therefore, in the present thesis work, an alternative way of obtaining a Si/metal system has been developed, with the precise aim of reducing production costs of graphene direct production on Silicon wafers.

3.3.1 Nickel Galvanic Displacement Solution

The galvanic displacement deposition bath was composed by the following chemicals:

- 10% (w/v) NH_4F;
- 0.1 M $NiSO_4(H_2O)_6$;

For the immersion plating is sufficient to use 50 ml of solution, so it is important to make the appropriate proportions of chemicals.

Because of the fluorides in the solution a high density polyethylene beaker was employed; the beaker capacity was 50 ml.
First Nickel sulphate was put inside the beaker along with a magnetic anchor for solution stirring; soon after, a small amount of water was poured inside the beaker, in order to induce Nickel Sulphate dissociation.
When solid residual was present no more, the Ammonium Fluoride was added to the solution.
Persistent 300 rpm stirring was kept, until the solution was light green and transparent.
Solution pH was adjusted to 9 by means of a saturate Sodium Hydroxide solution, according to literature. The pH control was performed using litmus paper, because electronic pH measurement pods were encased in silica vial. When pH turned to 9, solution changed colour: from the original pale green it became dark blue.

Silicon monocrystalline wafers were supplied by ST MICROELECTRONICS. Silicon wafers were cut by means of a diamond saw into 0.5 by 1 cm^2; samples were degreased by a 10 minutes sonication step in acetone. After a first rinsing and nitrogen stream drying, the Silicon samples were put in a 40% Hydrofluoric Acid solution, in order to get rid of the native oxide and thus activate the silicon surface; then rinsing and drying followed again.

Plating was performed at 50°C, using a double – boiler configuration in order to not melt the beakers; solution had to be kept 5 mm above the sample surface and no stirring was necessary.

To understand the relation between plating time and quality of the deposited metal, a characterization step preceded the actual experimentation.

3.3.2 Nickel Film XRD Characterization

Solution characterization was mandatory in order to understand the behaviour of the solution ([58]) without the used of compact fluorescent lamps (CFLs). The characteristics of the solution have been investigated by plating 5 sacrificial samples for 5 different deposition times:

- 10 minutes;
- 15 minutes;
- 25 minutes;
- 30 minutes;
- 40 minutes.

For what concerned temperature, Nickel depositions have to be done at high temperatures, according to the literature.

XRD of all the deposited sample has been collected; data are reported in the following page normalized to the highest peak.

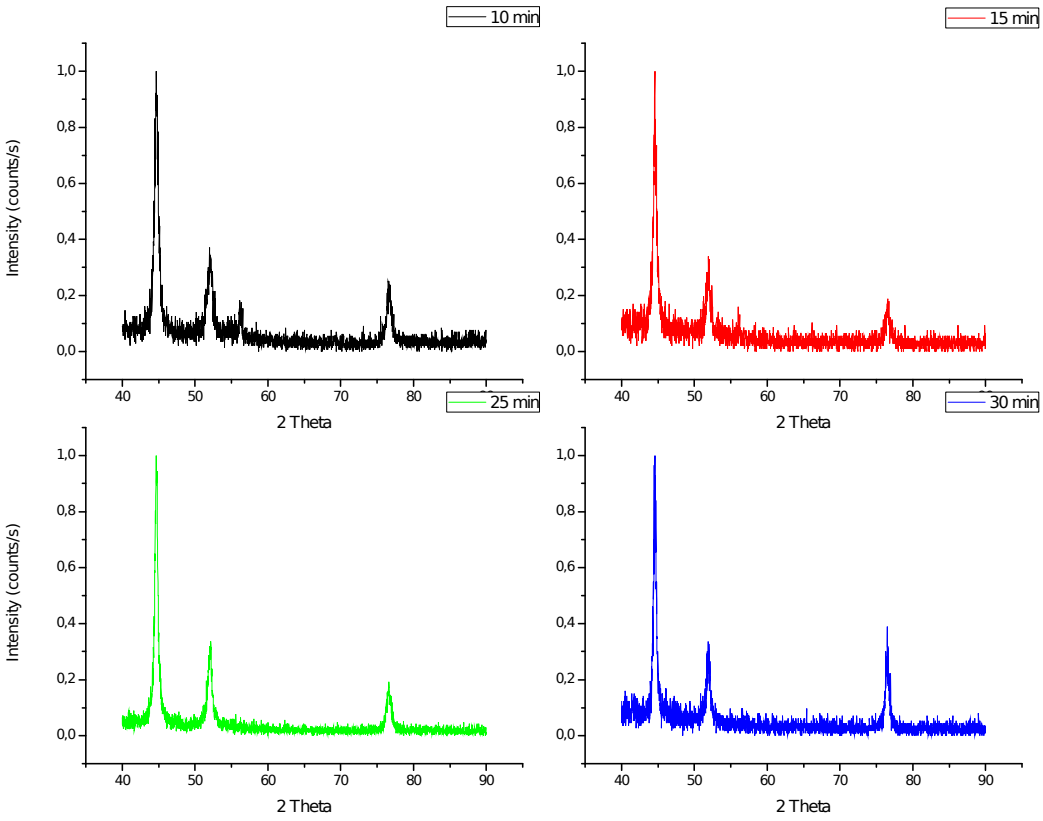

Fig. 3.20: XRD comparison of the 4 different Ni plated structures

It was possible to observe that for every sample the peak relative to the families of planes (111) were more intense than the other two peaks present.

Furthermore it could be observed that the crystallographic orientation defined by the family of planes (200) was more present than that defined by the family of planes (220), although in absolute value was always very low; this trend did not hold for the 30 minutes plated sample, for which the tendency is diverted, meaning that a longer deposition time would have led to a slightly different crystallographic structure.

Finally, a slight peaks broadening could be sought as the plating time increased, which was a sign of grain size growing.

Using Scherrer equation it was possible to relate the size of the crystallites to the deposition time:

$$\tau = \frac{K\lambda}{\beta \cos\theta}$$

where:

- τ is mean size of the ordered crystalline domains;
- K is a dimensionless shape factor;
- λ is the X – rays wavelength;
- β is the is the line broadening at half the maximum intensity (FWHM), after subtracting the instrumental line broadening, in radians;
- θ is the Bragg angle.

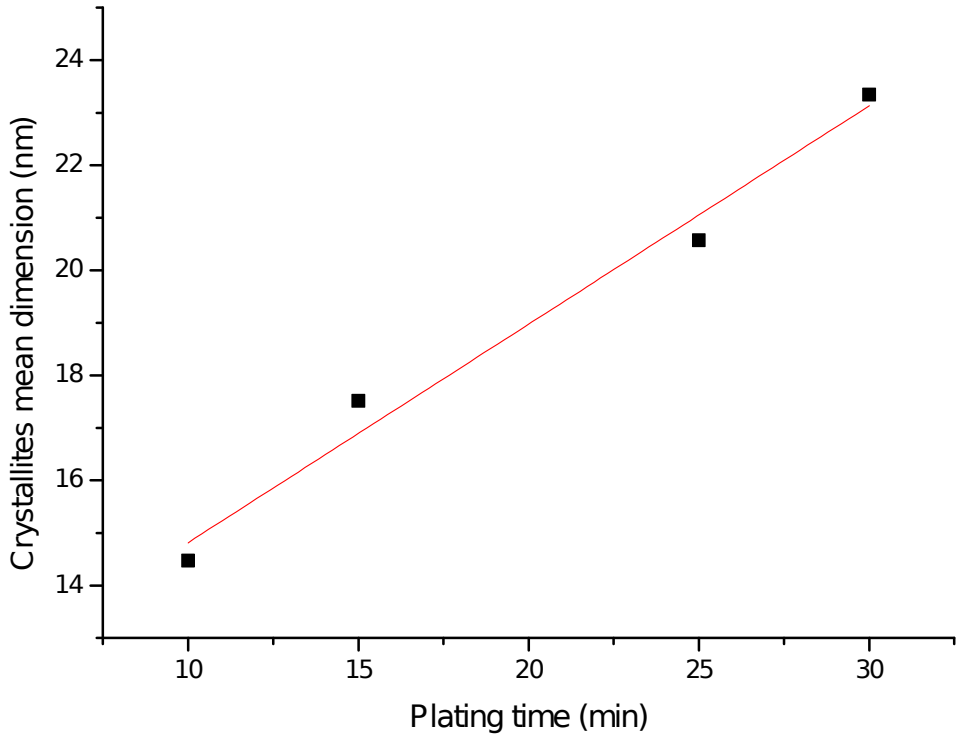

Fig. 3.21: application of the Scherrer equation to understand crystallites size evolution

Unfortunately the 30 minutes mark was not a free choice: the 40 minutes sample was totally delaminated because of the loss of adherence. Actually, at 35 minutes some pits occurred in the Nickel layer; hence this sample were not included in the analysis.
Interestingly also a lower limit to the deposition time was found: despite the homogeneity of the metal layer, the 10 minutes sample was not completely covered.
Nevertheless its XRD graph has been taken in consideration because of the informations about Nickel crystallographic structure in the first minutes of the plating process.

Lastly, taking a look at the 10 and 15 minutes samples XRD peaks, the Silicon Oxide (311) peak was not visible, while in the higher deposition times it was no more, which clearly pointed out the complete coverage of the sample with the Nickel metal layer.

3.3.3 Nickel Film SEM Characterization

In order to grasp the evolution of the Nickel layer thickness and quality evolution, a SEM characterization using primary electrons was performed onto the above cited samples; for those without complete metal coverage a suitable choice of the measure spots was done.

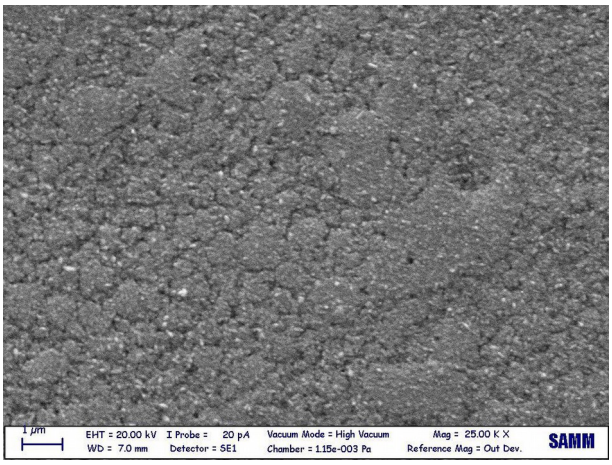

Fig. 3.22: 10 minutes Nickel deposit

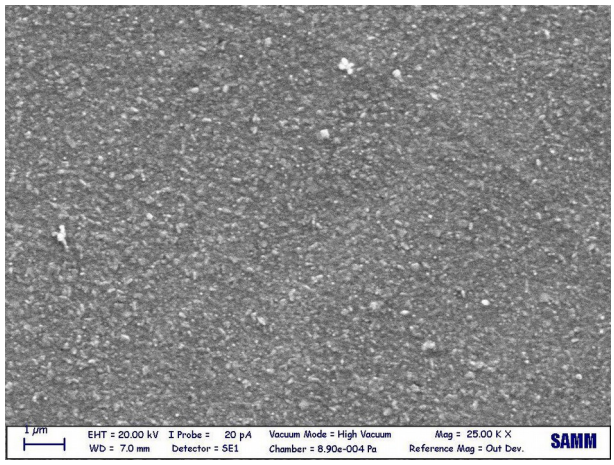

Fig. 3.23: 15 minutes Nickel deposit

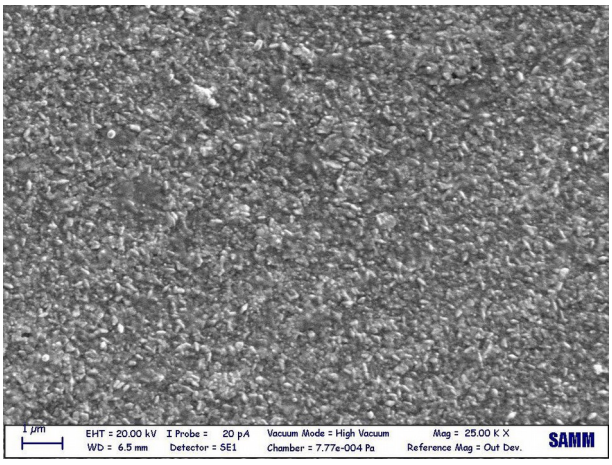

Fig. 3.24: 25 minutes Nickel deposit

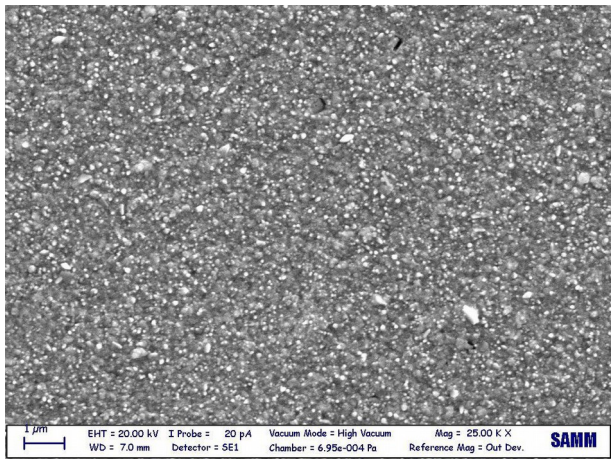

Fig. 3.25: 30 minutes Nickel deposit

The increasing density and homogeneity of the Nickel layer was appreciated as the plating time increased.

A profile analysis is presented too.

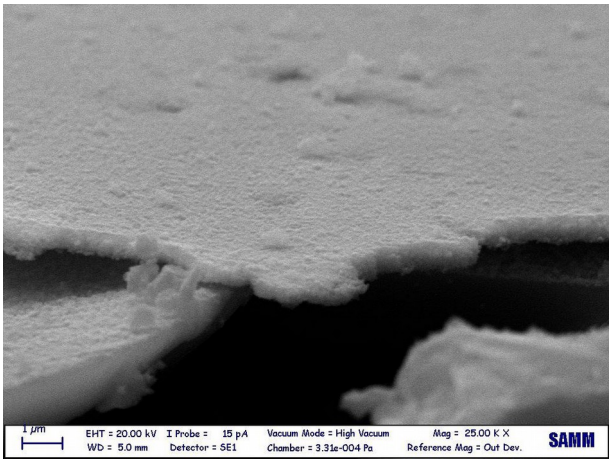

Fig. 3.26: 10 minutes deposited Nickel thickness

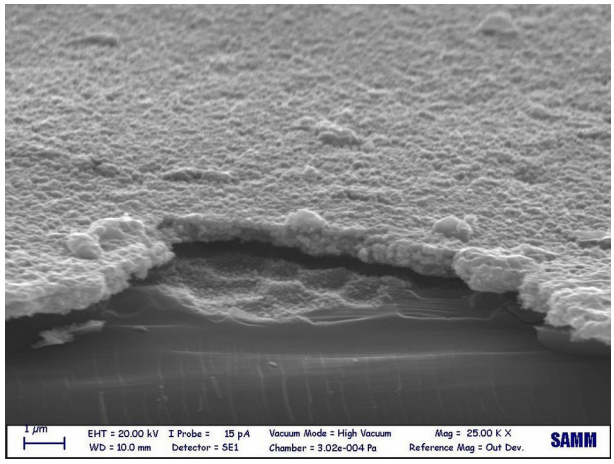

Fig. 3.27: 15 minutes deposited Nickel thickness

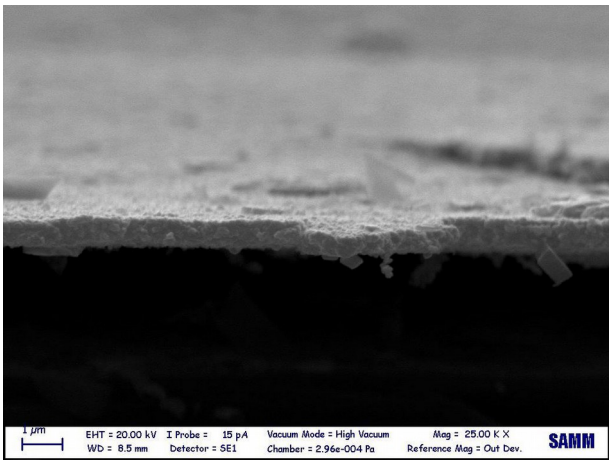

Fig. 3.28: 25 minutes deposited Nickel thickness

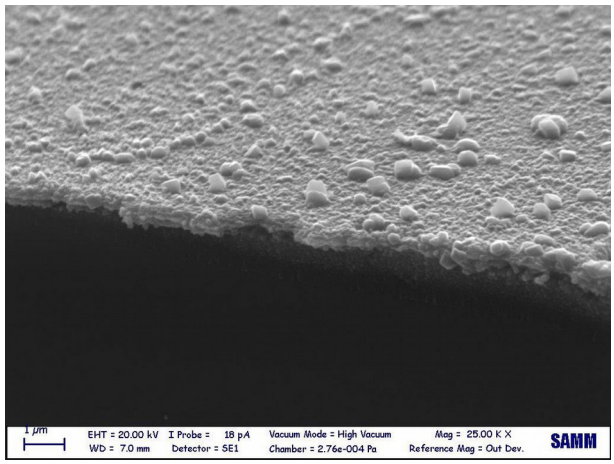

Fig. 3.29: 30 minutes deposited Nickel thickness

The Nickel film thickness did not increase in with a linear proportionality relation with the deposition time, as this pictures showed. This result may be expected if one reflects on the galvanic displacement deposition mechanism: as stated in chapter one, galvanic displacement is a self – limiting process because of the limited Silicon surface available for metal atoms reduction. Then, the metal film thickness could not increase indefinitely but reached roughly 600 nm already at 10 minutes and no further growth occurred at longer plating times.

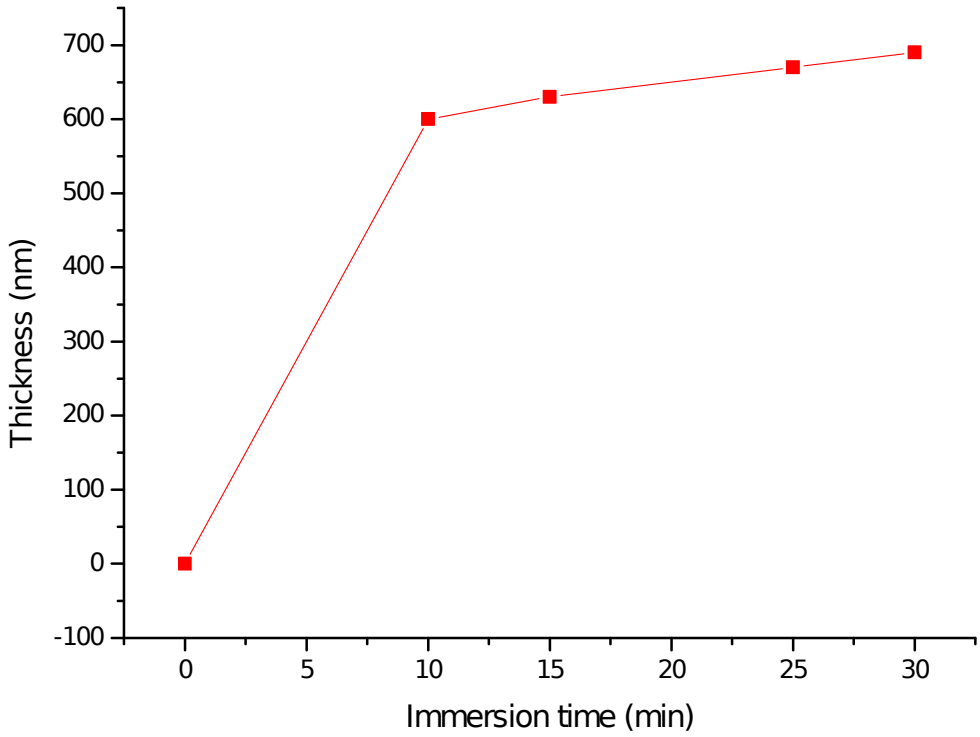

Fig. 3.30: Ni deposit thickness as a function of plating time

3.3.4 Nickel Film AFM Characterization

The AFM analysis was realized in order to understand key parameters of the plated surface, such as mean surface roughness. The analysis was performed on the 30 minutes sample, because of the higher film compactness and because of it should have displayed the highest surface roughness among all the Ni/Si samples. The AFM imaging was performed in contact mode.

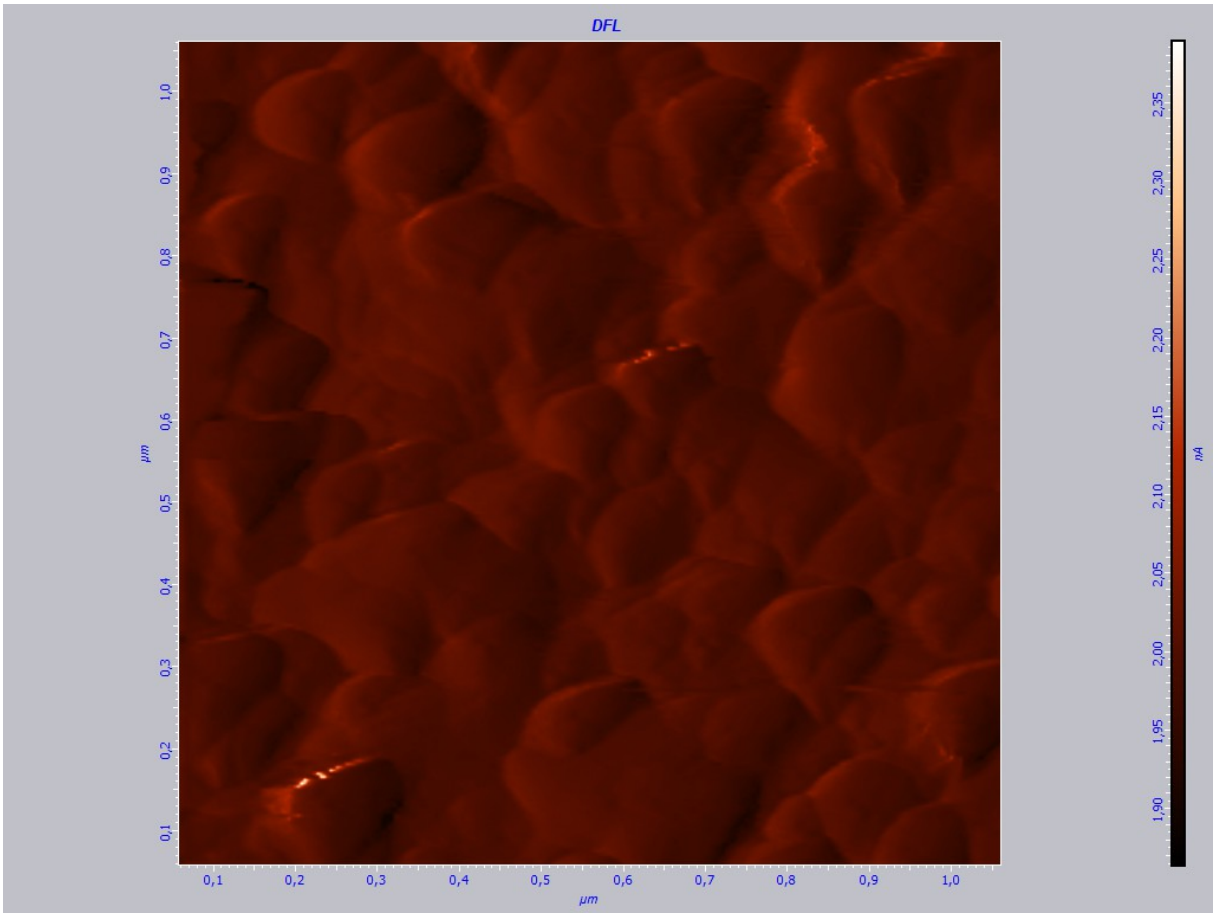

Fig. 3.31: dft image of the 30 min Ni/Si sample

And a 3D image was captured too:

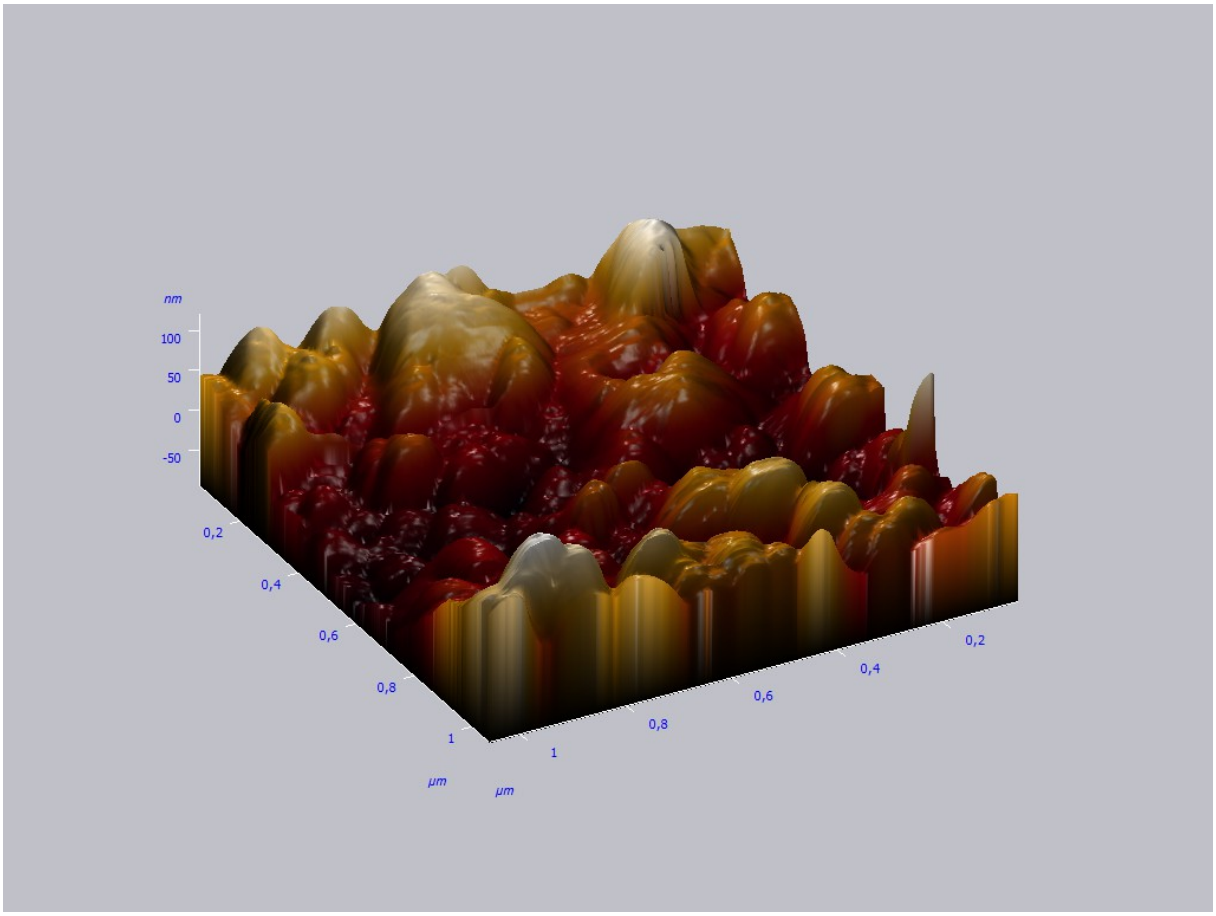

Fig. 3.32: 3D image of the 30 min Ni/Si sample

From AFM analysis a mean surface roughness of 33 nm was measured.

Thus, given all the above data, the 25 minutes deposition time sample was chosen for the graphene chemical vapour deposition to perform onto: actually it displayed quite intense XRD peaks, no Silicon (311) peak, a complete and homogeneous metal coverage and no sign of film delamination.

As already said, carbon solubility is very high so there was not the need of selecting particular preferential orientation of crystalline planes in order to enhance Carbon solubility; this led to no need of performing an annealing process to change the cited preferential orientation and Nickel microstructure.

This in turns is a great advantage, because any process involving the manipulation of the so deposited metal film would raise the costs and time burdens of the proposed technology, reducing the application possibilities of direct fabrication of graphene on Silicon Oxide.

3.3.5 FLG/Ni/Si Substrate and Raman Spectroscopy

The first experiment was performed on the cited Nickel sample, keeping the temperature at **1000°C** and the furnace dwelling time at **2 min.**

Sample surface morphology appeared as follows:

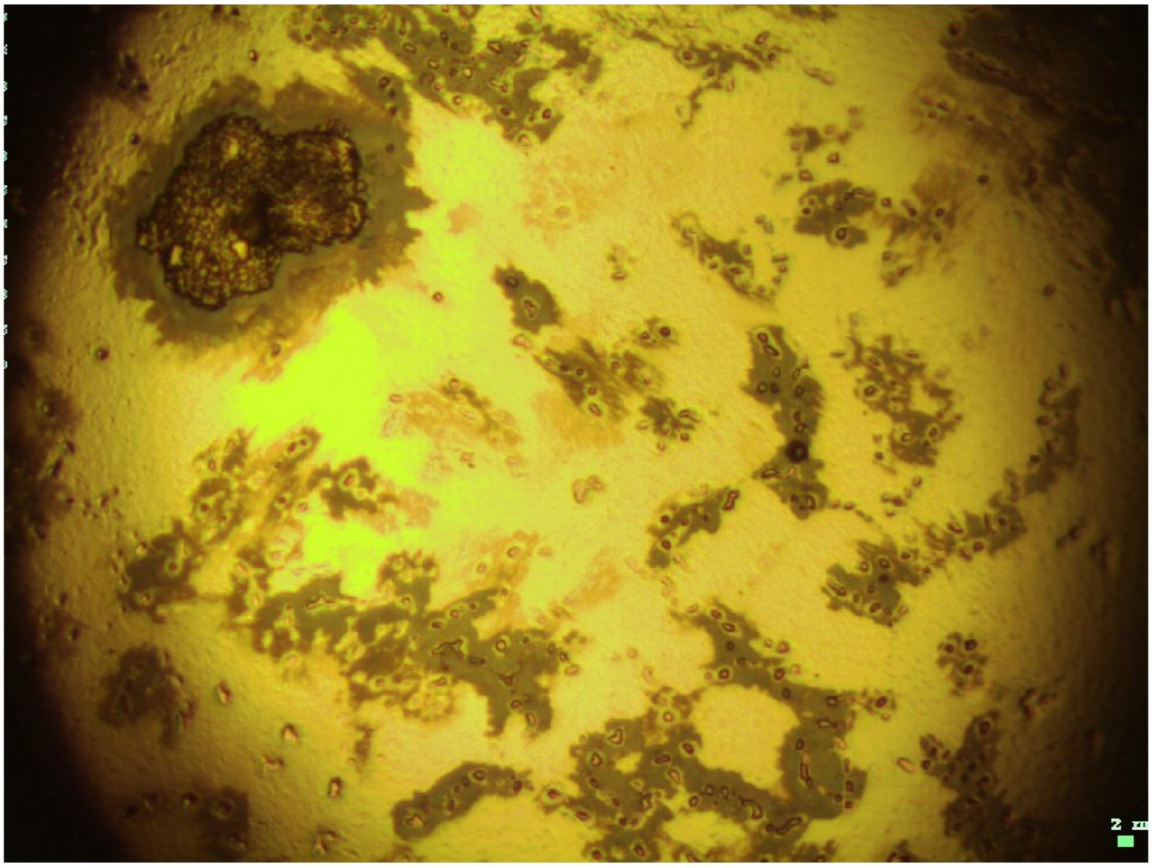

Fig. 3.33: optical image of the Ni/Si system after CVD at 1000°C

As could be sought, the surface morphology presented differences and analogies to the one obtained after graphene CVD on the self – standing Nickel film. Actually, inhomogeneities in the deposition were still perceived, but the structure was more web – like: brighter and darker areas seemed to be linked by light grey portions, possibly a graphene sub – monolayer.

A final remark: the pits that could be sought on the surface of the sample were due to the intrinsic aggressiveness of the solution, which corroded spots of Nickel.

The solution optimization could be a starting point for future works.

In order to understand the quality of the deposition, a complete Raman investigation was carried out. Indeed, all the different coloured regions (fig. 23) were analysed and the following scheme has been obtained:

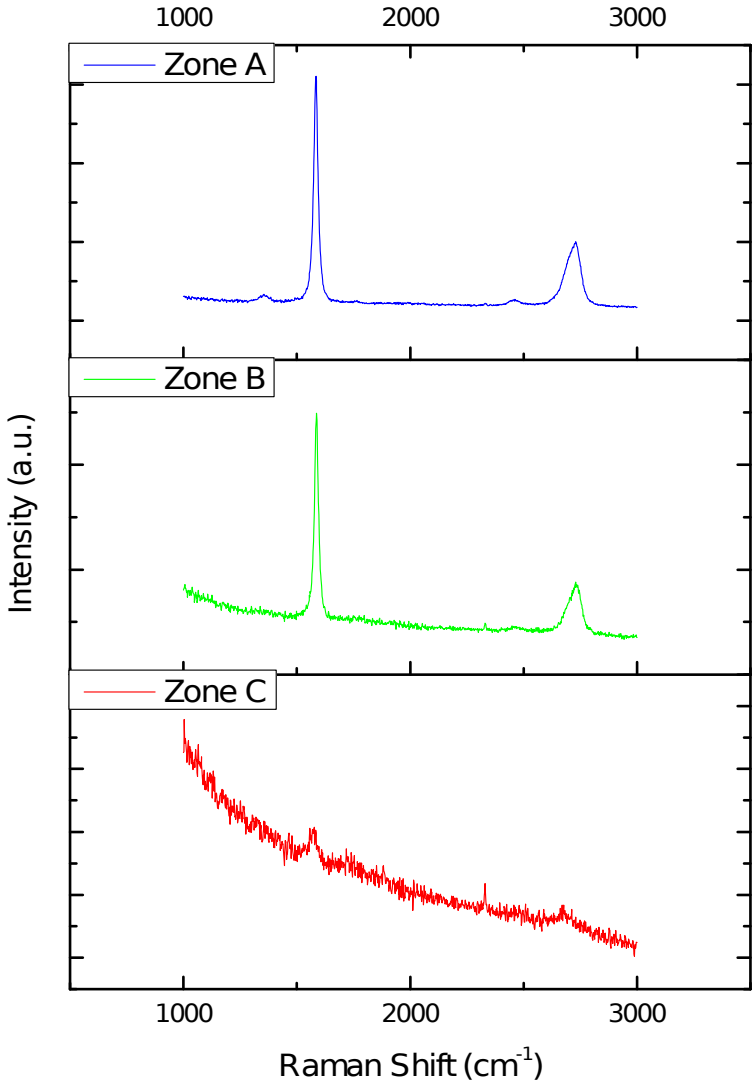

Fig. 3.34:comparison of Ni/Si system Raman spectra in different spots

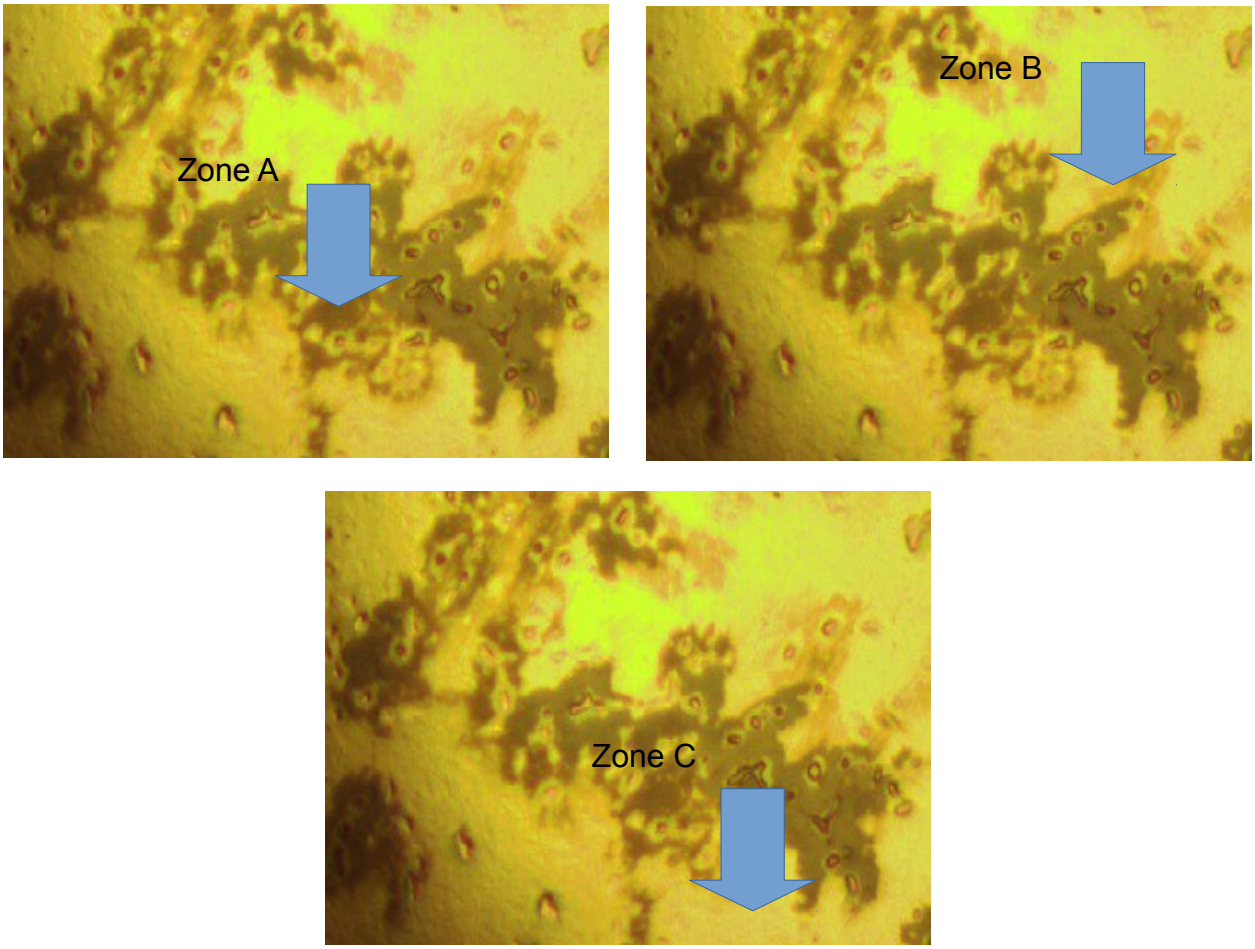

Fig. 3.35: different inspection points

A table reporting peak intensities and frequencies, as well as the I(G)/I(2D), follows:

	I(G)	G frequency [cm^{-1}]	I(2D)	2D frequency [cm^{-1}]	$\frac{I(G)}{I(2D)}$
Zone A	6205,7783	1583,7	2001,2662	2729,7	3,1
Zone B	2493,0574	1587,0	882,25244	2728,7	2,8
Zone C	(814,84259)	(1575,7)	(567,46027)	(2670,2)	(1,43)

In all three zones analysed, Raman spectroscopy detected graphitic structures, in accordance with the values of the I(G)/I(2D). The Zone C ratio (as well as the intensities) have been reported, but the high noise measurement made difficult spectrum analysis. This is in “good agreement” with the hypothesis that the brightest

zones are covered by a graphene sub – monolayer, which could be regarded as a defected, non continuous monolayer. A quantitative evaluation of the number of layers can be found in the bands deconvolution section and in the XPS analysis section.

The second experiment carried out considering a lower deposition temperature, just because of the high solubility of Carbon into the Nickel lattice. Therefore, the same CVD process was performed, but the reaction temperature was fixed at **900°C**; indeed, lowering the reaction temperature would lower again the production cost, making the process more valuable for the large scale industry. Furnace dwelling time was kept at **2 minutes.**

Here is an image of the resulting sample took with the optical microscope:

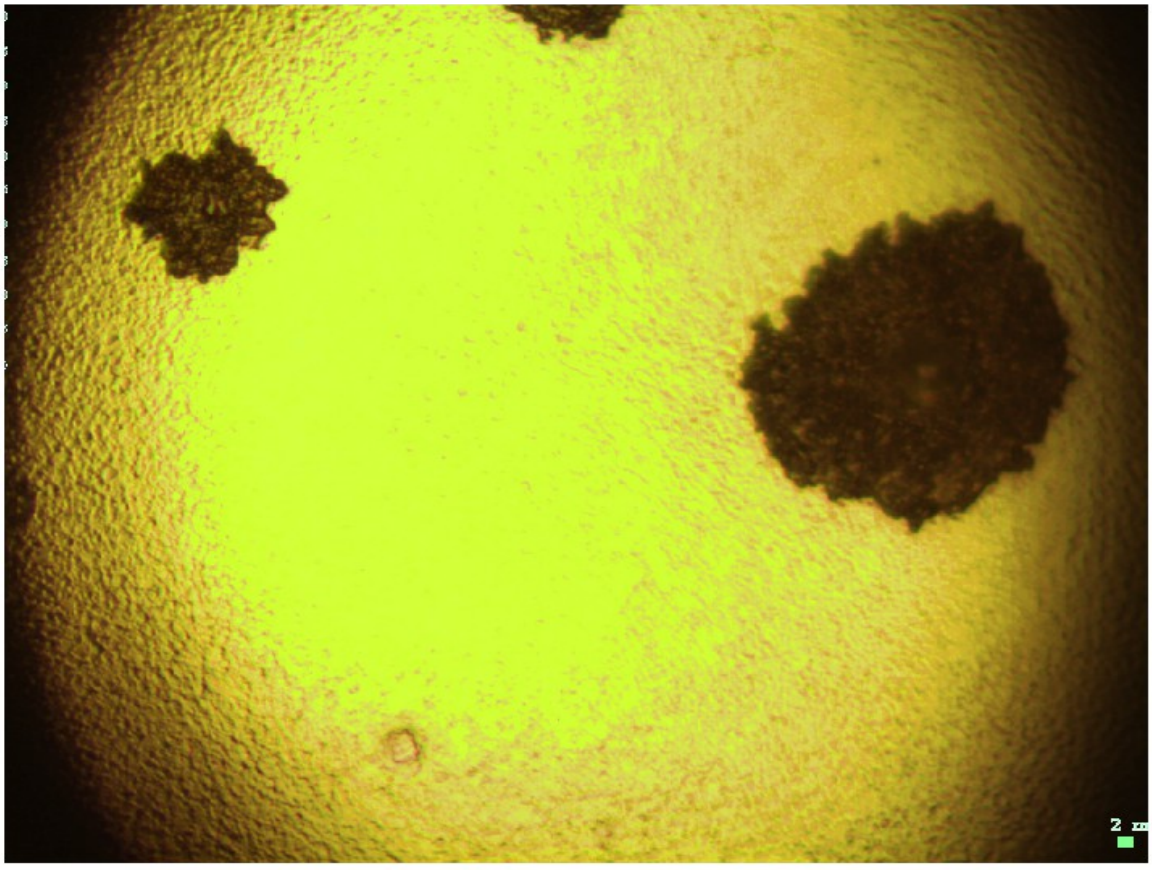

Fig. 3.36: optical image of the Ni/Si sample deposited at 900°C

The absence of any dark shade or web – like grey structure was the first thing noticed about this picture, a part from the pits induced by the solution environment.

A further investigation through Raman spectroscopy was then needed in order to understand the sample microscopic appearance.

Two random points were selected for the measurement, D point and E point: Indeed no visual difference was appreciable between the two points due to the high regularity of the surface.

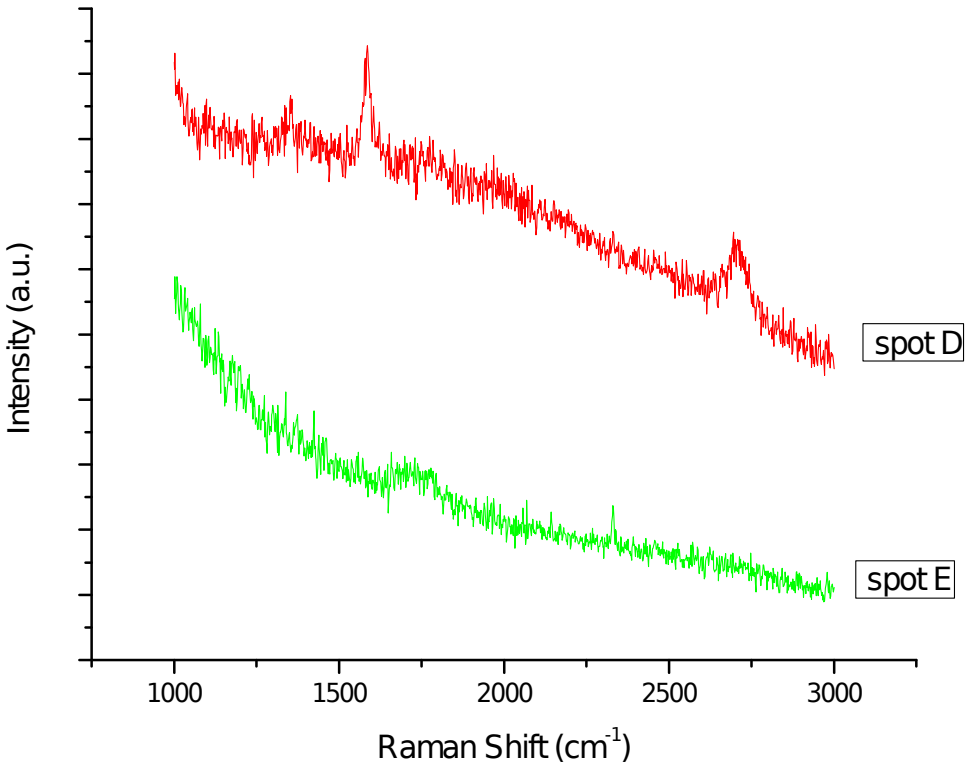

Fig. 3.37: Raman spectra of two random point on 900°C CVD Ni

As it can be seen, the background noise was still present but in the D spot Raman spectrum some peaks could be assigned.

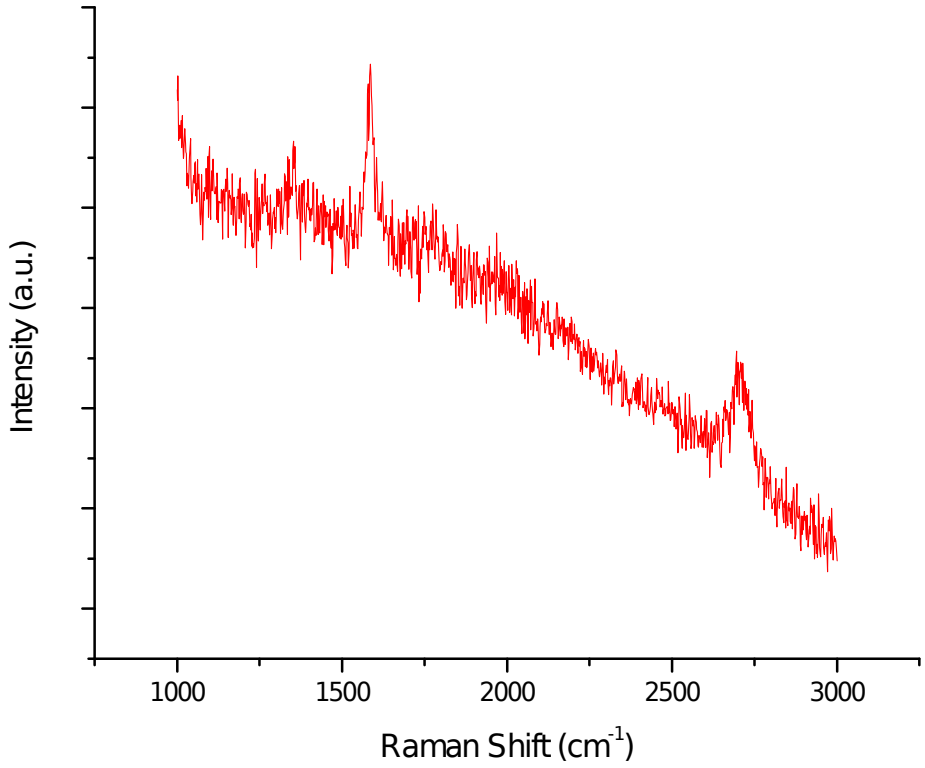

Fig. 3.38: 900°C CVD Ni spot D Raman spectrum

The presence of the D peak let understand that a disordered carbonaceous film was present. As for the previous sample's bright areas, it was likely that a sub – monolayer had been deposited once again.

Unfortunately this was not a good result, because a so non – structured layer could not be used as active layer for charge transport nor for a protection purposes because of its lack of complete surface coverage.

As it might appear clear the 900°C chemical vapour deposition process was labelled as not viable and the 1000°C one was picked up for further characterization and for the last experimental session of the present thesis work.

In fact, in order to make suitable the direct fabrication of graphene onto Silicon Oxide for the large scale industry, it must be adapted to the on hand production.
So the last part of the practical work was devoted to the application of the technology developed until here to a commercial MEMS wafer, supplied again by ST MICROELECTRONICS.

3.3.6 FLG/Ni/Si SEM Characterization

SEM analysis was performed on the 1000°C, 2 minutes FLG/Ni/Si sample, just for the sake of completeness: SEM was not able to reveal any trace of Carbon onto the surface just because of the analysis properties. In fact, the electrons beam just passed through the graphene layer because of it was thinner than 10 nm (the actual SEM resolution for this kind of substrates). Anyway, the surface image is reported; as it can be noticed, Nickel surface was far less rough, probably due to the CVD thermal treatment.

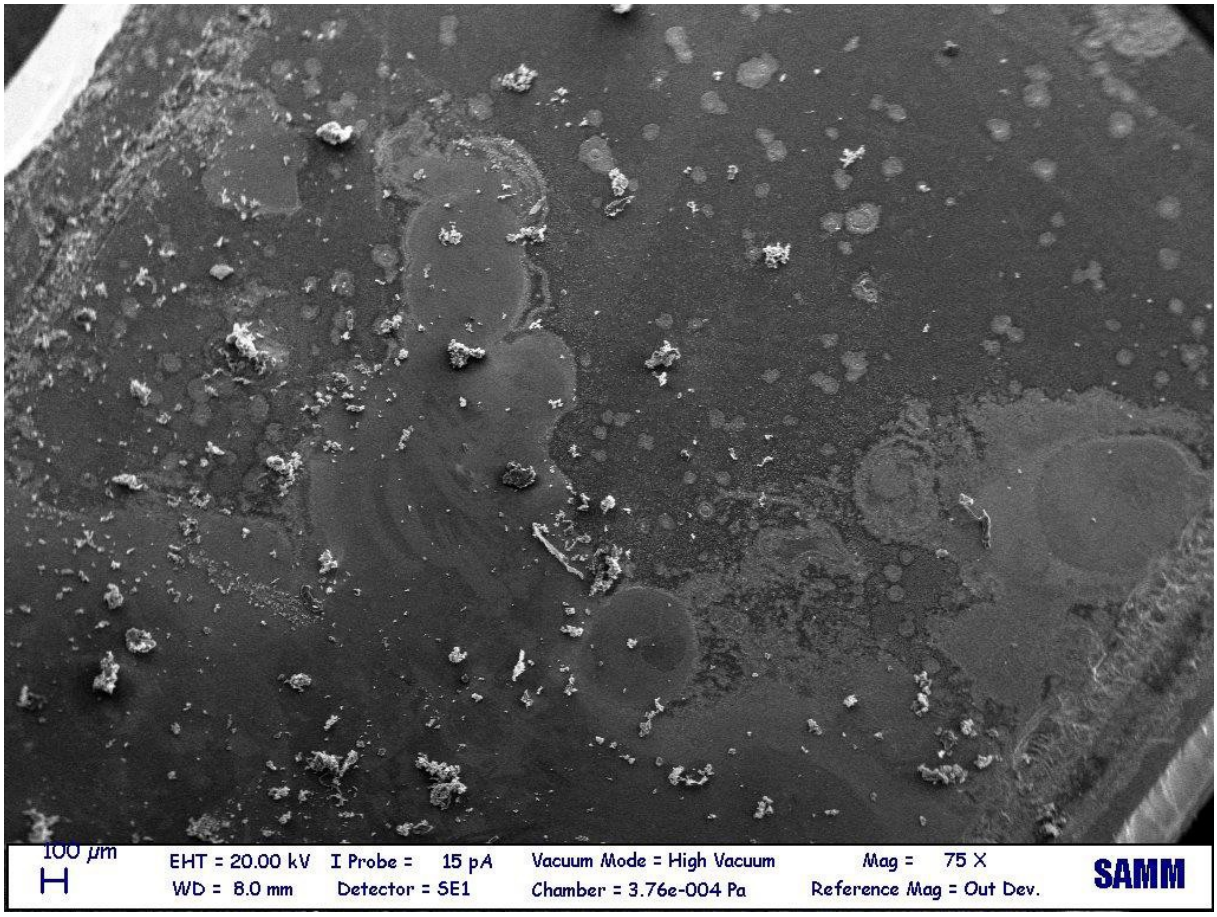

Fig. 3.39: 75x magnification CVD Ni/Si SEM image

A higher magnification picture was captured in order to find some significant feature:

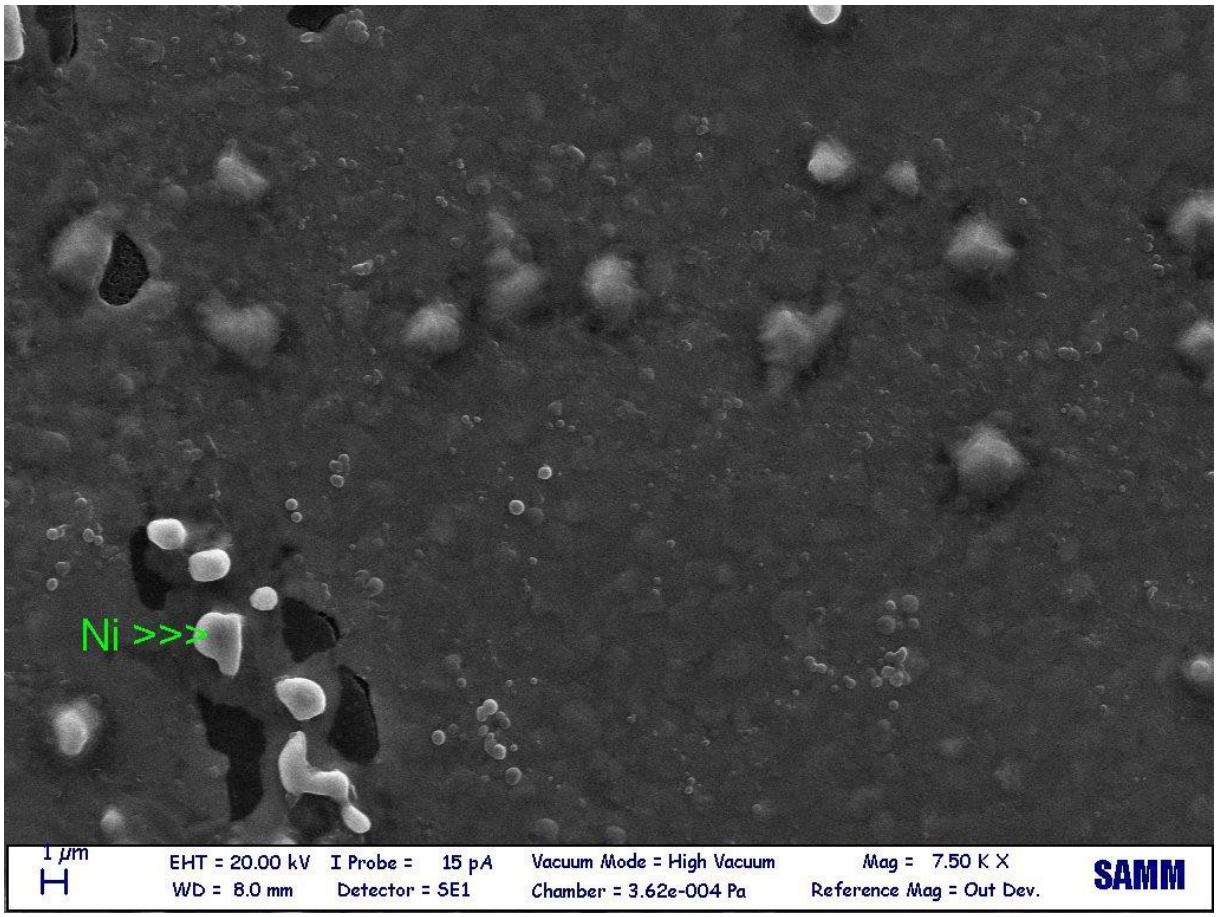

Fig. 3.40: 5000x magnification CVD Ni/Si SEM image

Again, no Carbon signal was detected.

3.3.7 FLG/Ni/Si AFM Characterization

Through an AFM analysis it is possible to observe how the heat treatment of the CVD process modify the structure of the alloy and how the graphene (or graphite) is structured. AFM analysis was realized on the Nickel/Silicon Oxide sample which underwent the 1000°C CVD process.

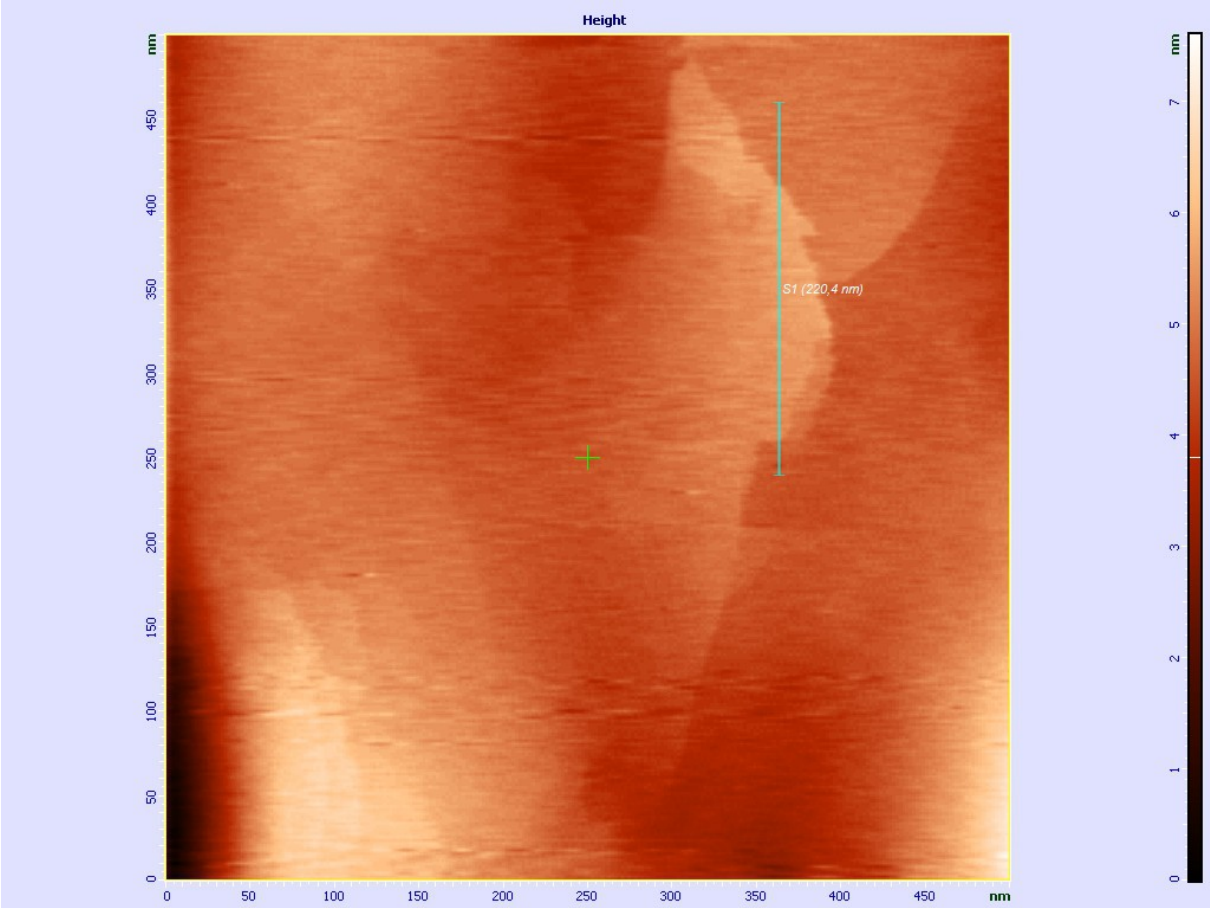

Fig. 3.41: dft image of the graphene deposited onto the Ni/Si system

It was possible to observe the presence of graphene sheets as flat areas delimited by boundary zones. Graphene seemed to be uniformly distributed over the entire area without overlapping; this is understood by the absence of wrinkles at the sheets boundaries.

This resulted clear also from the profile informations, as can be seen in fig.3.42:

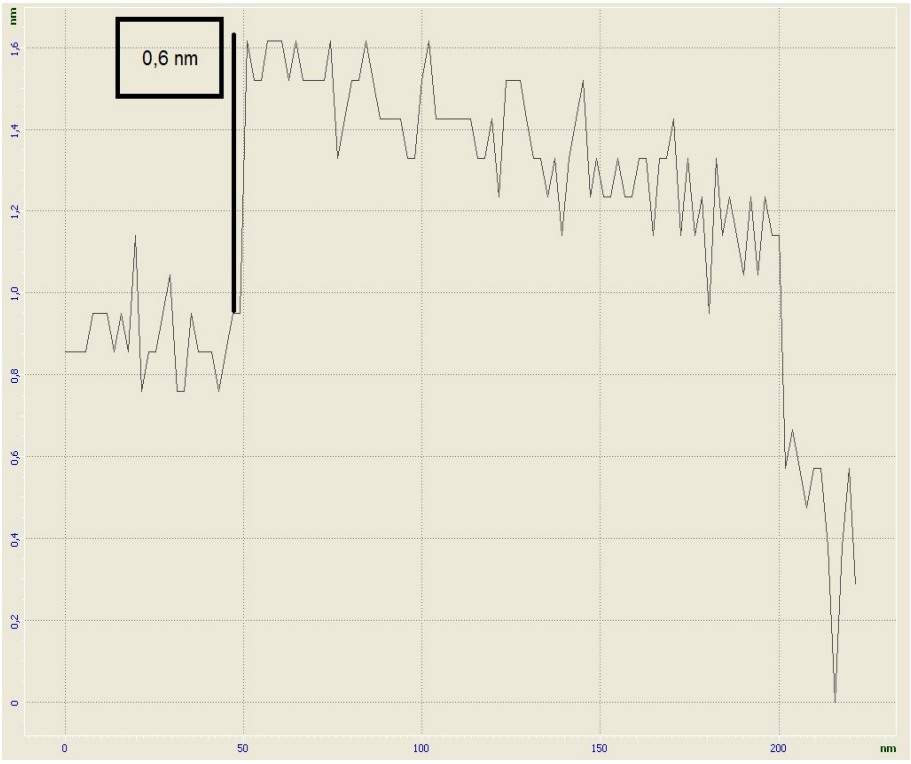

Fig. 3.42: qualitative evaluation of the graphene layers thickness

Given the profile graph of the inspected area, it was possible to make a first estimation of the graphene layers thickness *on top* of the Nickel surface; the y axis reported endoscopic lengths and, in particular, it could be said that 0,6 nm of graphene layers were present at the very top of the sample. Literature suggest a 0,335 nm [59] inter planar distance for graphite, so a simple ratio yielded, roughly, **2 graphene layers.** These data have to be intended referring to the highest feature measured on the surface of the sample.

And the 3D image of the film has been taken too:

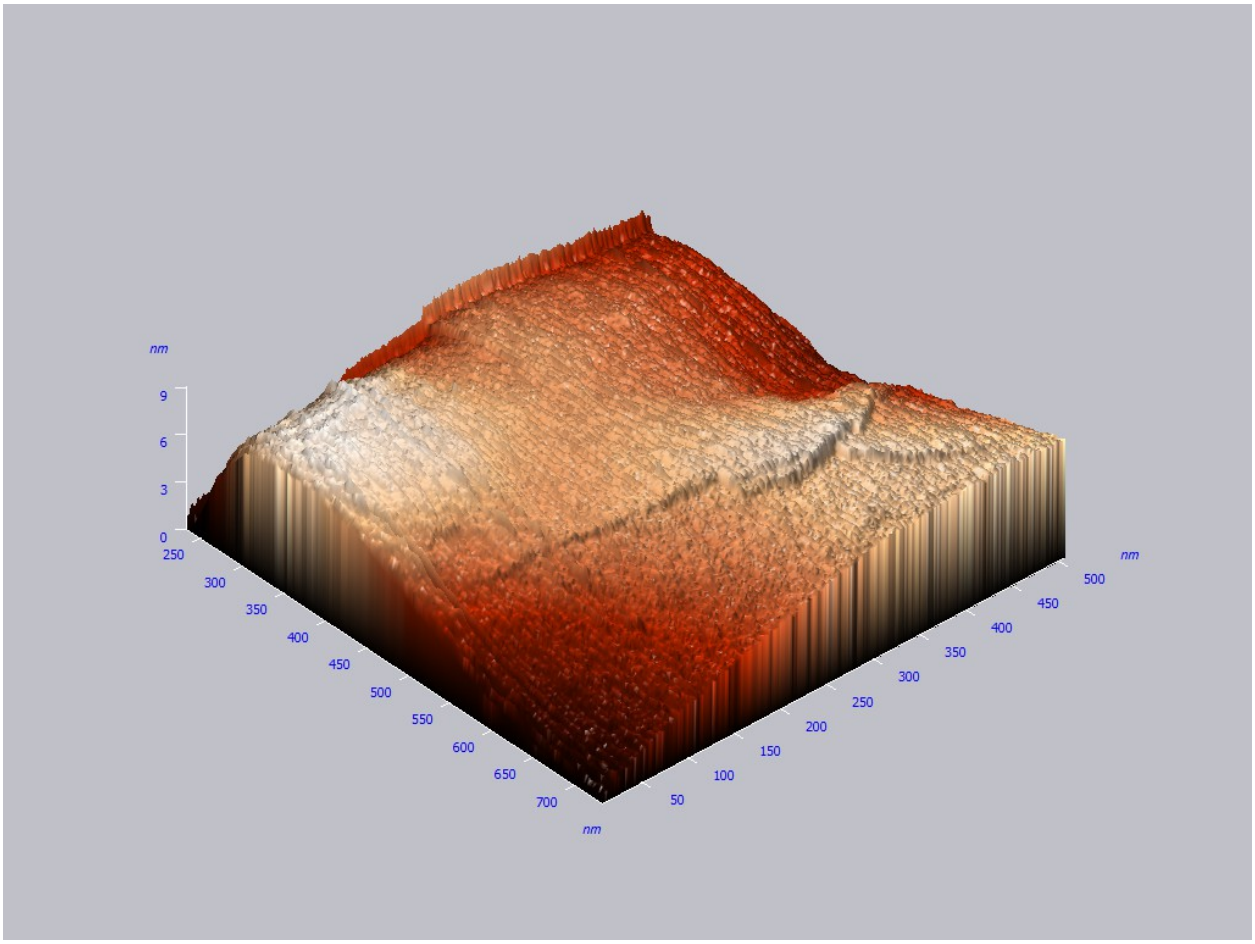

Fig. 3.43: 3D AFM image of few graphene layers

3.3.8 FLG/Ni/Si 2D Peak Deconvolution

The visual comparison between the collected spectra and literature models did show a validation for the four layers graphene [55]. It was not possible to assert that we deposited graphite because the shape of the measured 2D Raman bands of the proposed samples and the graphite one did not correspond.

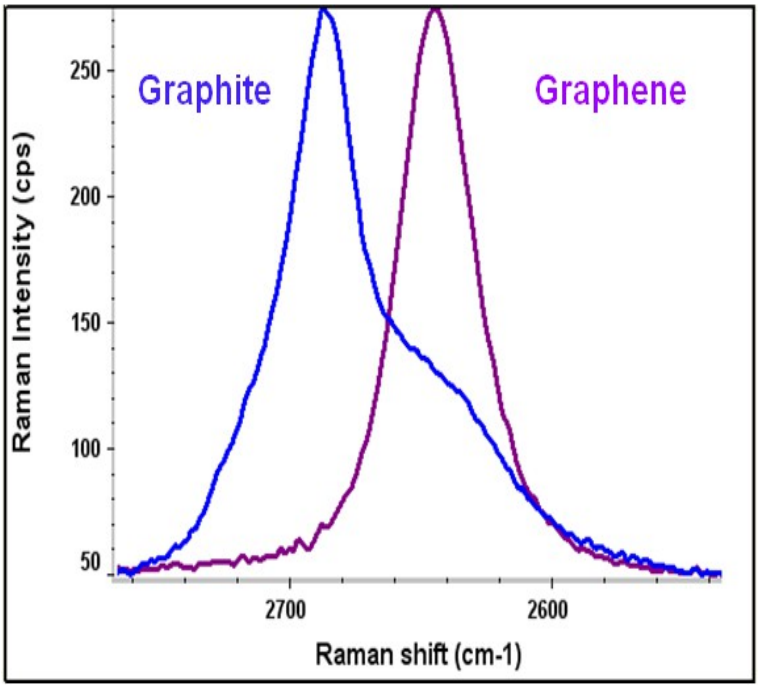

Fig. 3.44: graphene and graphite 2D peak shape differences

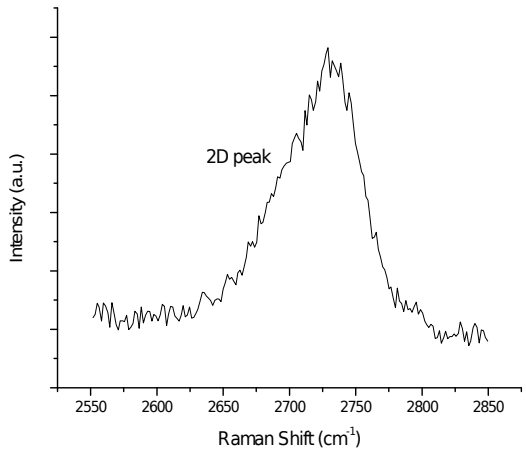

Fig. 3.45: 1000°C, 2 min CVD Ni/Si 2D peak shape

In contrast with graphene, the 2D bands corresponding to a four layers graphene showed more complex shapes, as the following picture shows:

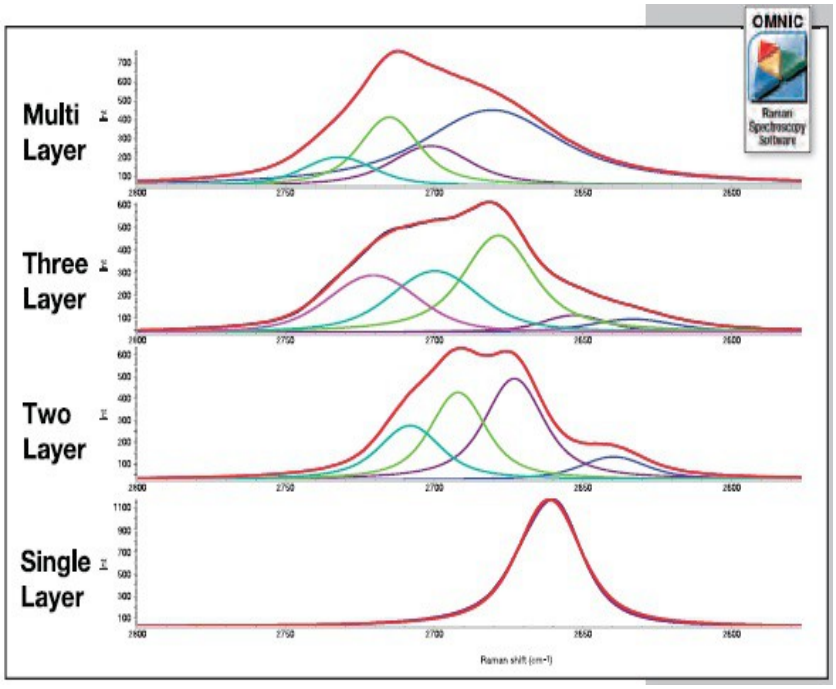

Fig. 3.46: 2D band evolution in FLG

Given that is not possible to attribute their position to a unique frequency, in order to extract characteristic frequencies, bands deconvolution with a defined set of Voigt curves has been employed.
The term characteristic frequencies intends the relative position of the Voigt curves in the spectral range.

Unfortunately the samples nature is extremely different with respect to the reference one: literature samples were mechanical exfoliated graphene foils, deposited onto a Silicon oxide structure by using a PMMA support; the presented sample were deposited directly onto an annealed metal and thus many differences arose.
Further more Voigt curves have been used and the result was a 4 – curves deconvolution for the flat Ni/Si (3.46 figure) and a 5 – curves deconvolution for the plated MEMS wafer (3.45 figure).

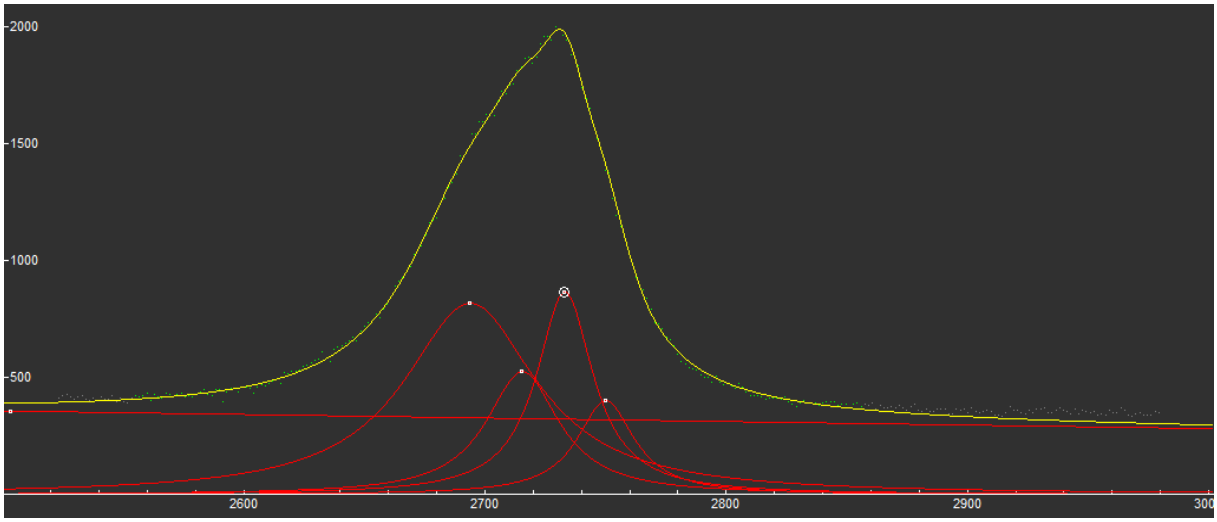

Fig. 3.47: 1000°C, 2 min Raman 2D peak deconvolution with Voigt curves

And the characteristic frequencies found were:

- 2692,96 cm^{-1};
- 2727,89 cm^{-1};
- 2728,08 cm^{-1};
- 2742,93 cm^{-1}.

These results gave credit to the assumption made before that **3 to 5 graphene layers** were present on the inspected sample.

3.3.9 FLG/Ni/Si XPS Analysis

Due to the difference between the literature reference graphene substrates and those realized in the present work, a XPS analysis has been performed onto the flat Ni/Si system. XPS analyses were carried out by using an Escalab 250Xi (Thermo Fisher Scientific Ltd, UK) equipped with a monochromatized Al Ka source, electromagnetic lenses,

6 – channeltron detector for spectroscopy and multichannel plate for chemical imaging. Acquired spectroscopic data were processed by the Avantage v.5 software.

All measurements were performed at CNR Roma.

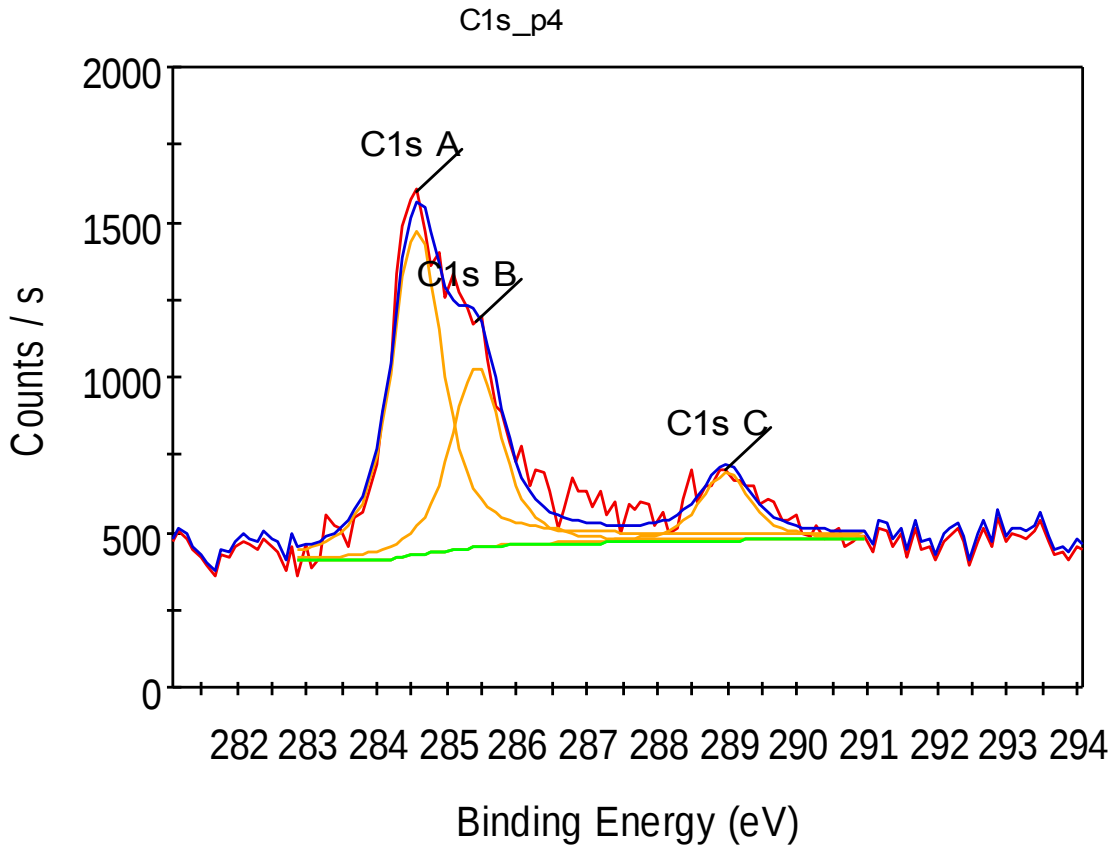

Fig. 3.48: XPS analysis of Ni/Si sample after CVD

Grazing angle measurements: from C1s/Ni2p3 ratio was determined the thickness of C overlayer, about 1,3 to 1,5 nm. Again, considering a 0,335 nm as inter planar distance, it could be said that **3 to 5 graphene layers** were present. It must be kept in mind that

XPS spatial resolution was higher than all of the other characterization methods employed (200 μm diameter) so it glimpsed a wide portion of the deposit: the values reported are to be intended as mean values.

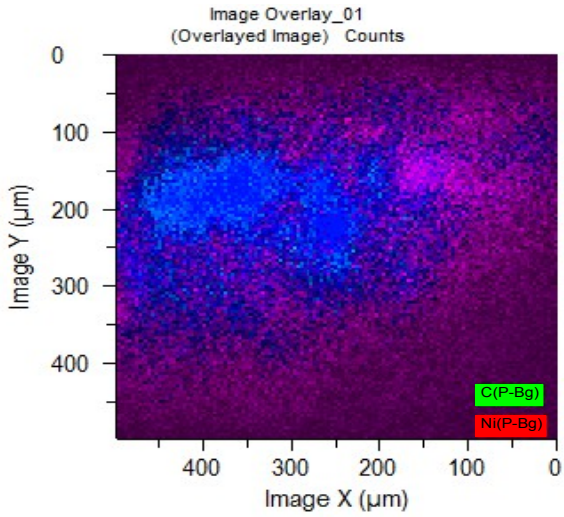

Fig. 3.49: Overlay of Ni2p and C1s images; blue corresponds to the more intense signal of Ni2p (i.e. thinner C overlayer)

Blue corresponds to the more intense signal of Ni2p (so a thinner Carbon overlayer), where is present graphene with an average thickness of 1,3 nm.

3.3.10 FLG/Ni/Si GDOES Investigation

Glow Discharge Optical Emission Spectroscopy is able to highlight the order films are deposed onto a surface, by means of a plasma produced on the same surface.
The mass spectrometers did recognized carbon layers on top of the Ni/Si surface, giving another clue of graphene presence on the device: in fact the sharpness of the Carbon peak gave credit of a low material concentration.

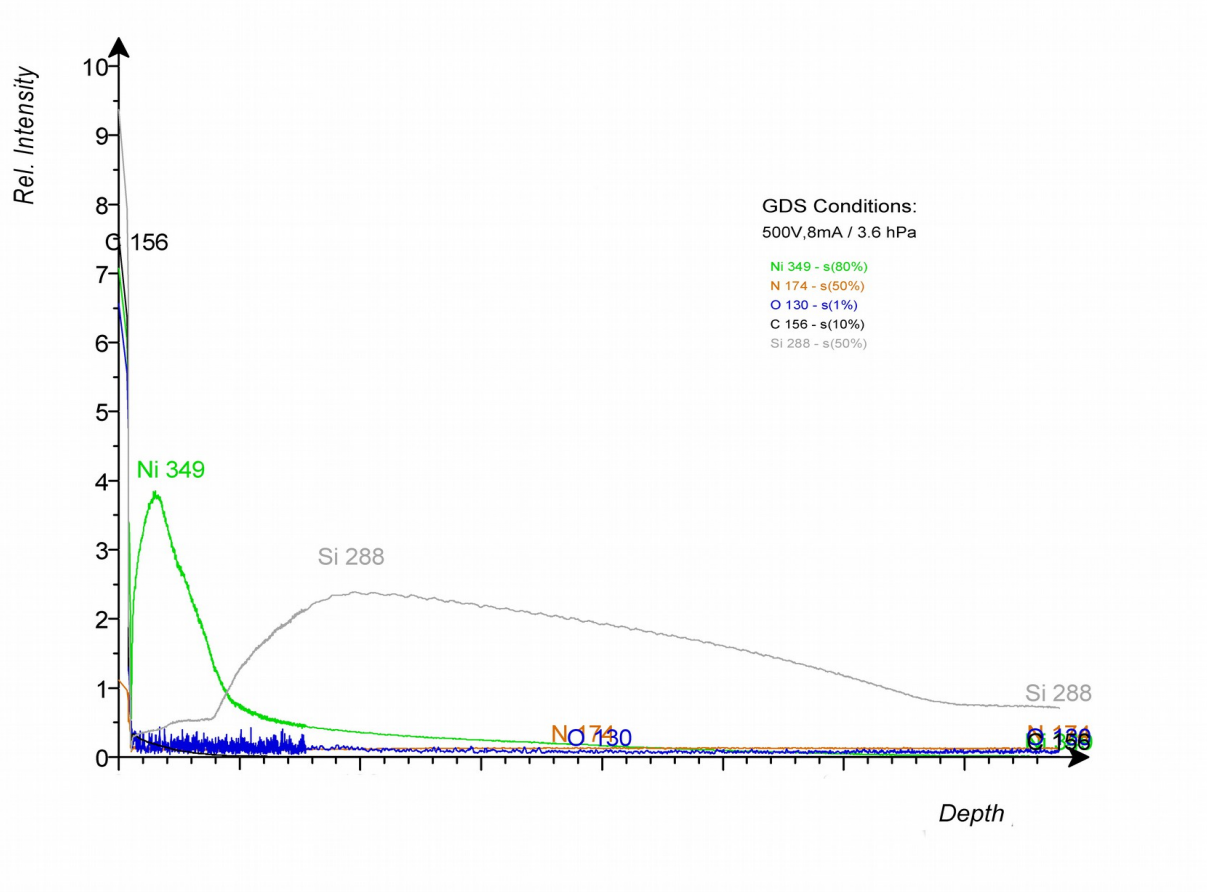

Fig. 3.50: GDOES analysis of the flat Ni/Si after CVD

It was possible to observe the very sharp Carbon peak on the sample's surface while after few nanometers the Nickel signal appeared; there is an overlap between Nickel and Silicon signals, which was probably due to an intermetallic compound formed at the Ni/Si interface.

3.4 MEMS Application

After the characterization of the graphene/FLG layer obtained onto the flat Ni/Si substrate, the natural evolution of the experimental route was the application of the proposed technology to a microstructured substrate.

Sample pretreatment was slightly different: the microstructured sample could not be immersed for 10 minutes in the Hydrofluoric Acid because of the possibility to etch away the floating parts of the device and no sonication was applied to avoid the disruption of the features because of the mechanical stresses induced by the sonic waves.

So a fast degreasing in acetone and a 1 minute HF etching were performed onto the micro device.

Nickel displacement plating was performed with no substantial changes; here is the samples aspect after galvanic displacement step, observed with optical microscope :

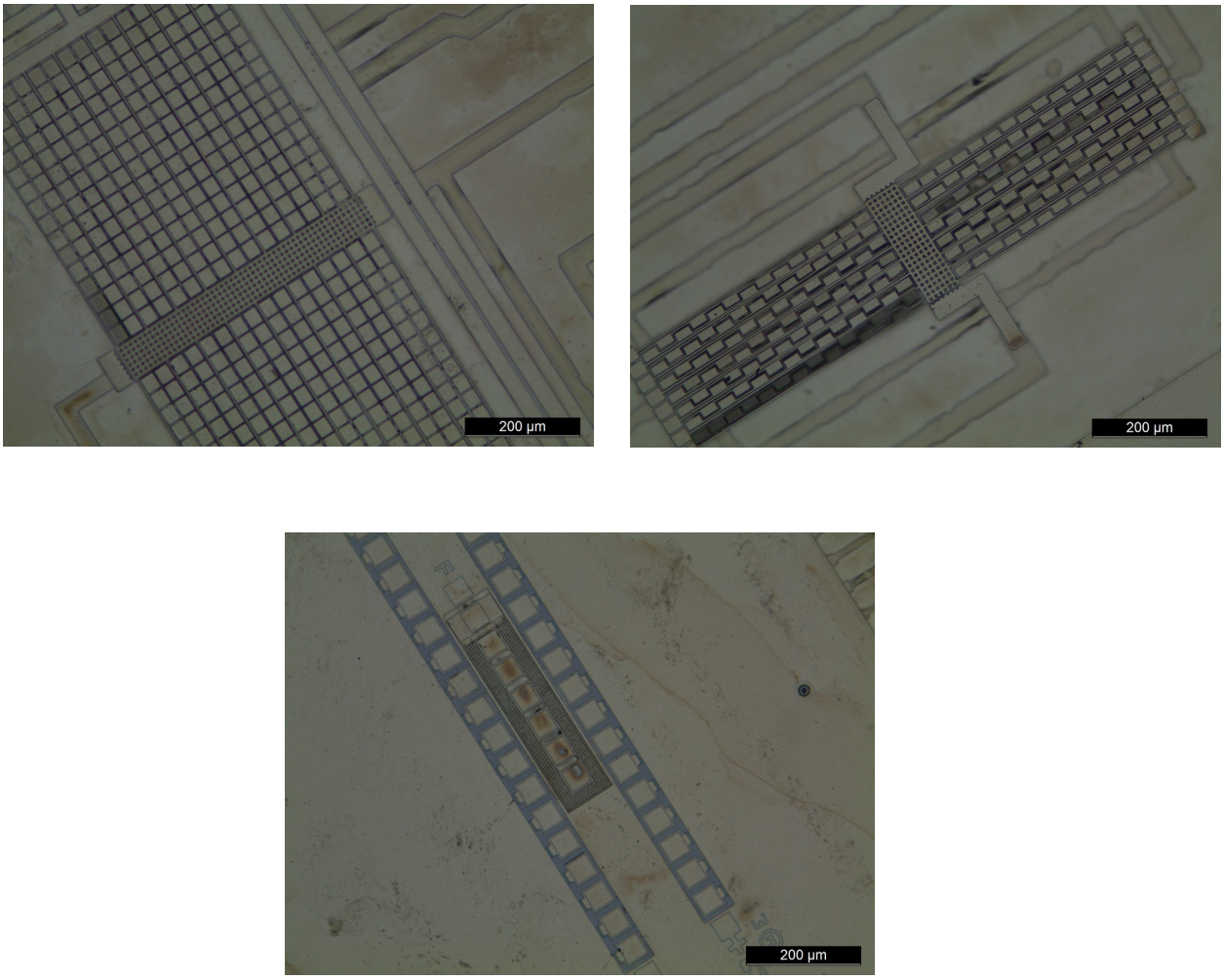

Fig. 3.51: MEMS after Nickel plating

Surface morphology appeared regular and homogeneous in all point but the areas covered by the protective photoresist, which were not covered.
The focus was onto the floating parts, which are those that most suffer stiction failure: these were all covered by a homogeneous metal film.

The thermal cycle the samples underwent was the following:

- 30°C/s heating ramp;
- 2 minutes at 1000°C;
- free cooling.

The CVD followed the step presented in the previous section without alterations.

Samples optical image were taken after graphene deposition (500x magnification):

Fig 3.52: MEMS substrate after CVD

Sample aspect was very similar to that of the flat Nickel and the floating parts coverage was complete. Dark and bright area was still present and again the web – like structure was visible.

Raman spectroscopy was then qualitative applied, just to verify the possibility of application of this technique:

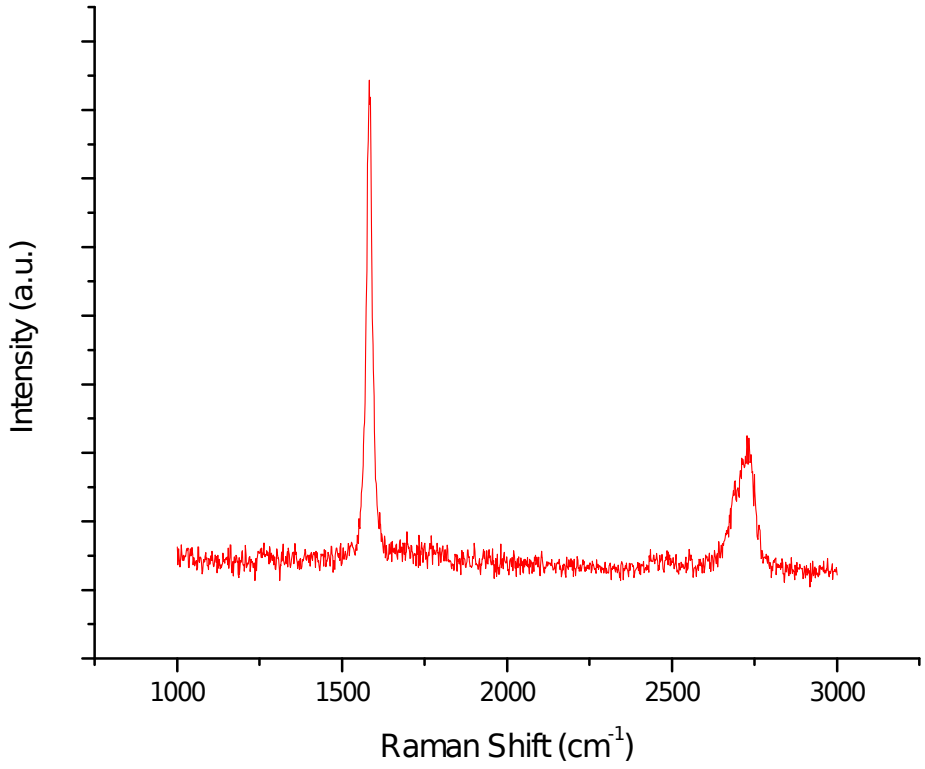

Fig. 3.53: CVD MEMS Raman spectrum

The spectrum was low intense but the shape was not unmistakable: both the G and the 2D peaks were present and the I(G)/I(2D) was more or less 3, which is a very good result.

3.4.1 CVD MEMS SEM Characterization

MEMS samples were subjected to SEM analysis even if no trace of Carbon was expected to be found (see 3.3.6 paragraph). Anyway the integrity of the micro features could be appreciated:

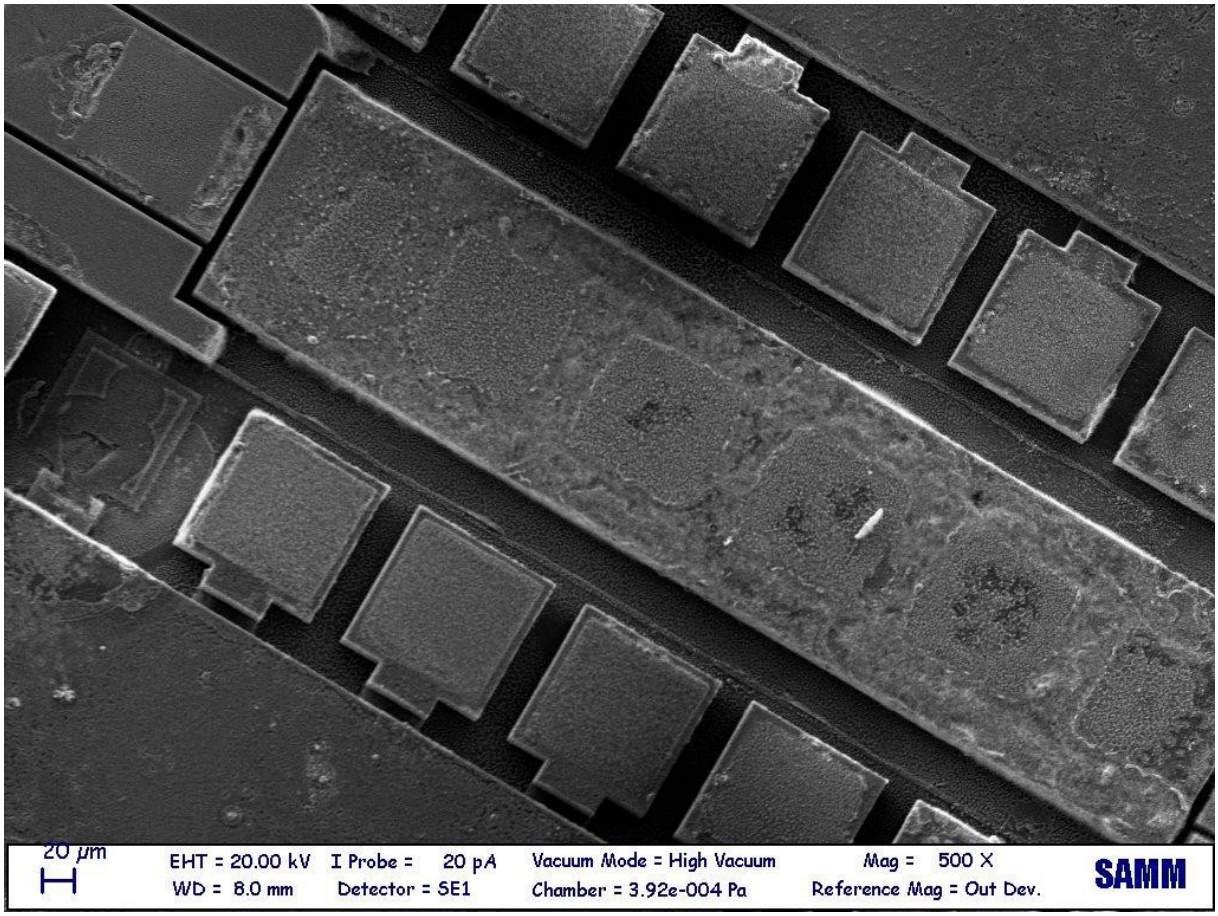

Fig. 3.54a: CVD MEMS SEM view

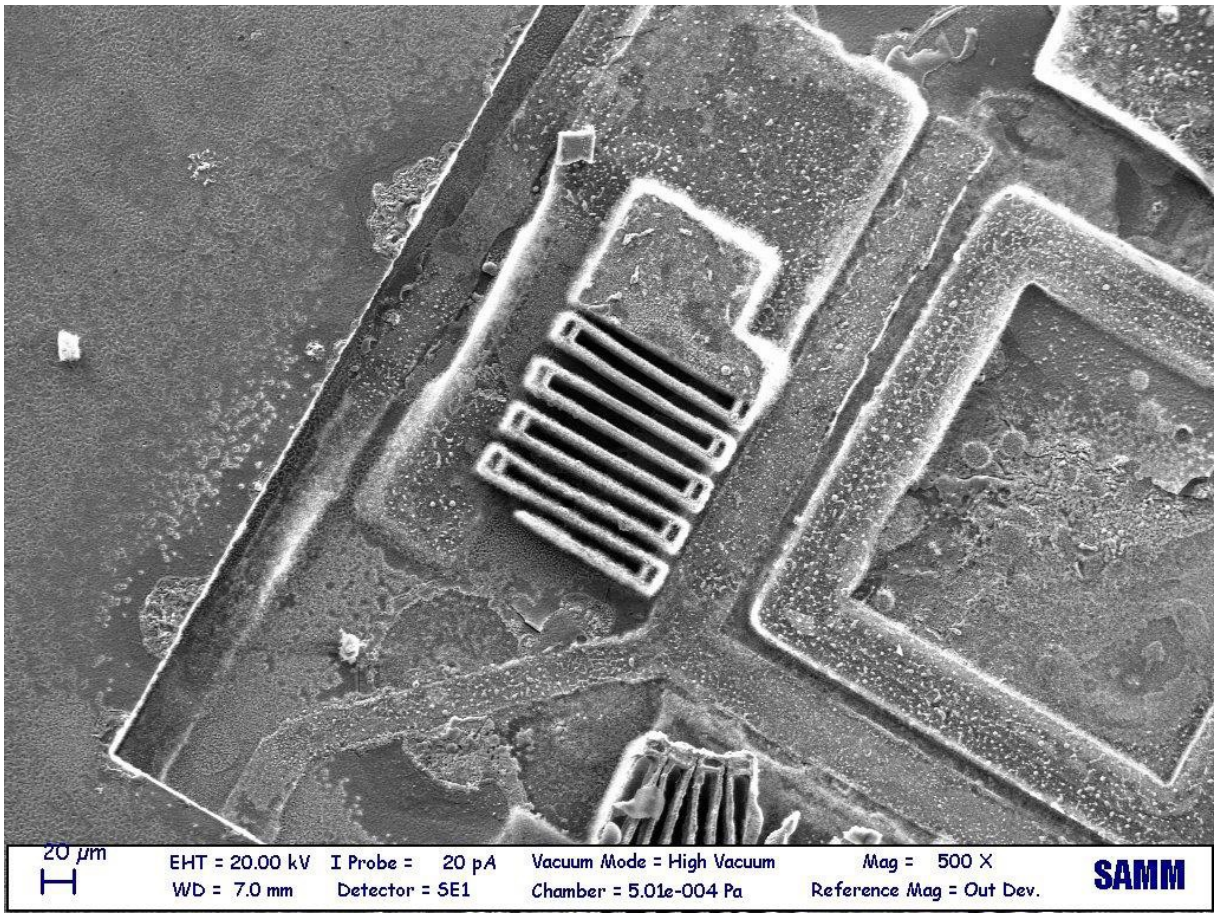

Fig. 3.54b: CVD MEMS SEM view

The homogeneous Nickel layer is visible and it seems it covered completely the floating parts: galvanic displacement is suitable for MEMS plating because of the limited thickness that can be deposited (500 – 600 nm), which is much lower than MEMS features (1 – 2 µm).

3.4.2 MEMS 2D Raman Peak Deconvolution

The procedure was the same of the 3.3.8 paragraph. Unlike the flat Ni/Si samples, MEMS sample had a more irregular 2D peak, which led to a major number of Voigt curves used for the deconvolution. This information, along with the relatively high I(G)/I(2D) led to the conclusion that **more than 5 layers was present, up to 7.**

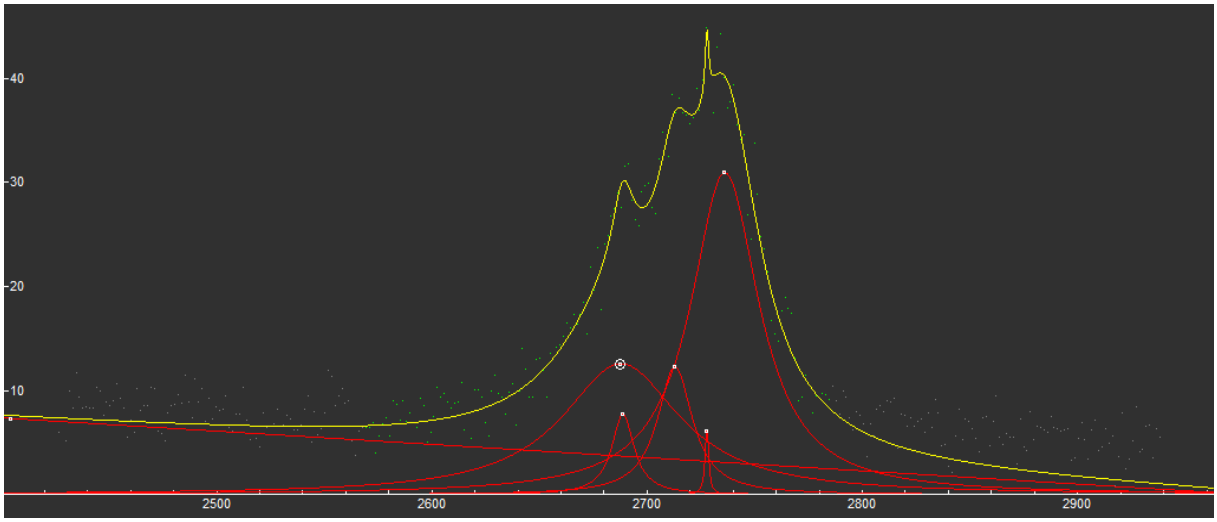

Fig. 3.55: CVD MEMS 2D Raman peak deconvolution with Voigt curves

And the characteristic frequencies found were:

- 2694,9 cm^{-1};
- 2735,0 cm^{-1};
- 2712,32 cm^{-1};
- 2727,7 cm^{-1};
- 2688,05 cm^{-1};

CHAPTER 4:

Conclusions

Electrons beam deposited transition metals films have proven to be a successful buffer layer for direct fabricating graphene on top of semiconductor surfaces, because of the high compatibility these materials show with respect to electronics and microelectronics applications [57].
The main disadvantages in using this technique are the equipment costs of the electron beam deposition, in particular the vacuum and high vacuum machinery.

In this thesis work galvanic displacement is proposed as alternative process to deposit a homogeneous metal layer onto activated surface of Silicon wafers. This technique has proven to be highly reproducible and highly adaptable for it was performed either on flat wafers and on microstructured ones (MEMS).

Before actually stepping into the deposition process, a preparatory set of experiments were performed onto electroformed, selfstanding, metal foils. The aim was to understand the graphene layer quality that could be achieved with two different
d – block metals: Copper and Nickel.

Graphene deposition was carried out with atmospheric Chemical Vapour Deposition technique using methane as a precursor. Deposition stream composition parameter was critically selected among all literature data, while deposition times and temperatures diverged with respect to the substrate to be covered with graphene: Copper and Nickel display different Carbon solubility, a feature that changes the inner nature of the graphene deposition mechanism onto them.

In particular, Copper took 3 deposition experiments to achieve the growth of a FLG like structure: the sample dwelt 2, 4 and 6 minutes in the tubular furnace at 1000°C.
On the other hand, nickel proved to be more easy to cover, and a single experiments, a 2 minutes deposition at 1000°C, was sufficient to obtain an acceptable result, that is, an ordered, few layered, graphene deposit.

From an analysis of the deposition made through the optical microscope, it was possible to observe hat the deposition was not uniform because there were areas with different colours. This difference in colour was attributed to the different quantities of deposited material.

The judgement upon the graphene deposit quality could have been made thanks to Raman spectroscopy and optical inspection. Actually, the samples' surface features were unmistakable and periodic: a single spot analysis was sufficient to link the resulting spectrum to all the similar optical peculiarities.

The most important parameters of the latter analysis were the presence of the G and 2D peaks, typical of carbon structures, the ratio between the intensities of the two peaks, the shape of the 2D peak and the change of the frequencies of the two peaks as a function of the number of layers deposited.
The informations so gathered motivated the choice made: Copper was covered by a disordered graphitic layer while Nickel presented a well rounded and highly ordered FLG structure grown on it. So the experimental work proceeded with the application of the graphene CVD onto Silicon flat wafers.

As already said, galvanic displacement was the plating method chosen for Silicon buffering with transition metals.
The data gathered on the quality of graphene deposit onto free standing metals led to the obvious choice of Nickel as go to plating material.

In order to understand the optimal plating time for having a homogeneous and adherent metal film grown onto Silicon, the solution was characterized using XRD,SEM and AFM analysis.

XRD analysis allowed us to appreciate the Nickel grains size growth when the plating time increased, because of the broadening of the diffraction peaks, and the complete surface coverage at higher deposition times (Silicon XRD peak disappeared).
SEM investigations gave us informations about the composition of the deposit (simple as it could be) and thickness evolution: in fact galvanic displacement is regarded as a self limiting deposition and this feature could be observed in the non linear behaviour of the metal thickness as a function of the plating time graph.
AFM revealed an overall good mean surface roughness (about 32 nm), which is under the mirror plate acceptance.

Finally CVD was performed onto the Ni/Si system with exactly the same parameters used for free standing Nickel: 1000°C was the reaction temperature and the sample dwelt for 2 minutes in the furnace.
With the sake of optimize the procedure, a second experiment was performed on a similar sample: the reaction temperature was lowered to 900°C, keeping 2 minutes as furnace dwelling time.

The same characterization path was followed for the above cited samples: optical investigation showed a web – like structure of dark and bright areas for the 1000°C deposited sample, while a clean and bright surface was observable for the 900°C deposited sample.
Raman spectroscopy was performed in a more accurate way: for the first sample all the different colour areas were analysed while for the second sample, given that any surface features were appreciable, two random spots were inspected.
It turned out that the dark areas on the first samples surface were characterized by FLG, ranging from 5 to 3 layers as the analysis proceeded from dark grey to light grey zones, while the bright areas seemed to be covered with a graphene “sub – monolayer” that is, a very defected and non continuous graphene film.
AFM analysis was realized in order to observe the presence of graphene domains and the profile measurement revealed a good agreement with Raman results: the measured graphene domain heigh was roughly 1,3 nm which, considering 0,335 as the graphite inter planar distance, corresponds to 4 graphene layers (FLG).
SEM did no reveal any trace of Carbon: the FLG layer was too thin and homogeneous to have sufficient contrast and the SEM was blind to it.
Finally XPS analysis was performed at CNR on the first experiment samples, in order to have another prove of the FLG thickness. The local chemical analysis reported a 1,3 to 1,5 thickness of Carbon deposit in the areas were Nickel signal was more relevant, that are, the light grey areas under lighted during Raman spectroscopy. The 3 to 5 graphene layers theory was confirmed.

The last part of the experimental work was devoted to apply the techniques presented above to an existing MEMS, in order to prove the procedure can be applied to microstructured wafers without altering the production flow.

The CVD process was the same of the first Ni/Si sample (1000°C reaction temperature and 2 minutes furnace dwelling).
Optical inspection revealed the same web – like structure find in the above reported samples and Raman confirmed the same result was obtained.

In order to find a relationship between flat Ni/Si Raman spectrum and that of the microstructured Ni/Si one, peak deconvolution was taken in consideration for the capacity to “resolve” the 2D Raman peak and give a qualitative evaluation of the deposited graphene layers number.
Malaard [55] work was considered for the sake of linking the number of deconvolution curves to the number of graphene layers and Voigt curves were chosen to perform the fitting. The work so done revealed a high number of graphene layers onto the microstructured sample, ranging from 5 to 7 in the dark areas.
It must be said that the microstructured sample presented a higher homogeneity of the deposition, which is probably due to the smaller surface (MEMS features) available for graphene growth.

In conclusion, it is possible to confirm galvanic displacement of transition metals as a valid alternative to physical vapour deposition methods for metal enhanced graphene deposition onto semiconductors, because of the reduced equipment costs and the higher compatibility with Silicon substrates.
The deposited graphene/FLG structures proved to be very ordered, which is important for exploiting the novel characteristics of the carbonaceous film and the domains were quite large (tens of microns), even if featured a non constant number of layers.
In order to step out from academic landscape the deposition procedure has to be tuned, in particular deposition parameters should be customized with respect to the very substrate to cover, also featuring molecular analytic models to avoid graphitic deposits, along with *ad hoc* cooling procedures, which have not been considered in this work.

Bibliography

[1] **Lavoisier AL.** Traité é lé mentaire de chimie. Paris; 1789

[2] **Graphene layer**. *IUPAC Gold Book*. International Union of Pure and Applied Chemistry. Retrieved 31 March 2012

[3] **The Nobel Prize in Physics 2010**. The Nobel Foundation. Retrieved 2013-12-03

[4] **H. P. Boehm, R. Setton, E. Stumpp**. *Pure and Applied Chemistry* 1994; **66** (9): 1893-1901

[5] **H. P. Boehm, A. Clauss, G. O. Fischer, U. Hofmann**. *Zeitschrift für anorganische und allgemeine Chemie* 1962; **316** (3-4): 119-127

[6] **Phillips, P.** *Ann. Phys*. (N.Y.) 2006; **321**: 1634

[7] **M. Gmitra, S. Konschuh, C. Ertler, C. Ambrosch-Draxl, and J. Fabian**. *Phys. Rev.* 1098-0121/2009/80(23)/235431(5)

[8] **Geim AK, MacDonald AH.** *Physics Today* 2007; **60**(8): 35-41

[9] **Kelly BT.** Physics of graphite. *London: Applied Science Publishers* 1981

[10] **Neto AHC, Guinea F, Peres NMR, Novoselov KS, Geim AK.** *Rev Mod Phys* 2009;
81(1): 109-62

[11] **Ando T.** *Prog. Theor. Phys.* 2008; **176**(Suppl.): 203-26

[12] **Matthew O'Brien and Barbara Nichols**. ARL-TR-5047: 1-2

[13] **Zhang YB, Small JP, Pontius WV, Kim P.** *Appl Phys Lett* 2005; **86**(7): 073104

[14] **Novoselov KS, Geim AK, Morozov SV, Jiang D, Zhang Y, Dubonos SV, et al.** *Science* 2004; **306**: 666

[15] **Blake P, Brimicombe PD, Nair RR, Booth TJ, Jiang D, Schedin F, et al.** *Nano Lett*
2008; **8**: 1704

[16] **Hernandez Y, Nicolosi V, Lotya M, Blighe FM, Sun Z, De S, et al.** *Nat Nanotechnol* 2008; **3**: 563

[17] **Lotya M, Hernandez Y, King PJ, Smith RJ, Nicolosi V, Karlsson LS, et al.** *J Am Chem Soc* 2009; **131**: 3611

[18] **Li X, Zhang G, Bai X, Sun X, Wang X, Wang E, et al.** *Nat Nanotechnol* 2008; **3**: 538.

[19] **Hummers WOR.** *J Am Chem Soc* 1958; **80**: 1339

[20] **Stankovich S, Dikin DA, Piner RD, Kohlhaas KA, Kleinhammes A, Jia Y, et al.**

Carbon 2007; **45**: 1558

[21] **Stankovich S, Piner RD, Chen XQ, Wu NQ, Nguyen ST, Ruoff RS.** *J Mater Chem* (2006);

[22] **Wang JJ, Zhu MY, Outlaw RA, Zhao X, Manos DM, Holoway BC.** ***Appl Phys Lett*** 2004; **85**: 1265

[23] **Wang JJ, Zhu MY, Outlaw RA, Zhao X, Manos DM, Holoway BC.** *Carbon* 2004; 42: 2867

[24] **Hass J, Heer WAd, Conrad EH.** *J Phys: Condens Matter* 2008; **20**: 323202

[25] **Varchon F, Feng R, Hass J, Li X, Nguyen BN, Naud C, et al.** *Phys Rev Lett* 2007; 99: 126805

[26] **Nakada, K., Fujita, M., Dresselhaus, G. & Dresselhaus,** *M. S. Phys. Rev. B* 1996; 54: 17954-17961

[27] **Li, X. L. et al.** *Science* 2008; **319**, 1229-1232

[28] **Kosynkin, D. V. et al.** *Nature* 2009; **458**: 872-876

[29] **Jiao, L., Zhang, L., Wang, X., Diankov, G. & Dai, H**. *Nature* 2009; **458**: 877–880

[30] **Cai J, Ruffieux P, Jaafar R, Bieri M, Braun T, Blankenburg S, et al**. *Nature* 2010; 466: 470

[31] **Somani PR, Somani SP, Umeno M**. *Chem Phys Lett* 2006; **430**: 56

[32] **Li X, Cai W, Colombo L, Ruoff RS**. Nano Lett 2009; **9**: 4268

[33] ASTM International. In B374-96 (2003) Standard Terminology Relating to Electroplating; ASTM International: West Conshohocken, PA, 2003

[34] **Helen H. Lou, Yinlun Huang.** *Encyclopedia of Chemical Processing.* DOI: 10.1081/EECHP- 120007747

[35] **E. W. Becker, W. Ehrfeld, P. Hagmann, A. Maner, D. Munchmeyer**. Microelectronic engineering 1986; **4**: 35

[36] **Stelter, M.; Bombach, H.** *Advanced Engineering Materials* 2004; **6**: 558

[37] **Milan Paunovic and Mordechay Schlesinger,** Fundamentals of Electrochemical Deposition, Second Edition, 2006 John Wiley & Sons, Inc.

[38]:Review on break through MEMS technology

[39]:**Jeremy A.Waldraven,** "Introduction to application and industry for MEMS",Sandia Labs

[40]:www.analog.com

[41]:www.MEMS.sandia.gov

[42]:**J. Micromech.Microeng**, “Time and frequency response of two-arm

micromachined thermal actuators", 13 (January 2003) 40-46
[43]:**J. J. Yao and M. F. Chang**, "A surface micromachined miniature switch for telecom. applications with signal frequencies from DC up to 4GHz," Transducers, June 1995, pp. 384-387
[44]:**Walker, S. J., Nagel, D. J., Report** on "Optics & MEMS," Naval Research Laboratories, Materials Science and Technology Division, May 15, 1999
[45]:**Arney, S., Aksyuk, V. A., Bishop, D. J., Bolle, C. A., Frahm, R. E., Gasparyan, A., Giles, C. R., Goyal, S., Pardo, F. L., Shea, H. R., Lin, M. T. and White, C. D.**, "Design Reliability of MEMS/MOEMS for Lightwave Telecommunications," Proc. of the 27th ISTFA, Nov. 2001, pp. 345-348
[46]:www.ti.com
[47]:**R. R. Allen, J. D. Meyer, W. R. Knight**, "Thermodynamics and Hydrodynamics of Thermal Ink Jets," Hewlett Packard Journal, May 1985.
[48]:**P. Galambos, K. Zavadil, R. Givler, F. Peter, A. Gooray, G. Roller, and J. Crowley**, "A Surface Micromachined Electrostatic Drop Ejector," 11th Intl. Conf. on Solid-State Sensors and Actuators, Munich, Germany, June 2001, pp. 906-909. Paper 27.1
[49]:**S. Bohm, W. Olthuis, and P. Bergveld**, "A μTAS Based on Microdialysis for On-line Monitoring of Clinically Relevant Substances," Proceedings of the μTAS Workshop, 1998, pp. 31-34
[50]:**L. Bousse**, "Whole Cell Biosensors," Sensors andActuators B (Chem), B34(1-3), 1996, pp. 270-275
[51]:**J. M. Ramsey, S. C. Jacobson, and M. R. Knapp,"Microfabricated** Chemical Measurement Systems,"Nature Medicine, Vol. 1, 1995, pp. 1093-1096
[52]:K**urt E. Petersen**,"Silicon as a mechanical material", IEEE
[53]: **Nitaigour Premchand Mahalik,** "Micromanufacturing and Nanotechnology", Springer, ISBN 3-540-25377-7, 2006
[54]: **Xuesong Li, Weiwei Cai, Luigi Colombo, and Rodney S. Ruoff,** Department of Mechanical Engineering and the Texas Materials Institute, UniVersity Station C2200, The University of Texas at Austin, Austin, Texas 78712-0292, and Texas Instruments Incorporated, Dallas, Texas 75243
[55]: **L.M. Malard, M.A. Pimenta, G. Dresselhaus ,** M.S. Dresselhaus Departamento de Física, Universidade Federal de Minas Gerais, Belo Horizonte-MG 30123-970, Brazil
[56]: **H. Ago**, PRESTO-JST, "Synthesis, Characterization, and Applications of Single-

and Double-Layer Graphene Grown on Epitaxial Metal Films; 227th ECS Meeting, May 24 – 28 2015

[57]: **Daniel Q.McNerny, B. Viswanath, Davor Copic, Fabrice R.Laye, Christophor Prohoda; Anna C. Brieland-Shoultz, Erik S.Polsen, Nicholas T.Dee, Vijayen S. Veerasamy & A.John Hart**; "Direct fabrication of graphene on Sio2 enabled by thin film stress engineering", Scientific Reports 4 : 5049

[58]: **Yu Yao, john Rodriguez, Jie Cui, Alsion Lennon, Stuart Wenham**; "Uniform plating of thin Nickel layers for silicon solar cells", Energy Procedia 38 (2013) 807 - 815

[59]: **Delhaes, P.,** Graphite and Precursors, CRC Press, ISBN 90-5699-228-7

[60]: J**in-Ho Choi, Zhancheng Li, Ping Cui, Xiaodong Fan, Hui Zhang, Changgan Zeng & Zhenyu Zhang,** Scientific Reports 3, Article number: 1925 doi:10.1038/srep01925